Order Number 9414043

An experimental method for structural intensity and source location

Zhang, Yong, Ph.D.

Iowa State University, 1993

U·M·I
300 N. Zeeb Rd.
Ann Arbor, MI 48106

An experimental method for structural intensity and source location

by

Yong Zhang

A Dissertation Submitted to the

Graduate Faculty in Partial Fulfillment of the

Requirements for the Degree of

DOCTOR OF PHILOSOPHY

Department: Aerospace Engineering and Engineering Mechanics
Major: Engineering Mechanics

Approved:

Signature was redacted for privacy.

In Charge of Major Work

Signature was redacted for privacy.

For the Major Department

Signature was redacted for privacy.

For the Graduate College

Iowa State University
Ames, Iowa
1993

TABLE OF CONTENTS

LIST OF FIGURES

LIST OF TABLES

ACKNOWLEDGMENTS

I would like to sincerely thank my dissertation advisors, Dr. Anna L. Pate and Dr. J. Adin Mann III, for their invaluable advise and guidance in this research. Also, I am grateful to the other members of my Program of Study Committee, Dr. David K. Holger, Dr. James E. Bernard, Dr. Martin J. Vanderploeg and Dr. Alison B. Flatau, for their helpful advice.

I would like to acknowledge the financial support of the Office of Naval Research.

For the encouragement and support they have always given me, I want to thank my parents, Mr. Zhiquan Zhang and Mrs. Chengyu Yang. I am in debt to them, especially to my mother. I also want to thank my two sisters, for their taking care of my mother when she was sick in bed.

I especially want to thank my wife, Wenqin, and daughters, Chong and Celia, for their understanding, patience and support. I am grateful that I have a warm and loving family with me.

Finally, thanks to all other ISU faculty and staff that I didn't thank personally.

CHAPTER 1. INTRODUCTION

1.1 Objectives

In practical vibration problems, it is essential to understand why and how a structure vibrates so as to reduce (or enhance) the vibration and, therefore, the sound radiation. The goal of this thesis is to develop an experimental method to determine the structural intensity and force distribution function in order to locate sources and to trace the energy transmission in a vibrating structure.

Much research has been done on the formulation of the structural intensity. Different formulas have been derived. However, there has not been research to reveal the relations between different formulas. One of the objectives of the thesis is to study the formulations and the physical significance of structural intensity. In this part of the work, we are going to study the differences between two formulations that are based on different assumptions. Meanwhile, the relations between structural intensity for different wave types will be discussed.

Earlier research used a method to locate sources by solving for the inplane components of vibrating shells and plates based on the knowledge of the out of plane motion and loading of the structures. This thesis will introduce the idea of using a force distribution function to locate sources. It shows that the force distribution function can show the source location clearly for a plate type structure with the help

of some signal processing techniques.

The spatial Fourier transformation techniques are used in the calculation of the structural intensity and the force distribution function. Therefore, signal processing techniques such as windowing in the spatial domain and filtering in the wavenumber domain are necessary to overcome numerical difficulties that occur in the calculations due to the Fourier transforms being performed with discrete and finite data. In this thesis, we also studied the influences of windowing and filtering on the calculation of structural intensity and force distribution function.

Since the calculation of both the structural intensity and the force distribution function requires the information of the plate normal displacement (or velocity), the measurement methodologies and data processing techniques are also discussed.

It is also intended that the influences of ribs and constrained layer damping on the structural intensity and the force distribution function be studied for plate type structures.

In summary, the objectives of the thesis are to understand structural intensity physically, to refine the methodology to determine the structural intensity and force distribution function from measurements so as to locate sources, and to study the influences of ribs and damping on plates.

1.2 Literature Review

The work that is closely related to structural intensity in plates is plate vibration theory. The work on plate vibration is reviewed before the studies on structural intensity are reviewed.

1.2.1 Plate vibration theories

General three-dimension elasticity requires three partial differential equations to describe the vibration of an elastic medium [1, 2]. Because of their complexity, these exact equations are rarely used to solve for the vibrational response of practical structures, although they are employed in evaluating the natural frequencies and modes, as well as the response to a point load, of simple structures such as simply-supported plates [3]. In practical applications, there are always some assumptions used to simplify the governing equations.

The most widely used approximation to the three-dimensional theory is the thin-plate approximation which is usually referred to as bending (or classical) theory [4]. In this theory, the plate motion is governed by Lagrange's equation. It is assumed that every straight line in the plate which was originally perpendicular to the middle surface of the plate remains straight after deformation and perpendicular to the deflected middle surface, and that the middle surface remains unstretched. Due to such assumptions, the Lagrange's equation of plate motion contains only the out of plane component of the plate motion. And it is useful for frequencies for which the wavenumber is much larger than the plate thickness.

The development of approximate theories which are accurate enough for the bending wavelength on the order of the plate thickness may be attributed to Reissner [5], Uflyand [6], and Mindlin [7]. Mindlin, in deriving the thin-plate equations, introduced the influence of shear and rotary inertia in addition to the bending effect in classical theory. The assumption is that a straight line originally normal to the neutral plane will remain straight but not necessarily normal after deformation. Here, the shear stresses is still assumed to be uniformly distributed over the plate thickness

which is not the case in practical problems. Mindlin introduced a shear correction factor which accounts for the linear approximation to the shear stresses. In this set of plate equations, the inplane components of motion are included in addition to the out of plane motion that is found in classical theory. So, in Mindlin's theory, there are three partial differential equations versus one in classical theory.

1.2.2 Structural intensity

The study of structural intensity began in the early seventies [8]. Research primarily concentrated on the intensity formulation and measurement techniques.

Structural intensity is a quantity that describes the energy transmission in structures. It is defined as the product of stress tensor and the velocity of vibrating particles [9]. These quantities in vibrating elastic medium are not directly measurable. So, the study of the structural intensity formulation is aimed at expressing structural intensity in terms of measurable physical quantities such as the surface velocity or displacement of a vibrating elastic medium by making assumptions. However, these assumptions depend on the structure being studied.

Noiseux [8] and Pavić [10] formulated the structural intensity based on the assumptions that are used in the classical plate theory. As a result of this, the structural intensity formula for plates contains only the out of plane component of the plate surface velocity, and the order of spatial derivatives of the velocity appearing in the formula can be as high as third order. Special measurement arrangements using several accelerometers were proposed so that the spatial derivatives of the velocity can be performed using either the finite difference method or specially designed analog circuits.

Williams, Dardy, and Fink [11] proposed a noncontact measurement technique to obtain structural intensity using Pavić's intensity formulation. The noncontact measurement method, called SIMAP (Structural Intensity from the Measurement of Acoustic Pressure), does not change the plate loading as accelerometers do. Also, SIMAP uses only one probe, a hydrophone or microphone, and thus avoided the necessity of accurate phase calibrations. The structural intensity was calculated from the measured plate normal velocity using the Fast Fourier Transform (FFT) as a tool to take spatial derivatives. Pascal, Loyau and Mann [12] also discussed the technique to determine structural intensity using nearfield acoustic holography. Pate et al. [13], studied the technique to determine structural intensity from acoustic imaging. Other noncontact techniques of measuring the plate velocity, such as using a laser Doppler vibrometer, have been used by Hayek et al. [14]. In the work by Hayek et al. [14], the structural intensity was calculated using the finite difference method.

Romano, Abraham, and Williams [15], based on the definition of structural intensity and three-dimensional elasticity, and later Williams [16], based on an energy balance principal, derived general three-dimensional structural intensity formulas for thin shells and plates. Through certain assumptions, these equations can be simplified to Pavić's intensity formula [10]. Williams [16] also discussed the physical interpretation of all the terms in the structural intensity formulas.

Pascal, Loyau, and Mann [12], Williams [16], and Romano, Abraham, and Williams [15] also discussed the relationship between the plate normal acoustic intensity and the structural intensity. Romano, Abraham and Williams [33], Williams [16], Pascal et al. [12] also pointed out that the divergence of the structural intensity is equal to the power injected into the plate. So the divergence of the structural

intensity can be used to locate the sources.

1.2.3 Force distribution function

There has not been many explicit studies on the force distribution function to locate sources in the structures. However, in their paper about the application of structural intensity for thin shells and plates, Romano and Williams [15] pointed out that through a set of governing equation of vibrating plates or shells, it is possible to solve for the inplane components of motion provided that the out of plane motion and the loading to the structures are known. They further pointed out that the vector expression of the inplane motion can show the source location. Based on this same idea, Zhang, Pate, and Mann [17] used Mindlin's plate equations of motion to solve for force distribution function based on the measured plate surface velocity. The results show that source location can be clearly shown.

1.3 Introduction

Based on the objectives of the thesis and the work reviewed in the literature, the scope of research of this thesis is shown in Figure 1.1. The following topics will be covered in the order described below.

Theories related to the structural intensity and force distribution function will be discussed in Chapter 2. The physical significance of structural intensity and differences among different formulas, as well as the force distribution function based on Mindlin's plate equations, are discussed.

The implementation of the calculation of the structural intensity and the force distribution function will be described in Chapter 3.

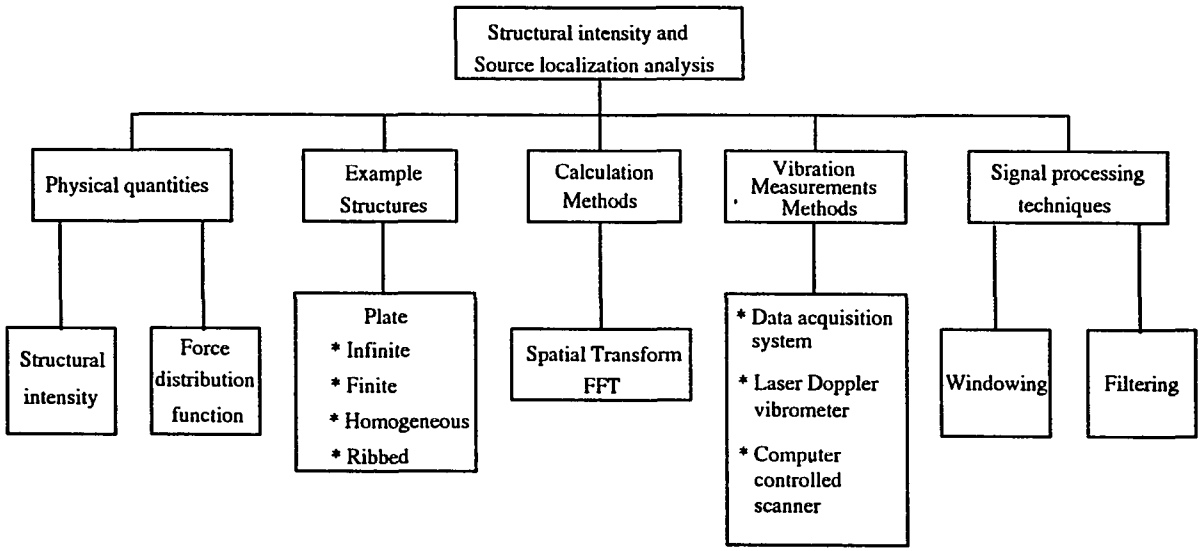

Figure 1.1: Scope of Research

The vibration measurement system is described in Chapter 4. A B-spline algorithm will be introduced to smooth the measured data.

Chapter 5 will discuss some of the signal processing techniques that are necessary in calculating the structural intensity and force distribution function from the velocity measurements. These techniques are not based on plate theories. They are used in this research is because of numerical difficulties in the calculations. A major concern will be placed on understanding the effectiveness and limitation of windowing and filtering on the accuracy of calculations.

Experimental and computational results will be presented in Chapter 6. These results will include those for homogeneous and ribbed plates.

Finally, in Chapter 7, conclusions and suggestions for further research will be presented.

CHAPTER 2. THEORETICAL ANALYSIS

As has been pointed out in the introduction, previous studies of structural intensity has focused on its formulation and measurement. In the structural intensity formulation, assumptions have to be made in order to express the structural intensity in terms of measurable quantities. This chapter discusses the differences in the structural intensity formulations that are based on different assumptions. Also, since in practical cases, the velocity and force (stresses) are expressed in complex form, carrying not only magnitudes but also phase information, the calculated structural intensity is complex. This leads to active and reactive intensities as in the case of sound intensity. This chapter will also explore some of the physical significance of active and reactive intensities by looking at some individual wave types.

As far as source location is concerned, previous research primarily used structural intensity as a tool to show source location. In this research, a force distribution function is introduced that is later proven to be very effective in locating sources. In this chapter, Mindlin's plate motion equations are used to solve for the force distribution function for plates based on the measured plate normal velocity. In fact, for any type of structure, a force function can be obtained provided a set of governing equations of motion can be found and some components of motion can be determined by either experimental or analytical methods.

From the force distribution function, a power function can be obtained that shows the power input to the plate. This chapter will also describe the power function.

2.1 Structural Intensity

2.1.1 Definition

The general definition of structural intensity at a arbitrary point in an elastic medium is [9]:

$$\vec{I} = -(\frac{\partial \vec{s}}{\partial t}) \cdot [\sigma], \tag{2.1}$$

where:

$(\frac{\partial \vec{s}}{\partial t})$ = particle velocity = $\dot{\vec{s}}$,

$[\sigma]$ = stress tensor.

Physically, if there is no energy source in the elastic medium, then the time rate of change of the strain energy in the volume v of an elastic medium equals the energy flux through the volume's boundary, A:

$$\int\int\int_V \frac{\partial E}{\partial t} dV = \int\int_A \vec{I} \cdot \vec{n} dA \tag{2.2}$$

where:

$\vec{n}$ is the outward normal of the volume V.

The particle velocity in Equation (2.1) is oscillating about its mean, and it does not represent rigid body motion. And so are the stresses. Both quantities are very small values.

Since the structural intensity is defined as the product of the velocity and the stress, it is the work done by the stress in the direction of the velocity. In other words, it is the work done in the direction of the velocity through a unit area. It is clear that structural intensity represents energy transported at a given point through a unit area. This can also be verified by examining the dimension of the structural intensity. Since the dimension for particle velocity is [Length/Time] and for stress is [Force/Length^2], the dimension for the structural intensity is [Force-Length/Time/Length^2], i.e., [Power/Length^2]. By this definition, structural intensity is a vector quantity that not only gives the amount of energy, but also shows the direction of the energy that is transported. For the general three dimensional case, it has three components, for example, $\underline{I}_x, \underline{I}_y$ and $\underline{I}_z$ in cartesian coordinates. For plate-like structures, the out of plane components $\underline{I}_z$ is ignored so only the inplane components, $\underline{I}_x, \underline{I}_y$, remain.

The structural intensity in Equation (2.1) is the *instantaneous* structural intensity because it represents the energy flow as a function of time, i.e., it changes not only with the location in the elastic medium (x, y, z), but also with time.

Since the structural intensity in the above definition is in terms of the particle velocity and the stress, which are not directly measurable quantities, the structural intensity is going to be formulated in terms of measurable quantities such as the surface normal velocity in plate-like structures. In the next section, the formulations and their differences will be discussed.

Structural intensity, as defined in Eqn. (2.1), is a function of the spatial coordinates x, y and z. For plates and shells, it changes over the area , as well as over the thickness of the plates or shells. For thin plates or shells, the average of the structural

intensity over the thickness of a plate or shell is defined as the *structural intensity resultants* :

$$I_x = \langle \int_{-\frac{h}{2}}^{\frac{h}{2}} \underline{\mathrm{I}}_x dz \rangle_t, \tag{2.3}$$

$$I_y = \langle \int_{-\frac{h}{2}}^{\frac{h}{2}} \underline{\mathrm{I}}_y dz \rangle_t, \tag{2.4}$$

where:

$\langle\rangle_t$ means time average, and h is the plate thickness.

The reason the time average is introduced here is that the time averaged energy flow in the plate is related to power. We will keep the time average sign through all the structural intensity formulas.

In the rest of this thesis, the structural intensity resultants are studied and are referred to as the structural intensity.

2.1.2 Formulations

Two different sets of structural intensity formulations for plates will be discussed. They are based on different assumptions [7, 18]. Pavić's formula is based on pure bending plate theory, while Romano's is based on Mindlin's plate theory which includes rotary inertial and shear effects. Now, we look at the two sets of formulations separately.

1. Pavić's Formulation:

Pavić's structural intensity formula is derived directly from the physics of the plate vibration. For a section of a thin plate shown in Figure 2.1, x and y are the coordinates of the middle plane of the plate. The coordinate z is normal to the plate

middle plane. The energy flowing through a unit length of the face perpendicular to x axis, i.e., the structural intensity in the x direction, I_x, is equal to the power transmitted by the forces and moments on their corresponding displacements (linear and rotational). On the face perpendicular to the x axis, there exist the shear force Q_x, caused by the shear stress σ_{xz}, the bending moment M_x, caused by the normal stress σ_x, and the twisting moment M_{xy}, caused by the inplane shear stress σ_{xy}. The displacements corresponding to Q_x, M_x, and M_{xy} are the normal displacement w, the bending rotational displacement θ_y and the twisting rotational displacement θ_x. Thus, the power flowing through a unit length of the plate section perpendicular to the x axis is [8]:

$$I_x = M_x\dot{\theta}_y + M_{xy}\dot{\theta}_x + Q_x\dot{w}. \tag{2.5}$$

Similarly, in the y direction:

$$I_y = M_y\dot{\theta}_x + M_{yx}\dot{\theta}_y + Q_y\dot{w}, \tag{2.6}$$

where:

I_x and I_y are the intensity components in the x and y direction, respectively, and

$$\dot{w} = \frac{\partial w}{\partial t}, \tag{2.7}$$

$$\dot{\theta}_x = \frac{\partial^2 w}{\partial y \partial t}, \tag{2.8}$$

$$\dot{\theta}_y = \frac{\partial^2 w}{\partial x \partial t}, \tag{2.9}$$

$$M_x = \int_{-\frac{h}{2}}^{\frac{h}{2}} \sigma_x z \, dz, \tag{2.10}$$

$$M_{xy} = \int_{-\frac{h}{2}}^{\frac{h}{2}} \sigma_{xy} z \, dz, \tag{2.11}$$

$$Q_x = \int_{-\frac{h}{2}}^{\frac{h}{2}} \sigma_{xz} \, dz, \tag{2.12}$$

$$M_y = \int_{-\frac{h}{2}}^{\frac{h}{2}} \sigma_y z \, dz, \tag{2.13}$$

$$M_{yx} = \int_{-\frac{h}{2}}^{\frac{h}{2}} \sigma_{yx} z \, dz, \tag{2.14}$$

$$Q_y = \int_{-\frac{h}{2}}^{\frac{h}{2}} \sigma_{yz} \, dz, \tag{2.15}$$

To determine the above mentioned force and moment resultants, the following assumptions are introduced [8, 11,18]:

- Normal of the middle plane remains normal after plate deflection;
- Normal stress component on the face parallel to plate surface is neglected, i.e., $\sigma_z = 0$;
- Middle plane of the plate remains unstretched.

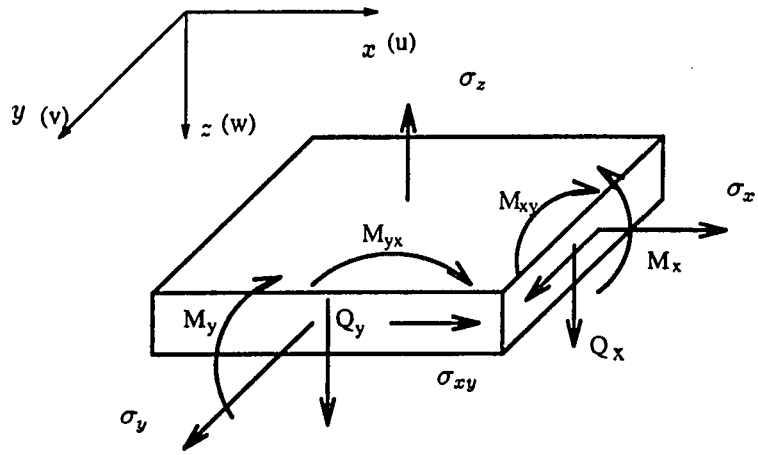

Figure 2.1: A section of a plate

As a result of the assumptions, the three displacement components of the plate are simplified as [18]:

$$u = -z\frac{\partial w}{\partial x}, \tag{2.16}$$

$$v = -z\frac{\partial w}{\partial y}, \tag{2.17}$$

$$w = w(x, y). \tag{2.18}$$

The corresponding stresses are:

$$\sigma_x = \frac{Ez}{1-\nu^2}\left(\frac{\partial^2 w}{\partial x^2} + \nu\frac{\partial^2 w}{\partial y^2}\right), \tag{2.19}$$

$$\sigma_y = \frac{Ez}{1-\nu^2}(\frac{\partial^2 w}{\partial y^2} + \nu\frac{\partial^2 w}{\partial x^2}), \tag{2.20}$$

$$\tau_{xy} = -\frac{Ez}{1+\nu}\frac{\partial^2 w}{\partial x \partial y}. \tag{2.21}$$

where:

E is the Young's modulus of the plate material;

ν is Poisson's ratio of the plate material.

For the section of a plate that is shown in Figure 2.1, the force and moment resultants are proportional to the second and third order of partial derivatives the plate normal displacement w:

$$M_x = -D(\frac{\partial^2 w}{\partial x^2} + \nu\frac{\partial^2 w}{\partial y^2}), \tag{2.22}$$

$$M_{xy} = -D(1-\nu)\frac{\partial^2 w}{\partial x \partial y}, \tag{2.23}$$

$$Q_x = D\frac{\partial}{\partial x}(\frac{\partial^2 w}{\partial x^2} + \frac{\partial^2 w}{\partial y^2}), \tag{2.24}$$

$$M_y = -D(\frac{\partial^2 w}{\partial y^2} + \nu\frac{\partial^2 w}{\partial x^2}), \tag{2.25}$$

$$M_{yx} = M_{xy}, \tag{2.26}$$

$$Q_y = -D\frac{\partial}{\partial y}(\frac{\partial^2 w}{\partial x^2} + \frac{\partial^2 w}{\partial x^2}), \tag{2.27}$$

where:

$D = \frac{Eh^3}{12(1-\nu^2)}$;

and h is the plate thickness.

Inserting equations (2.25) - (2.30) into Equations (2.5), (2.6), and integrate over the thickness of the plate, the structural intensity resultants for a plate based on the pure bending assumptions are:

$$I_x = \langle D \left[-(\frac{\partial^2 w}{\partial x^2} + \nu \frac{\partial^2 w}{\partial y^2}) \frac{\partial \dot{w}}{\partial x} - (1-\nu) \frac{\partial^2 w}{\partial x \partial y} \frac{\partial \dot{w}}{\partial y} + (\frac{\partial^3 w}{\partial x^3} + \frac{\partial^3 w}{\partial x \partial y^2}) \dot{w} \right] \rangle_t, \quad (2.28)$$

$$I_y = \langle D \left[-(\frac{\partial^2 w}{\partial y^2} + \nu \frac{\partial^2 w}{\partial x^2}) \frac{\partial \dot{w}}{\partial y} - (1-\nu) \frac{\partial^2 w}{\partial x \partial y} \frac{\partial \dot{w}}{\partial x} + (\frac{\partial^3 w}{\partial x^2 \partial y} + \frac{\partial^3 w}{\partial y^3}) \dot{w} \right] \rangle_t, \quad (2.29)$$

Equations (2.28) and (2.29) show that, for thin plates based on pure bending assumptions, the structural intensity is only related to the normal displacement and velocity and up to third order spatial derivatives of the normal displacement and velocity in addition to the material properties and plate dimensions.

There are three terms in each of the Equations (2.28) and (2.29). These terms correspond to three wave types: bending, twisting and shearing. Taking Equation (2.28) as an example, the three terms are:

$-(\frac{\partial^2 w}{\partial y^2} + \nu \frac{\partial^2 w}{\partial x^2}) \frac{\partial \dot{w}}{\partial y}$ $\longrightarrow$ corresponding to bending wave,

$-(1-\nu) \frac{\partial^2 w}{\partial x \partial y} \frac{\partial \dot{w}}{\partial x}$ $\longrightarrow$ corresponding to twisting wave,

$(\frac{\partial^3 w}{\partial x^2 \partial y} + \frac{\partial^3 w}{\partial y^3}) \dot{w}$ $\longrightarrow$ corresponding to shearing wave.

In other words, they represent the power transmitted by bending, twisting and shearing waves, respectively.

2. Romano's formulation:

Romano, Williams, and Abraham [4] derived the structural intensity for plates and cylindrical shells based on the definition of the structural intensity that is shown in Equation (2.1) and three dimensional elasticity. The velocity vector $\frac{\partial \vec{s}}{\partial t}$ term was replaced by three displacement components of the plates or shells. And the three displacements were expanded into a Taylor series about the middle surface ($r = a$):

$$\begin{pmatrix} u(a+\rho) \\ v(a+\rho) \\ w(a+\rho) \end{pmatrix} = \begin{pmatrix} u(a) \\ v(a) \\ w(a) \end{pmatrix} + \begin{pmatrix} u^{(1)}(a) \\ v^{(1)}(a) \\ w^{(1)}(a) \end{pmatrix} \frac{\rho}{1!} + \begin{pmatrix} u^{(2)}(a) \\ v^{(2)}(a) \\ w^{(2)}(a) \end{pmatrix} \frac{\rho^2}{2!} + \ldots, \tag{2.30}$$

where:

ρ is the distance of a point in the plate and shell to middle plane,

a is the radius of the cylinder.

Using the above equation and the definition of the structural intensity in Equation (2.1) for a thin cylindrical shell and averaging over the thickness of the plate, the structural intensity in a cylindrical coordinate is [15]:

$$I_z = -\{\dot{w}Q_z + \dot{v}N_{z\phi} + [\frac{\dot{v}}{a} - \frac{1}{a}\frac{\partial \dot{w}}{\partial \phi}]M_{z\phi} + \dot{u}N_z - \frac{\partial \dot{w}}{\partial z}M_z\}, \tag{2.31}$$

$$I_\phi = \{\dot{w}Q_\phi + \dot{v}N_\phi + [\frac{\dot{v}}{a} - \frac{1}{a}\frac{\partial \dot{w}}{\partial \phi}]M_\phi + \dot{u}N_{\phi z} - \frac{\partial \dot{w}}{\partial z}M_{\phi z}\}, \tag{2.32}$$

where the Q's, M's and N's are the force and moment resultants [19, 20].

For a plate, let the radius of the cylinder go to infinity, and note that:

$$\frac{1}{a}\frac{\partial}{\partial \phi} \rightarrow \frac{\partial}{\partial s} \rightarrow \frac{\partial}{\partial x}, \tag{2.33}$$

The structural intensity of the plate is therefore:

$$I_x = -[\dot{w}Q_x - \frac{\partial \dot{w}}{\partial x}M_x - \frac{\partial \dot{w}}{\partial y}M_{xy} + \dot{u}N_x + \dot{v}N_{xy}], \tag{2.34}$$

$$I_y = -[\dot{w}Q_y - \frac{\partial \dot{w}}{\partial x}M_{yx} - \frac{\partial \dot{w}}{\partial y}M_y + \dot{u}N_{yx} + \dot{v}N_y], \tag{2.35}$$

where $I_x, I_y, w, Q_x, M_x, M_{xy}, Q_y, M_{yx}$, and M_y are defined in the same way as in deriving Pavić's structural intensity formula in Equations (2.5) to (2.15), and:

$$N_x = \int_{-\frac{h}{2}}^{\frac{h}{2}} \sigma_x \, dz, \tag{2.36}$$

$$N_{xy} = \int_{-\frac{h}{2}}^{\frac{h}{2}} \sigma_{xy} \, dz, \tag{2.37}$$

$$N_{yx} = \int_{-\frac{h}{2}}^{\frac{h}{2}} \sigma_{yx} \, dz, \tag{2.38}$$

$$N_y = \int_{-\frac{h}{2}}^{\frac{h}{2}} \sigma_{yx} \, dz. \tag{2.39}$$

From the above definition, it is clear that N_x is the normal force resultant on the face perpendicular to the x axis, N_{xy} is the inplane shear force resultant on the face perpendicular to the x axis, N_{yx} is the inplane shear force resultant on the face perpendicular to the y axis, and N_y is the normal force resultant on the face perpendicular to the y axis.

Here, the first three terms in both Equations (2.34) and (2.35) are similar to the three terms in Equations (2.5) and (2.6). There are two additional terms in Equations (2.34) and (2.35).

So far, the derivation of structural intensity has been *exact* except that the higher order terms have been neglected. The reason that the procedure is *exact* is that the geometry of the structure is not yet included. In order to be able to express the structural intensity in terms of measurable quantities, the Q's, M's and N's need to be expressed in terms of the normal velocity of the plate surface as in the case of Pavić's formulation (see Equations (2.22) to (2.27)).

The three dimensional elasticity stress tensor is used:

$$\sigma_{ij} = \lambda \delta_{ij} u_{kk} + \mu u_{i,j} + \mu u_{j,i}, \tag{2.40}$$

where:

$$\delta_{ij} = \begin{cases} 1 & i = j \\ 0 & i \neq j \end{cases},$$

$u_{i,j} = \frac{\partial u_i}{\partial x_j}$,

$u_{kk} = \sum_{i=1}^{3} u_{ii}$,

λ and μ are the Lamé elastic constants of the plates or shells.

We also assume that for a thin plate, the normal of the middle plane defined as a straight line before deformation will not remain normal to the middle plane after deformation. This is different from the assumption for Pavić's formulation. As a result of this assumption, the relation between the inplane displacements u and v will not be the same as in Equations (2.7) to (2.9) for Pavić's formulation. Mindlin [2] assumed that the inplane displacements u and v are proportional to z and the normal displacement w is independent of z:

$$u = z\psi_x(x, y), \tag{2.41}$$

$$v = z\psi_y(x, y), \tag{2.42}$$

$$w = w(x, y), \tag{2.43}$$

The functions ψ_x and ψ_y are arbitrary functions of x and y. For $\psi_x = -\frac{\partial w}{\partial x}$ and $\psi_y = -\frac{\partial w}{\partial y}$, the above assumption is the same as for Pavić's assumption in Equations (2.16) to (2.18). This assumption corresponding to the fact that the out of plane shear effect is taken into account so that the stress components σ_{xz} and σ_{yz} exist and the corresponding shear deformations, γ_{xz} and γ_{yz} also exist.

The force and moment resultants based on the above displacements and the three dimensional stress tensor are:

$$M_x = \frac{h^3}{12}\left[(\lambda + 2\mu)\frac{\partial \psi_x}{\partial x} + \lambda\frac{\partial \psi_y}{\partial y}\right], \tag{2.44}$$

$$M_{xy} = \frac{h^3}{12}\mu(\frac{\partial \psi_x}{\partial y} + \frac{\partial \psi_y}{\partial x}), \tag{2.45}$$

$$Q_x = h\mu\left[\psi_x + \frac{\partial w}{\partial x}\right], \tag{2.46}$$

$$M_{yx} = M_{xy}, \tag{2.47}$$

$$M_y = \frac{h^3}{12}\left[\lambda\frac{\partial \psi_x}{\partial x} + (\lambda + 2\mu)\frac{\partial \psi_y}{\partial y}\right], \tag{2.48}$$

$$Q_y = \mu h(\psi_y + \frac{\partial w}{\partial y}), \tag{2.49}$$

$$N_x = 0, \tag{2.50}$$

$$N_{xy} = 0, \tag{2.51}$$

$$N_y = 0, \tag{2.52}$$

$$N_{yx} = 0, \tag{2.53}$$

The corresponding structural intensity is:

$$\begin{aligned} I_x &= \langle\{-\frac{h^3}{12}\left[(\lambda+2\mu)\frac{\partial\psi_x}{\partial x}+\lambda\frac{\partial\psi_y}{\partial y}\right]\frac{\partial\dot{w}}{\partial x} \\ &\quad -\frac{h^3}{12}\mu\left[\frac{\partial\psi_x}{\partial y}+\frac{\partial\psi_y}{\partial x}\right]\frac{\partial\dot{w}}{\partial y} \\ &\quad +h\mu\left[\psi_x+\frac{\partial w}{\partial x}\right]\dot{w}\}\rangle_t, \end{aligned} \tag{2.54}$$

$$\begin{aligned} I_y &= \langle\{-\frac{h^3}{12}\mu\left[\frac{\partial\psi_x}{\partial y}+\frac{\partial\psi_y}{\partial x}\right]\frac{\partial\dot{w}}{\partial x} \\ &\quad -\frac{h^3}{12}\left[\lambda\frac{\partial\psi_x}{\partial x}+(\lambda+2\mu)\frac{\partial\psi_y}{\partial y}\right]\frac{\partial\dot{w}}{\partial y} \\ &\quad +h\mu\left[\psi_y+\frac{\partial w}{\partial y}\right]\dot{w}\}\rangle_t. \end{aligned} \tag{2.55}$$

Equations (2.54) and (2.55) show that based on the assumptions that consider shear effects, the structural intensity is related not only to the normal displacement of the plate, but also to the in plane components of the plate. On the other hand,

the calculation of the structural intensity requires only first order spatial derivatives of the displacements with respect to x and y.

As in Pavić's formula, Romano's formula also consists of three terms that correspond to three wave types: bending, twisting and shearing. For Equation (2.54), these terms are:

$-\frac{h^3}{12}\left[(\lambda+2\mu)\frac{\partial\dot{\psi}_x}{\partial x}+\lambda\frac{\partial\psi_y}{\partial y}\right]\frac{\partial\dot{w}}{\partial x}$ —— bending,

$-\frac{h^3}{12}\left[\lambda\frac{\partial\dot{\psi}_x}{\partial x}+(\lambda+2\mu)\frac{\partial\psi_y}{\partial y}\right]\frac{\partial\dot{w}}{\partial y}$ —— twisting,

$+h\mu\left[\psi_y+\frac{\partial w}{\partial y}\right]\dot{w}$ —— shearing.

The reason the shear and rotary inertia effects are considered in Mindlin's plate theory is that the classical theory based on pure bending assumption is only good for the waves that are long in comparison with the thickness of the plate. As the wave length diminishes, the velocity in the three-dimensional theory has as its upper limit the velocity of Rayleigh surface waves. Hence the classical plate theory cannot be expected to give good results for sharp transients or for the frequencies of modes of vibration of high order. Mindlin [7] showed that the shear and rotary inertia effects are more important at higher frequencies than at lower frequencies.

2.1.3 Comparison of structural intensity formulations

From the description of the structural intensity formulations, it is seen that the differences between Pavić's and Romano's formula are primarily:

1. Pavić's formulation is based on the classical plate theory which requires that the normal to the middle plane remain normal after deformation, while Romano's formulation is based on Mindlin's plate theory in which the normal of the middle does not need to remain normal after deformation. As a result, the inplane displacement

components for the two cases are different. For Pavić's formula, the in plane displacements are described in Equations (2.16) to (2.18). For Romano's formula, they are described in Equations (2.41) to (2.43). In both cases, they are linear functions of the distance from the plate middle plane. However the rotation angles are different.

2. Pavić's uses the stress expression that is similar to that of the plane stress assumption, while Romano's uses the general three dimensional stress expression.

3. As a result of the above different displacements and stresses, the force and moment resultants on the plate sections, the M's and Q's, are different. Comparing Equations (2.25) to (2.30) with Equations (2.44) to (2.49), it is seen that for Pavić's formulation, the force and moment resultants, and therefore the structural intensity, are related to only the out of plane displacement component, w, While the Romano's formula requires all three displacement components.

4. On the other hand, Pavić's needs up to the third order partial derivatives of the displacement with respect to x and y, while Romano's only need the first order derivatives. In calculations with experimental data, lower derivatives are more accurate to calculate than the higher derivatives. Chapter 3 will discuss the calculation method using Fast Fourier Transforms (FFT) and the influence of the order of derivatives on the calculation accuracy.

5. Both Pavić's structural intensity formula (2.28), (2.29) and Romano's formula (2.54), (2.55) show that the structural intensity is caused by three types of forces and moments, the bending moments M_x and M_y, the twisting moments M_{xy} and M_{yx}, and the out of plane shear force Q_x and Q_y, and their corresponding angular and linear displacements.

6. Romano's formula is based on Mindlin's plate theory that considers the shear

and rotary inertia effects. But these effects are more important for high frequency vibrations, i.e., frequencies corresponding to a wavenumber that is in the same order or shorter than the plate thickness. For a thin aluminum plate with thickness of 0.01 meters, the lowest frequency corresponding to the flexural wavelength of the plate thickness is about 980 kHz, which is well above the frequency range of our interest. In the low frequency range, shear and rotary inertia do not have much influences on the structural intensity in plates.

Figure 2.2 and Figure 2.3 show the structural intensity for an infinite homogeneous plate with a point source calculated from Pavić's formula and Romano's formula, respectively. In both figures, the plot on the left is active structural intensity and the plot on the right is the reactive structural intensity (the active and reactive structural intensities are discussed in the next section). For now, it is enough to say that the active structural intensity is the time average of the instantaneous structural intensity defined in Equation (2.1). The plate is made of aluminum and the plate thickness is 0.01 meters. The calculation is performed on a 2.0 by 2.0 meters area. Figure 2.4 and Figure 2.5 show the x component of the active structural intensity from the two formulas in 3-D plots. Since a 32 by 32 grid is used in the calculation and the point force is located on a grid node, the point force is not located exactly at the center of the plate. Therefore, the active structural intensity is not exactly symmetric about the center of the plate. The non-symmetry in these results indicates an error in the calculation since it is done on a finite plate with discrete data. Figure 2.6 and Figure 2.7 show the difference and the percentage error for the x component of the active intensity. It is seen that there is not much difference between the two results. The active intensity is considered here because its physical significance is

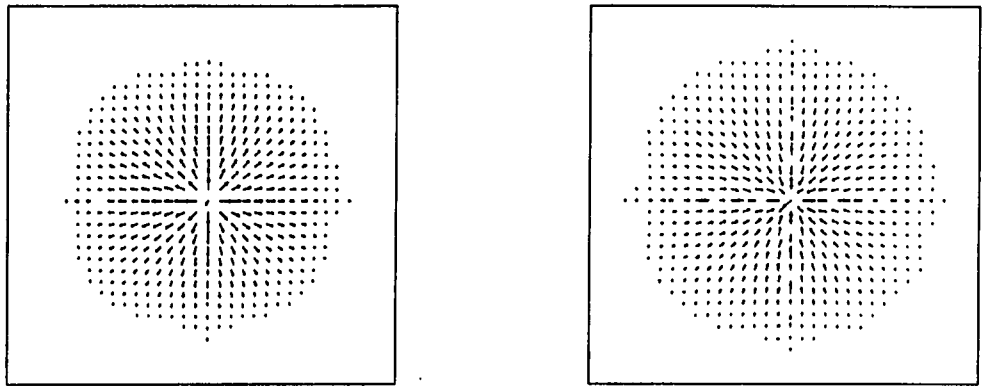

Figure 2.2: Structural intensity for an infinite homogeneous plate with a point source, f=250 Hz, Pavić's formula, (left. active, right. reactive)

most understood. The active intensity represents the time average power.

2.1.4 Active and reactive structural intensity

In both Pavić's and Romano's structural intensity formulas, the structural intensity is expressed in terms of plate displacement and its spatial derivatives. In Equations (2.28), (2.29) and (2.54), (2.55), the structural intensity is a real quantity. The structural intensity can also be expressed as a complex quantity,

$$\vec{I} = \vec{I}_r + j\vec{I}_i, \tag{2.56}$$

where

$\vec{I}_r$ is the real part of the structural intensity,

$\vec{I}_i$ is the imaginary part of the structural intensity.

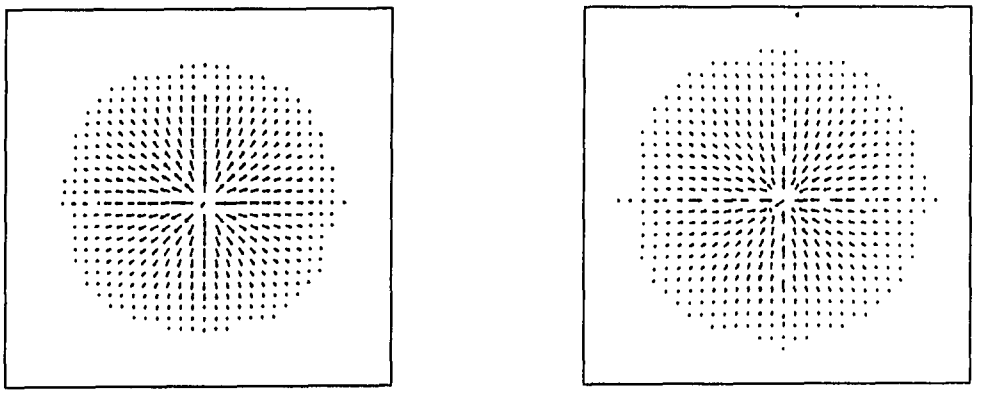

Figure 2.3: Structural intensity for an infinite homogeneous plate with a point source, f=250 Hz, Romano's formula, (left. active, right. reactive)

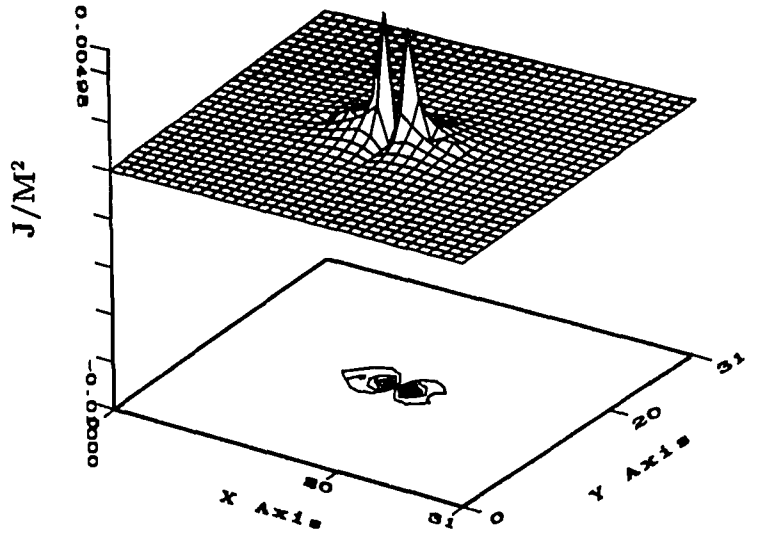

Figure 2.4: X component of active structural intensity for an infinite homogeneous plate with a point source, f=250 Hz, Pavić's formula

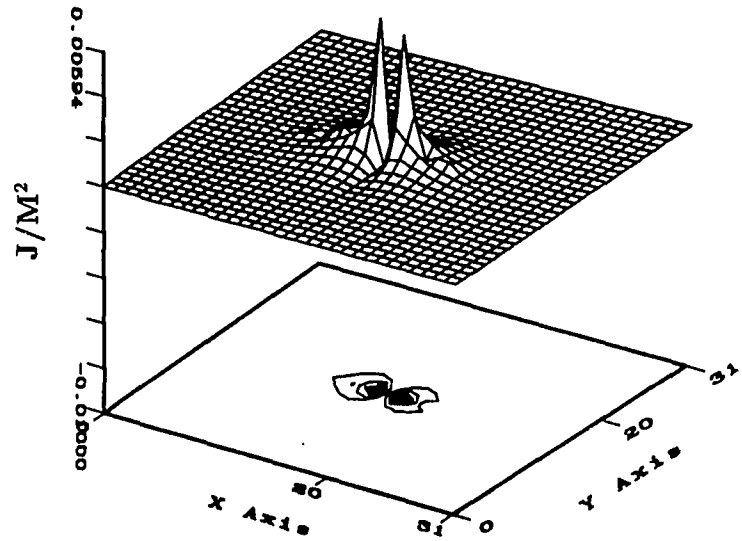

Figure 2.5: X component of active structural intensity for an infinite homogeneous plate with a point source, f=250 HZ, Romano's formula

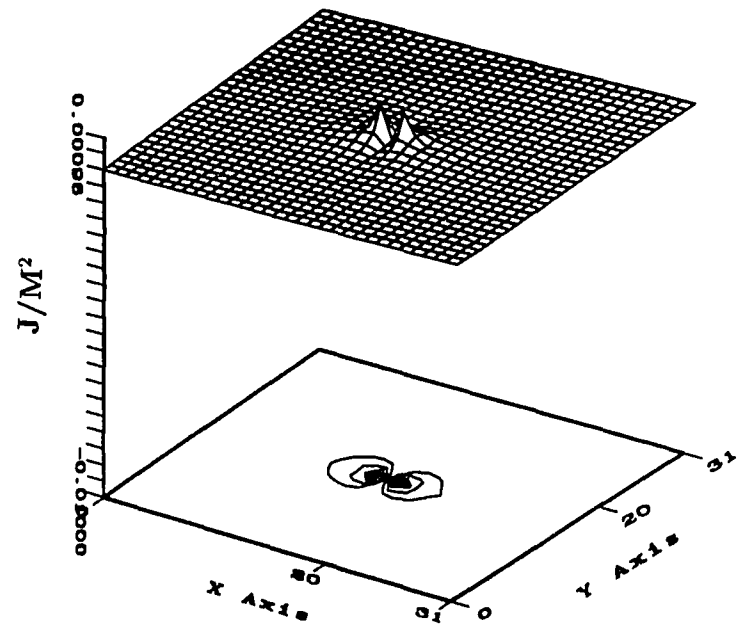

Figure 2.6: Difference between the structural intensities in Figure 2.4 and Figure 2.5

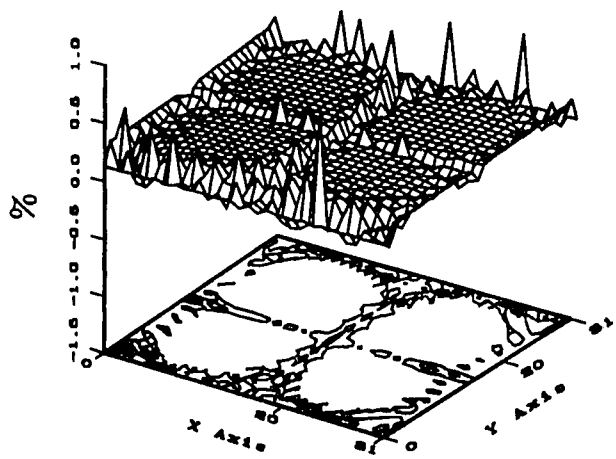

Figure 2.7: Percentage difference between the structural intensities in Figure 2.4 and Figure 2.5

The real part of the structural intensity is called *active structural intensity* while the imaginary part is called *reactive intensity.* The active structural intensity is the time average of the instantaneous intensity.

The reasons for the structural intensity to be complex are:

1. The measured plate surface displacement (or velocity) is complex. This means that the displacement function of the plate surface contains not only the magnitude, but also the phase information.

2. The materials in practical cases usually have some damping. The influence of damping on the plate vibration is usually included by using a complex Young's modulus. The material is assumed to have a loss factor, η. Then the Young's modulus with damping, E_d, is [21]:

$$E_d = E(1 + j\eta), \tag{2.57}$$

where:

E is the Young's modulus of the material without considering the damping effect,

$j = \sqrt{-1}$.

For plate structural intensity, this damping is introduced by the plate bending stiffness D. The plate bending stiffness that includes the damping influence is:

$$\begin{aligned} D_d &= \frac{E_d h^3}{12(1-\mu^2)} \\ &= D(1 + j\eta), \end{aligned} \tag{2.58}$$

η assumed to be 0.02 (2 % damping) in the calculations of this thesis.

Now, let us look at the physical meanings of the active and reactive intensity through some simple wave forms:

1. Longitudinal wave.

A one dimensional longitudinal wave propagating in the x direction has the form [22, 23]:

$$\xi = A(x)e^{j(\omega t - \phi(x))}, \tag{2.59}$$

where ξ is the particle displacement in x direction, $A(x)$ is the wave magnitude, ω is the circular frequency and $\phi(x)$ is the phase of the wave. The corresponding stress in the x direction is:

$$\sigma_{xx} = B\frac{\partial \xi}{\partial x}, \tag{2.60}$$

where:

$B = E(1-\nu^2)(1+2\nu)$.

According to Equation (2.1), the structural intensity is the product of the stress and its corresponding velocity. From references [24] and [25], if both the stress and the velocity are sinusoidal functions of time, then the time average of their product is the first function multiplied by the complex conjugate of the second function:

$$I_x = \frac{1}{2}\dot{\xi} \cdot \sigma_{xx}^*, \tag{2.61}$$

where:

$\dot{\xi} = \frac{\partial \xi}{\partial t}$,

σ_{xx}^* is the complex conjugate of σ_{xx}.

Insert Equations (2.62) and (2.63) into Equation (2.64), the structural intensity becomes:

$$I_x = -\frac{A^2}{2}\omega B\frac{\partial \phi(x)}{\partial x} + j\frac{A}{2}\omega B\frac{\partial A(x)}{\partial x}. \tag{2.62}$$

This shows that the active structural intensity is proportional to the phase gradient in the direction of wave front propagation[26]. Thus, it shows that the energy is transported in the direction of wave front propagation. And the amount of energy is proportional to the square of the wave magnitude, the frequency and the stiffness of the structure.

The reactive structural intensity, which is the imaginary part in Equation (2.62), is proportional to the gradient of the wave magnitude. As a result of this, the reactive structural intensity vector points to the peaks of the maximum wave magnitudes.

2. Transverse shear wave.

The transverse shear wave displacement and stress are [22, 23]:

$$w = A(x)e^{j(\omega t - \phi(x))}, \tag{2.63}$$

$$\tau_{xz} = G\frac{\partial w}{\partial x}. \tag{2.64}$$

The resulting structural intensity from the above displacement and stress is:

$$\begin{aligned} I_x &= \frac{1}{2}\dot{w} \cdot \tau_{xz}^* \\ &= -G\frac{A^2}{2}\omega\frac{\partial\phi(x)}{\partial x} + jG\frac{A}{2}\omega\frac{\partial A}{\partial x}. \end{aligned} \tag{2.65}$$

Again, the active structural intensity is proportional to the phase gradient and the reactive structural intensity is proportional to the magnitude gradient.

3. Pure bending wave.

For pure bending wave traveling in x direction, the stresses that existing on the intersection perpendicular to x axis are [22, 23]:

$$\sigma_x = -Ez\frac{\partial^2 w}{\partial x^2}, \tag{2.66}$$

$$\tau_{xz} = -\frac{E}{2}\frac{\partial^3 w}{\partial x^3}[(\frac{h}{2})^2 - z^2], \tag{2.67}$$

where w is the normal displacement, E is the Young's modulus, and z is the distance from the neutral plane of the plate.

According to Equation (2.1), the structural intensity is:

$$I_x = \frac{1}{2}[\dot{u} \cdot \sigma_x^* + \dot{w} \cdot \tau_{xz}^*], \tag{2.68}$$

where the displacements u and w are:

$$u = jA\omega e^{j(\omega t - \phi_x)}, \tag{2.69}$$

$$w(x) = A(x)e^{j(\omega t - \phi_x)}, \tag{2.70}$$

Substituting Equations (2.69) and (2.70) into Equations (2.66) and (2.67), and then inserting the results into Equation (2.68), the structural intensity for pure bending motion in a thin plate is:

$$I_x = -\frac{E\omega h^3}{12}\{[A_r + \frac{A}{4}B_r] + j[A_i + \frac{A}{4}B_i]\}, \tag{2.71}$$

where:

$$A_r = A\frac{\partial \phi_x}{\partial x}(\frac{\partial^2 A}{\partial x^2} - A(\frac{\partial \phi_x}{\partial x})^2) + \frac{\partial A}{\partial x}(2\frac{\partial A}{\partial x}\frac{\partial \phi_x}{\partial x} + A\frac{\partial^2 \phi_x}{\partial x^2}),$$

$$A_i = -\frac{\partial A}{\partial x}(\frac{\partial^2 A}{\partial x^2} - A(\frac{\partial \phi_x}{\partial x})^2) - A\frac{\partial \phi_x}{\partial x}(2\frac{\partial A}{\partial x}\frac{\partial \phi_x}{\partial x} + A\frac{\partial^2 \phi_x}{\partial x^2}),$$

$$B_r = 3\frac{\partial^2 A}{\partial x^2} + 3\frac{\partial A}{\partial x}\frac{\partial^2 \phi_x}{\partial x^2} + A\frac{\partial^3 \phi_x}{\partial x^3} + A(\frac{\partial \phi_x}{\partial x})^3,$$

$$B_i = [\frac{\partial^3 A}{\partial x^3} - 3\frac{\partial A}{\partial x}(\frac{\partial \phi_x}{\partial x})^2 - 3A\frac{\partial^2 \phi_x}{\partial x^2}\frac{\partial \phi_x}{\partial x}][(\frac{h}{2})^2 - z^2].$$

Since the structural intensity is in such a complicated format, it is not clear what contributes to the active and reactive structural intensities.

2.2 Force Distribution Function

One of the primary purposes to study the structural intensity is to locate sources on the vibrating structures. There have not been many studies on other methods

to locate sources. Romano and Williams [15] pointed out that the vector form of the plate inplane displacement components can be used for locating a source. In this thesis, a force distribution function method is introduced for locating sources in plate-like structures. This method is based on the fact that there exists a set of governing equations of motion which relates the plate motion with its excitation forces and that certain motion components can be determined by either experimental or analytical methods.

In this research, Mindlin's plate motion equation is used for the purpose of calculating the force distribution function. At the same time, the plate inplane motion components are determined for the purpose of calculating the structural intensity using Romano's structural intensity formula.

After making assumptions that are described in Equations (2.44) to (2.46) [7, 31], Mindlin developed the following equations of motion for a plate. These equations take into account the shear and rotary inertia effects.

$$\frac{D}{2}[(1-\nu)\nabla^2\psi_x + (1+\nu)\frac{\partial\phi}{\partial x}] - \kappa^2 Gh(\psi_x + \frac{\partial w}{\partial x}) = \frac{\rho h^3}{12}\frac{\partial^2\psi_x}{\partial t^2}, \tag{2.72}$$

$$\frac{D}{2}[(1-\nu)\nabla^2\psi_y + (1+\nu)\frac{\partial\phi}{\partial y}] - \kappa^2 Gh(\psi_y + \frac{\partial w}{\partial y}) = \frac{\rho h^3}{12}\frac{\partial^2\psi_y}{\partial t^2}, \tag{2.73}$$

$$\kappa^2 Gh(\nabla w + \phi) + q = \rho h\frac{\partial^2 w}{\partial t^2}, \tag{2.74}$$

where:

ρ is the volume density of the plate material,

κ is shear correction coefficient determined by [7],

$o = \frac{\partial \psi_x}{\partial x} + \frac{\partial \psi_y}{\partial y}$,

G = shear modulus,

q = force distribution function

D, ν, h, ψ_x and ψ_y are the same as before.

In this set of equations, there are four quantities, w, ψ_x, ψ_y, and q, besides the parameters that are related to material properties and the plate dimensions. The first three, w, ψ_x, ψ_y, are the three displacement components. The q function is the force density on the surface of the plate. If one of the displacement components is known, the other two displacement components and the force distribution function can be determined from Equations (2.72) to (2.74). In practice, we can measure the plate out of plane displacement w. Then, the two inplane displacement components, ψ_x, ψ_y, and the force density function q, can be solved for.

The two inplane displacement components, ψ_x and ψ_y can be used in the calculation of the structural intensity using Romano's structural intensity formula. The force distribution function q shows the force on the plate. Therefore, it can be used for the purpose of locating sources.

2.3 Power Function

It is obvious that if there is a force acting at an arbitrary point on the plate surface, and the plate vibrates at a certain velocity, then the force is doing work on the plate, i.e., the force injects power into the plate. From the above section, the force distribution function is obtained so that the force at every point of the plate surface is known. The plate surface normal displacement (or velocity) is obtained from measurements. The power function $p = p(x, y)$ can be defined as the product

of the force distribution function and the velocity and calculated by:

$$p(x,y) = \frac{1}{2} Re\{q(x,y) \cdot v(x,y)^*\}, \tag{2.75}$$

where:

Re indicates the real part of the product,

$q(x,y)$ is the force distribution function,

$v(x,y)^*$ is the complex conjugate of normal velocity.

The power function can also be used to show the source location of the plate. Theoretically, by multiplying the power function by the area of the plate, the input power to the plate can be calculated. So, the power function can also be used to estimate the input power to the plate. In the next chapter, the calculation of input power from the power function will be discussed along with determining the input power from the structural intensity.

CHAPTER 3. CALCULATION METHODS

From the description of Chapter 2, the structural intensity for thin plate is expressed by two different formulas. Pavić's formula (Equations (2.28) and (2.29)) consists of the normal displacement (or velocity) and up to the third order spatial derivatives of the normal displacement, while the Romano's formula (Equations (2.54) and (2.55)) is in terms of all three displacement (or velocity) components and their first order spatial derivative. It is clear that the key to calculating the structural intensity is to calculate accurate derivatives of the plate displacement (or velocity) if only the normal component of the displacement (or velocity) is known. This chapter will discuss the methods to calculate the spatial derivatives and the inplane displacement components of the plate.

As has been pointed out in Chapter 2, a force distribution function can be obtained from Mindlin's plate equations of motion provided that the out of plane component of plate displacement is known. This chapter will outline the method to solve for the force distribution function from Mindlin's equations.

In this research, Fourier Transforms are used to perform derivatives that are needed in calculating the structural intensity and to solve Mindlin's equation of motion to obtain the force distribution function. In this chapter, the Fourier Transform method to take derivatives will be described. Also, the methods of implementing the

equations will be described.

This chapter will also describe the way to calculate the input force magnitude from the force distribution function and the way to calculate the input power magnitude from the structural intensity and the power function.

3.1 Fourier Transform Formula

The basic formula that is used in taking spatial derivatives is:

$$\frac{\partial^m}{\partial x^m}\frac{\partial^n}{\partial y^n}[w(x,y)] = \mathcal{F}^{-1}\{(jk_x)^m(jk_y)^n\mathcal{F}[w(x,y)]\}, \tag{3.1}$$

where $\mathcal{F}$ represents a forward Fourier transform and $\mathcal{F}^{-1}$ represents an inverse Fourier Transform. For a two dimensional spatial function $g(x,y)$, the forward Fourier Transform with respect to spatial variables (x,y) is defined as [27, 28]:

$$G(k_x,k_y) = \mathcal{F}\{g(x,y)\} = \int_{-\infty}^{+\infty}\int_{-\infty}^{+\infty} g(x,y)e^{-j2\pi k_x x}e^{-j2\pi k_y y}dxdy, \tag{3.2}$$

where

k_x, k_y are wave numbers in x and y directions, respectively,

$G(k_x,k_y)$ is the wavenumber domain spectrum of the function $g(x,y)$.

The inverse Fourier Transform of the wavenumber domain spectrum $G(k_x,k_y)$ transforms the function back to real domain (x,y) [27, 28]:

$$g(x,y) = \mathcal{F}^{-1}\{G(k_x,k_y)\} = \int_{-\infty}^{+\infty}\int_{-\infty}^{+\infty} G(k_x,k_y)e^{j2\pi k_x x}e^{j2\pi k_y y}dk_x dk_y. \tag{3.3}$$

Equation (3.1) means that for a function $w(x,y)$ in real space (x,y), the mth derivative with respect to x and the nth derivative with respect to y is the inverse

Fourier Transform of a new function which is the Fourier Transform of the original function $w(x,y)$ multiplied by the wavenumber k_x raised to the mth power and the wavenumber k_y raised to the nth power. As a result of this equation, calculating spatial derivatives becomes a process of algebra. Also, in solving for the force distribution function, Mindlin's plate equations, which are partial differential equations, become linear algebraic equations. Thus, the process of solving partial differential equations becomes the process of solving linear algebraic equations. The details of this change will be shown in the following sections.

The key calculation in Equation (3.1) is the Fourier Transform. In this research, a Fast Fourier Transform algorithm is used because discrete sampled data is used. The Fourier Transform of the plate displacement, $w(x,y)$, is taken with respect to spatial variables x and y. The result of the Fourier Transform is the wavenumber spectrum of the displacement.

From Equation (3.1), it can be seen that in the wavenumber domain, the spectrum of the displacement, $W(k_x,k_y)$, is multiplied by $k_x^m k_y^n$. This term can be very large when higher than first order derivatives are calculated, (i.e., m, n greater than 1). Any numerical error in $W(k_x,k_y)$ at high k_x and k_y can be significantly enlarged. Figures 3.1, 3.2 and 3.3 show how the noise at large k values is enlarged. Figure 3.1 is the wavenumber spectrum $W(k_x,k_y)$ of a typical displacement $w(x,y)$. The main information is in the peak centered in the plot. However, there is some noise away from the center, although they are not large. Figure 3.2 shows the function $k_x W(k_x,k_y)$. This function is used for calculating $\frac{\partial w}{\partial x}$ according to Equation (3.1). It can be seen that the noise at large k_x values are enlarged so that this plot looks noisier than that in Figure 3.1. To calculate the third order derivative of the ve-

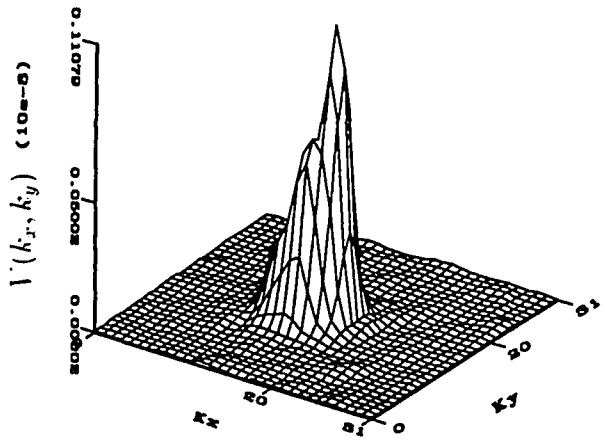

Figure 3.1: Wavenumber domain spectrum of a plate displacement $W(k_x, k_y)$

locity with respect to x, $\frac{\partial^3 w}{\partial x^3}$, the wavenumber spectrum $W(k_x, k_y)$ is multiplied by k_x^3. Figure (3.3) shows the function $k_x^3 W(k_x, k_y)$. Obviously, the noise is enlarged so that the main information is not outstanding any more. So, as has been pointed out in Chapter 2, in calculating the structural intensity, Romano's formula (Equations (2.54), (2.55)) often gives better numerical results than Pavić's formula, Equations (2.28) and (2.29) because the former requires lower order of spatial derivatives of the plate displacement (or velocity), reducing error caused by noise in the data.

At this point, we can see a major computational problem that arises by using Equation (3.1). In actual calculations, because of noise in the data, some signal processing techniques such as windowing and filtering are necessary in calculating the structural intensity and force distribution function. Filtering will be used to remove the noise amplified by multiplying $W(k_x, k_y)$ by k_x or k_x^3. This will be discussed in detail in Chapter 4.

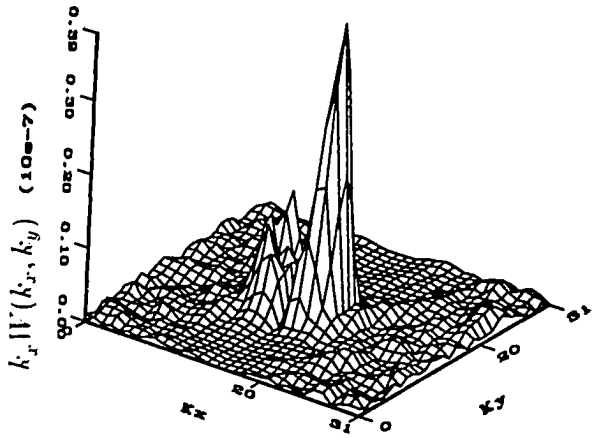

Figure 3.2: Wavenumber domain function $k_x W(k_x, k_y)$ for calculating $\frac{\partial w}{\partial x}$

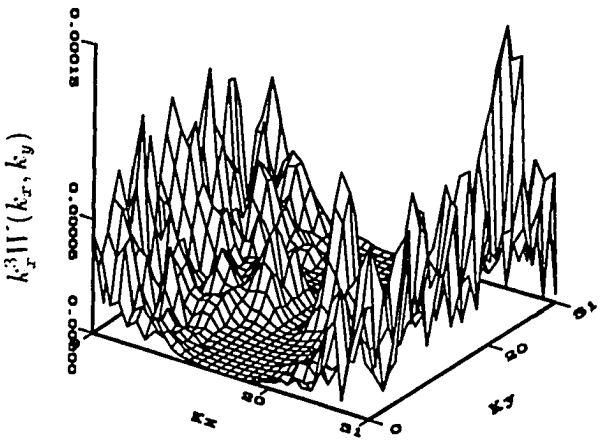

Figure 3.3: Wavenumber domain function $k_x^3 W(k_x, k_y)$ for calculating $\frac{\partial^3 w}{\partial x^3}$

3.2 Calculation of the Structural Intensity

Based on Equation (3.1), the structural intensity is calculated according to Equations (2.28) and (2.29) for Pavić's formulation, and according to Equations(2.54) and (2.55) for Romano's formulation.

Because the displacement and the structural intensity are complex quantities, the calculation is performed in the complex form, resulting in active and reactive structural intensity, which has been discussed in Chapter 2. The calculation procedure of the structural intensity using Pavić's formula (2.28),(2.29) is shown in the block diagram in Figure 3.4. There are nine derivatives included in Equations (2.28) and (2.29). They are: $\frac{\partial^3 w}{\partial x^3}$, $\frac{\partial^3 w}{\partial x^2 \partial y}$, $\frac{\partial^3 w}{\partial x \partial y^2}$, $\frac{\partial^3 w}{\partial y^3}$, $\frac{\partial^2 w}{\partial x^2}$, $\frac{\partial^2 w}{\partial x \partial y}$, $\frac{\partial^2 w}{\partial y^2}$, and $\frac{\partial v}{\partial x}$, $\frac{\partial v}{\partial y}$. These term are calculated by first performing an FFT of the out of plane displacement $w(x, y)$,and then using Equation (3.1) to calculate the derivatives. Finally, all the derivatives are inserted into Equations (2.28) and (2.29) to get the structural intensity.

Equations (2.28) and (2.29) each consists of three terms. Each term is a product of two partial derivatives or the sum of partial derivatives. After all the derivatives are calculated using Equation(3.1), the time average is calculated by taking the complex conjugate of the second quantities in each term before the multiplication. This method is based on the assumption of sinusoidal vibration in time [24].

The procedure for calculating the structural intensity using Romano's formula (2.54) and (2.55) is shown in Figure 3.5. In Romano's formula, the structural intensity includes all three displacement components. So, Mindlin's plate equation of motion, Equations (2.72) to (2.74), are used to solve for the inplane displacement components. This will be discussed in the next section along with the calculation of the force distribution function. With all three displacement components known, the Equations

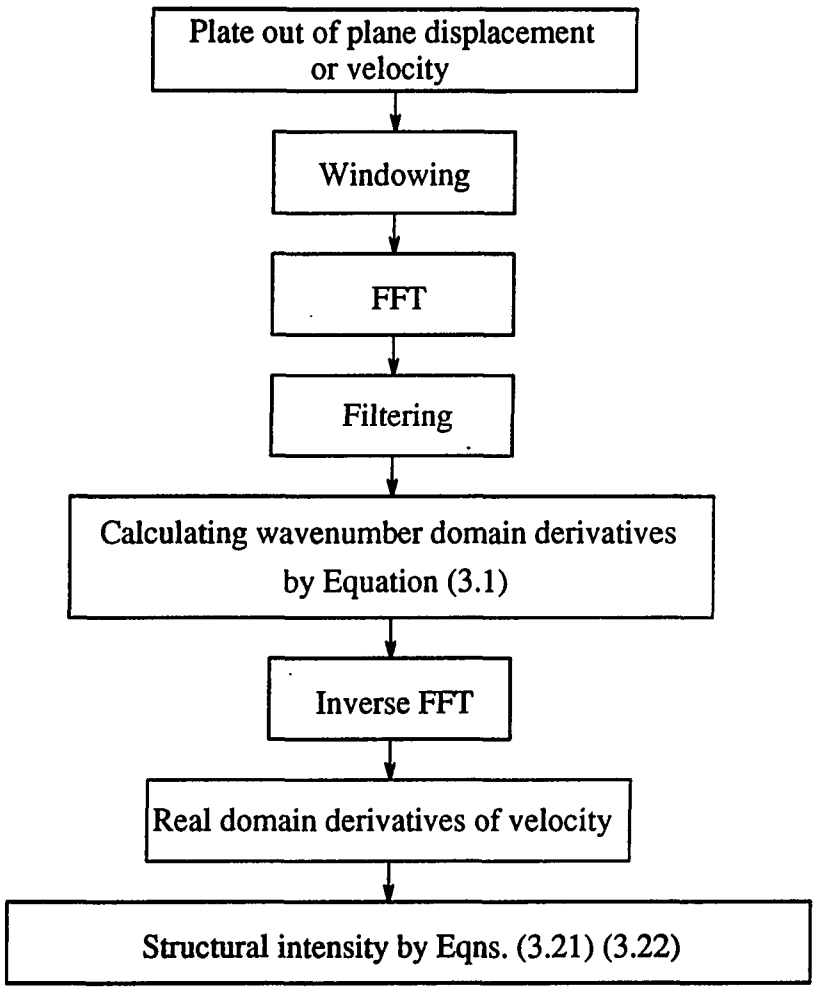

Figure 3.4: Procedure to calculate structural intensity from Pavić's formulation

(2.54) and(2.55) are rewritten as:

$$I_x = -\frac{h^3}{12} \cdot T_{x1} \cdot \frac{\partial w^*}{\partial x} - \frac{h^3}{12}\mu \cdot T_{x2} \cdot \frac{\partial w^*}{\partial y} + h\mu \cdot T_{x3} \cdot w^*, \tag{3.4}$$

$$I_y = -\frac{h^3}{12}\mu \cdot T_{y1} \cdot \frac{\partial w^*}{\partial x} - \frac{h^3}{12} \cdot T_{y2} \cdot \frac{\partial w^*}{\partial y} + h\mu \cdot T_{y3} \cdot w^*, \tag{3.5}$$

where:

$T_{x1} = (\lambda + 2\mu)\frac{\partial \psi_x}{\partial x} + \lambda \frac{\partial \psi_y}{\partial y}$,

$T_{x2} = \frac{\partial \psi_x}{\partial y} + \frac{\partial \psi_y}{\partial x}$,

$T_{x3} = \psi_x + \frac{\partial w}{\partial x}$,

$T_{y1} = \frac{\partial \psi_x}{\partial y} + \frac{\partial \psi_y}{\partial x}$,

$T_{y2} = \lambda \frac{\partial \psi_x}{\partial x} + (\lambda + 2\mu)\frac{\partial \psi_y}{\partial y}$,

$T_{y3} = \psi_y + \frac{\partial w}{\partial y}$,

* means the complex conjugate which is used to do time average.

The Fourier Transform of all the T's is used to transform them into wavenumber domain:

$$\bar{T}_{x1}(k_x, k_y) = (\lambda + 2\mu)(jk_x)\Psi_x + \lambda(jk_y)\Psi_y, \tag{3.6}$$

$$\bar{T}_{x2}(k_x, k_y) = (jk_y)\Psi_x + (jk_x)\Psi_y, \tag{3.7}$$

$$\bar{T}_{x3}(k_x, k_y) = \Psi_x + (jk_x)W, \tag{3.8}$$

$$\bar{T}_{y1}(k_x, k_y) = (jk_y)\Psi_x + (jk_x)\Psi_y, \tag{3.9}$$

$$\bar{T}_{y2}(k_x, k_y) = \lambda(jk_x)\Psi_x + (\lambda + 2\mu)(jk_y)\Psi_y, \tag{3.10}$$

$$\bar{T}_{y3}(k_x, k_y) = \Psi_y + (jk_y)W, \tag{3.11}$$

where:

$\Psi_x = \mathcal{F}\{\psi_x\}$,

$\Psi_y = \mathcal{F}\{\psi_y\}$,

$W = \mathcal{F}\{w\}$.

Now, all the $\bar{T}'s$ can be directly calculated from wavenumber domain displacement components Ψ_x, Ψ_y and W. The displacement in wavenumber domain, W, is obtained by taking the Fourier Transform of the out of plane displacement w, which is measured. The inplane displacement functions in wavenumber domain, Ψ_x and Ψ_y, are calculated from Mindlin's plate motion equation, which will be discussed in the next section.

Taking the inverse Fourier Transform of the $\bar{T}'s$, the real domain $T's$ can be obtained. The structural intensity can be, therefore, calculated by inserting the $T's$ back to Equations (3.4) and (3.5). Other derivative terms in Equations (3.4) and (3.5) are calculated according to Equation (3.1) as has been described in Pavić's formula.

For both the Pavić's and Romano's structural intensity formulas, the structural intensity is composed of three terms. These terms correspond to three wave types, bending, twisting and shearing. In calculating the structural intensity, these terms can be plotted separately to show contributions from different waves to the structural intensity.

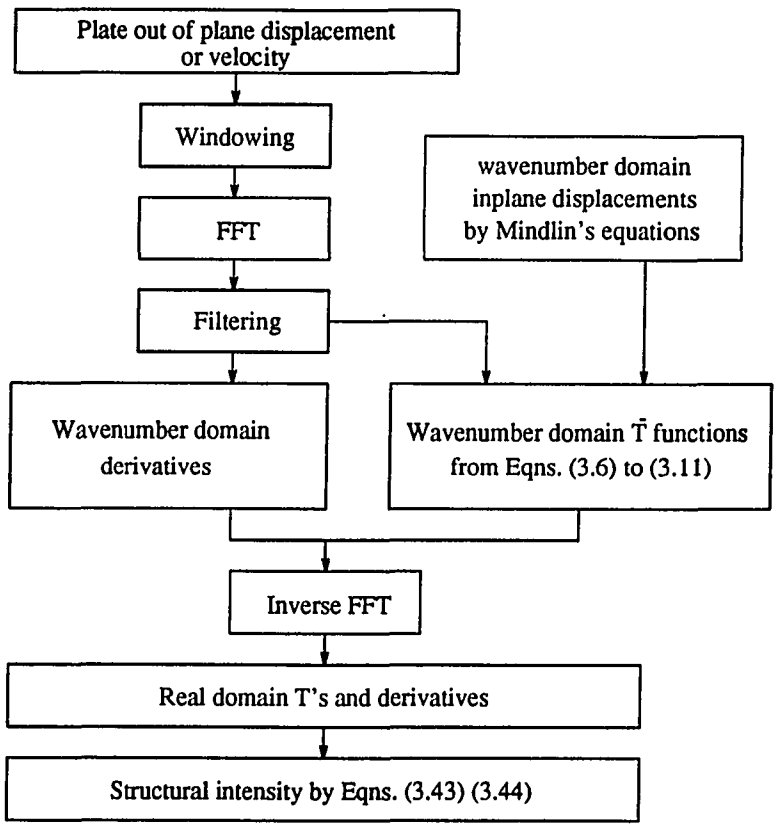

Figure 3.5: Procedure to calculate structural intensity from Romano's formulation

3.3 Calculation of the Force Distribution Function

From Mindlin's plate equations, Equations (2.72) to (2.74), the force distribution function, q is solved for by using Fourier Transforms. Taking a two dimensional spatial Fourier Transform of both sides of the three equations, transforms the three partial differential equations into three linear algebraic equations:

$$\alpha_1 \Psi_x + \beta_1 \Psi_y = j k_x \kappa^2 G h W, \tag{3.12}$$

$$\alpha_2 \Psi_x + \beta_2 \Psi_y = j k_y \kappa^2 G h W, \tag{3.13}$$

$$\begin{aligned} \kappa G h[(-k_x^2 - k_y^2)W + \Phi] + Q \\ = -\rho h \omega^2 W, \end{aligned} \tag{3.14}$$

where:

$\Psi_x = \mathcal{F}\{\psi_x\}$,

$\Psi_y = \mathcal{F}\{\psi_y\}$,

$\alpha_1 = \frac{D}{2}[-2k_x^2 - (1-\nu)k_y^2] - \kappa^2 G h + \frac{\rho h^3}{12}\omega^2$,

$\alpha_2 = -\frac{D}{2}(1+\nu)k_x k_y$,

$\beta_1 = \alpha_2$,

$\beta_2 = \frac{D}{2}[-(1-\nu)k_x^2 - 2k_y^2] - \kappa^2 G h + \frac{\rho h^3}{12}\omega^2$,

$W = \mathcal{F}\{w\}$,

$\Phi = \mathcal{F}\{\phi\}$,

$Q = \mathcal{F}\{q\}$.

When the measured plate displacement is known, its wavenumber domain function W can be calculated by using a two dimensional Fast Fourier Transform. The three unknowns of the above equations are Ψ_x, Ψ_y, and Q. Ψ_x and Ψ_y are the two inplane displacement components of the plate in the wavenumber domain, while Q is the force distribution function in the wavenumber domain. The two inplane displacement components can be solved for by using Equations (3.5) and (3.6) analytically:

$$\Psi_x = j\kappa^2 GhW \frac{k_x\beta_2 - k_y\beta_1}{\alpha_1\beta_2 - \alpha_2\beta_1}, \tag{3.15}$$

$$\Psi_y = j\kappa^2 GhW \frac{-k_x\alpha_2 + k_y\alpha_1}{\alpha_1\beta_2 - \alpha_2\beta_1}. \tag{3.16}$$

These two wavenumber domain inplane displacement components are used in calculating the wavenumber domain structural intensity components, $\bar{T}'s$ in Equations (3.6) to (3.11), for Romano's formula, Equations (2.54) and (2.55). The wavenumber domain structural intensity components are then transformed back to real domain by an inverse Fourier Transform to get the structural intensity in the real domain as shown in Figure 3.2.

The force distribution function is solved for directly from Equation (3.15). Taking inverse Fourier Transform of Equation (3.15) gives:

$$q = \mathcal{F}^{-1}\{-\rho h\omega^2 W - \kappa^2 Gh[(-k_x^2 - k_y^2)W + \Phi]\}. \tag{3.17}$$

The inverse Fourier Transform is performed by using the Fast Fourier Transform algorithm.

The procedure of calculating the force function is shown in Figure 3.6.

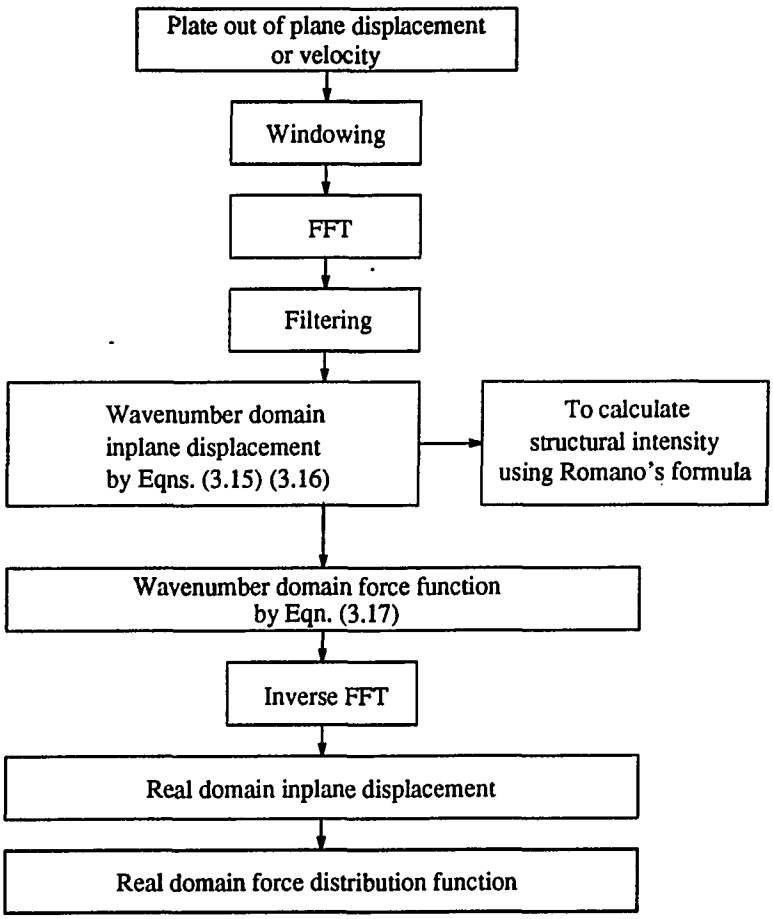

Figure 3.6: Procedure to calculate force distribution function

3.4 Calculation of Force Magnitude and Input Power

3.4.1 Force magnitude

The force distribution function q is the force density that is exerted on the plate surface. To determine the magnitude of the input force, this force density should be multiplied by an area $\triangle A$ that the force is acting on:

$$\mid F \mid = q \mid_{\triangle A} \cdot \triangle A, \tag{3.18}$$

where $\mid F \mid$ is the force magnitude. $q \mid_{\triangle A}$ is the value of q at the area $\triangle A$.

For a point force, the magnitude of the force should be:

$$\mid F \mid = \lim_{\triangle A \to 0} q \mid_{\triangle A} \cdot \triangle A, \tag{3.19}$$

meaning the force is in an infinitesimal area and the force distribution function has a infinite value at the point of the applied force so as to have a finite force magnitude $\mid F \mid$. In practical calculations, the force distribution function is not infinite, nor is the area to which the force is applied infinitesimal. Thus, Equation (3.18) can be used as an approximation to Equation (3.19), provided that $\triangle A$ be sufficiently small and $q \mid_{\triangle A}$ sufficiently large.

3.4.2 Input power

The input power to the plate can be calculated from both the structural intensity and the power function. From the power function (Equation (2.75)), which is the input power density on the plate surface, the input power can be calculated in the same way as the force magnitude is calculated:

$$| P | = p |_{\triangle A} \cdot \triangle A, \tag{3.20}$$

where $| P |$ is the input power. The quantity $p |_{\triangle A}$ is the value of p at the area $\triangle A$.

Similarly for a point force, the injected power to the plate is:

$$| P | = \lim_{\triangle A \to 0} p |_{\triangle A} \cdot \triangle A, \tag{3.21}$$

For practical calculations, Equation (3.20) can be used as an approximation to Equation (3.21).

From the structural intensity, the input power can also be estimated. Since the structural intensity for plates represents the energy flow through the thickness of the plate cross section, the following integration is the power that a point source has injected to the plate:

$$| P | = \lim_{\epsilon \to 0} \oint_s \vec{I} \cdot \vec{n} ds, \tag{3.22}$$

where the integration is performed over a circle s with a radius of ϵ which encloses the source. The vector $\vec{n}$ is the unit outer normal of the circle (see Figure 3.7 (a)).

In practical cases, the integration is approximated by a summation:

$$| P | \cong \sum_{i=1}^{m} (\vec{I}_i \cdot \vec{n}_i) \triangle s_i, \tag{3.23}$$

where the circle is divided into m segments. In the ith segment, the value of the structural intensity is projected to the normal of the circle and multiplied by the length of the segment $\triangle s_i$ (see Figure 3.7 (b)).

In this research, the calculation is performed over a rectangular grid. So the calculation of the input power using the structural intensity is along the periphery of a rectangular area (see Figure 3.7 (c)).

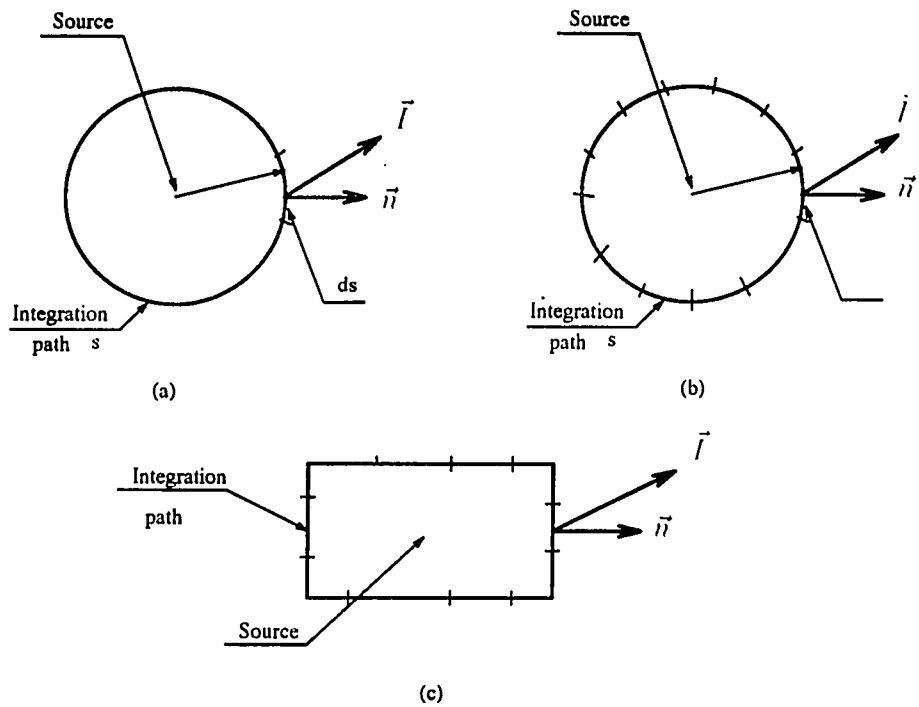

Figure 3.7: Three different ways of integrating input power using the structural intensity, (a). accurate integration, (b). approximate integration over a circular path, (c). approximate integration over a rectangular path

CHAPTER 4. MEASUREMENT

In this chapter, the measurement systems are described. Some measurement results will be shown. In the results, we can see that due to inefficient reflection of the laser beam at some points on the surface of the plate, there are some measurement errors that show up as dips in the measured velocity. A B-spline algorithm is developed to eliminate the dips, creating a smooth velocity distribution.

4.1 Measurement Systems and Procedure

As has been mentioned in the literature review, there are different measurement methodologies used to obtain the surface velocity or displacement of vibrating structures in order to calculate the structural intensity and the force distribution function.

In the investigation of this thesis, a laser Doppler vibrometer is used for the measurement of velocity. The measurement process is controlled by a MassComp computer which also performs the data acquisition. An electrical signal is generated and directed to the electromagnetic shaker to drive the plate. A computer controlled scanner moves the laser head (lens system) over a rectangular grid. The signal from the laser vibrometer is then sent to the multi-channel data acquisition system, and analyzed by the computer. Figure 4.1 shows a block diagram of the measurement system.

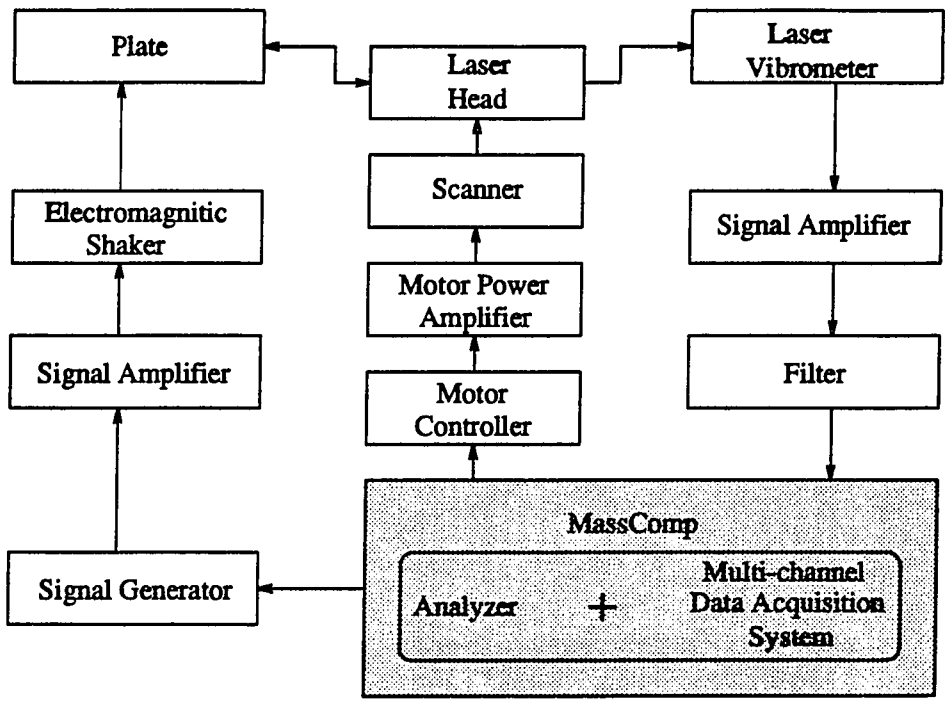

Figure 4.1: Computerized data acquisition system

Here, the MassComp computer and the computer controlled scanner will not be described in detail. The laser Doppler vibrometer, the measurement setup, the data acquisition programs and the measurement procedures will be described in detail in this section.

4.1.1 Laser Doppler vibrometer

The laser Doppler vibrometer used in this investigation is a Polytec OFV 1102HR fiber optical vibrometer. Figure 4.2 is a schematic of the interferometer in the Polytech system [29]. The laser beam is first split into two beams by the beamsplitter 1 (BS1). One route of the laser beam goes through the beamsplitter 2 (BS2) and is targeted on the surface being measured (Object 1) by the measurement lens. The reflected laser beam from the surface is sent back to the beamsplitter 2 (BS2) through the same lens system. The lens system contains a quarter wave retardation plate (QWP) which rotates the polarization of the measurement beam by 90 degrees. The beam is then reflected into the final beamsplitter (BS3) where it will be optically combined with the reference beam.

The reference beam that was originally split at BS1 is directed to the beamsplitter 4 (BS4), through which, the beam is sent to the reference lens system and targeted at Object 2. The reflected beam from Object 2 is then sent back to the BS4 where it is reflected to a Bragg Cell. The Bragg Cell is to frequency modulate the beam at a preset carrier frequency (RF in). Finally, the reference beam is combined with the measurement beam in BS3.

The laser beams from the measurement and reference lenses are then directed to photodetectors (D1) and (D2), respectively. Then, a differential pre-amp circuit is

used to cancel the phase shift introduced by the beamsplitters and to remove the DC offset present in the detectors' signals. The resulting signal represents the velocity of the measurement object.

The two lens systems in the Polytec fiber optic vibrometer gives the possibility that the difference between the velocities at two different measuring points can be measured directly by targeting the two laser beams at the two points. Also, this feature of the vibrometer can be used to eliminate any other vibratory signals from the measurement by placing the reference beam at a location containing the unwanted characteristics. In essence, the measured velocity signal will be referenced to the noise source, thus subtracting out the noise.

In the measurement for this investigation, only one laser beam is needed. Thus, a stationary reference head is attached to the reference arm so that no velocity is seen by the reference beam.

It is crucial in the velocity measurements using the laser Doppler vibrometer that there is enough reflection of the laser beam from the plate surface. To check the reflection of the plate surface, one should check the LED bar in the front panel of the Polytec laser vibrometer. There are three areas in the LED bar colored red, orange and green from the bottom to the top. The green part of the LED bar should be lit indicating there is enough reflection.

The coherence function is also a good parameter that can be used to check if the reflection is good enough for accurate measurement. When there is not enough reflection, the coherence between the laser signal and a reference force signal from the force transducer is low. Figures 4.3 and 4.4 show two coherence functions at two different points of a plate with absorptive boundaries and point excitation(details of

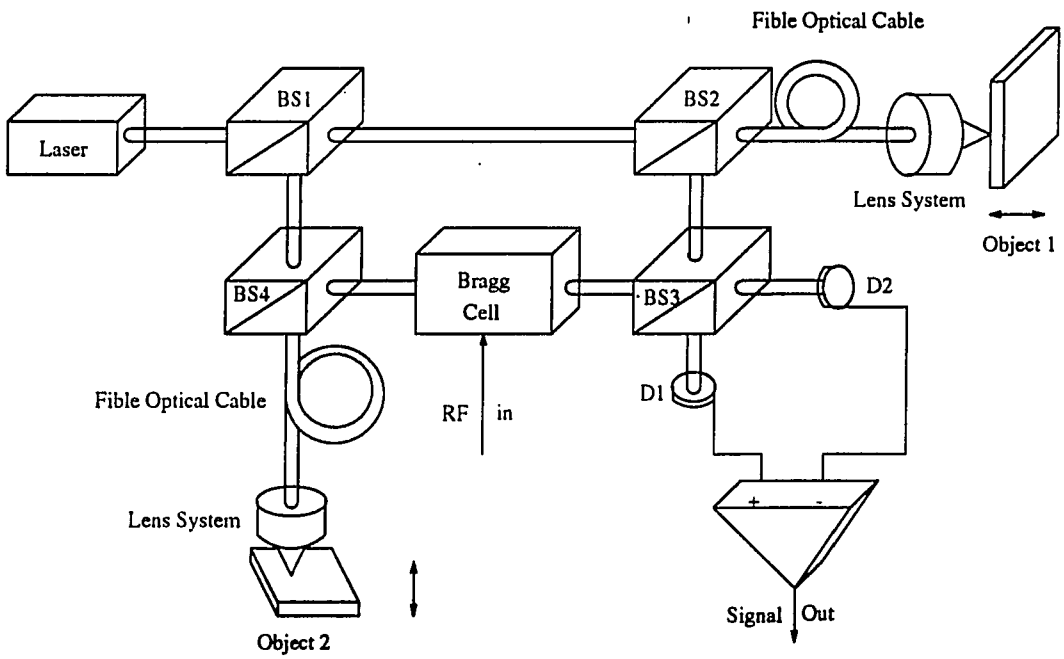

Figure 4.2: Schematic of the interferometer in the Polytec fiber optic vibrometer

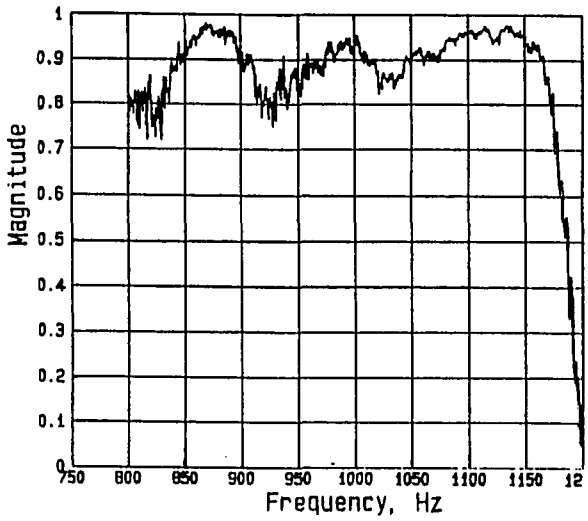

Figure 4.3: Coherence function measured on a plate with absorptive boundaries with a point excitation, at point (1, 1)

the plate will be described in the section describing the structures under test). The point corresponding to the Figure 4.3 does not have enough reflection. According to the author's experience, a coherence that is less than 0.9 indicates insufficient reflection.

4.1.2 Measurement set up

As shown in the block diagram of the measurement systems, Figure 4.1, the plate with certain boundary conditions is to be driven by an electromagnetic shaker at a given point. The shaker used in the research for this thesis is a Brüel & Kjær Vibration Exciter (Type 4809). The actual set up of the plate is shown in Figure 4.5. A signal from a signal generator excites the shaker. Between the shaker and the plate, there is a PCB force transducer that senses the input force to the plate. The

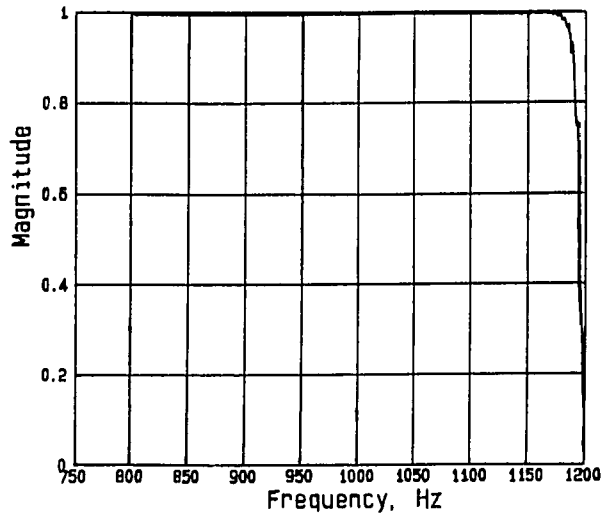

Figure 4.4: Coherence function measured on a plate with absorptive boundaries with a point excitation, at point (16, 15)

input force to the plate is then sent to one of the channels of the multi-channel data acquisition system as a reference signal.

At the same time, as the plate is vibrating under the shaker's excitation, the laser vibrometer's measurement lens system takes the surface velocity and sends this signal to another channel of the data acquisition system. The laser vibrometer's measurement lens system is carried by the computer controlled scanner.

4.1.3 Software for measurement

There are several programs on the MassComp computer developed over the last few years for use in the ISU Acoustics Lab for the different measurement and data acquisition purposes.

The program *intrun* was originally developed for acoustic intensity measure-

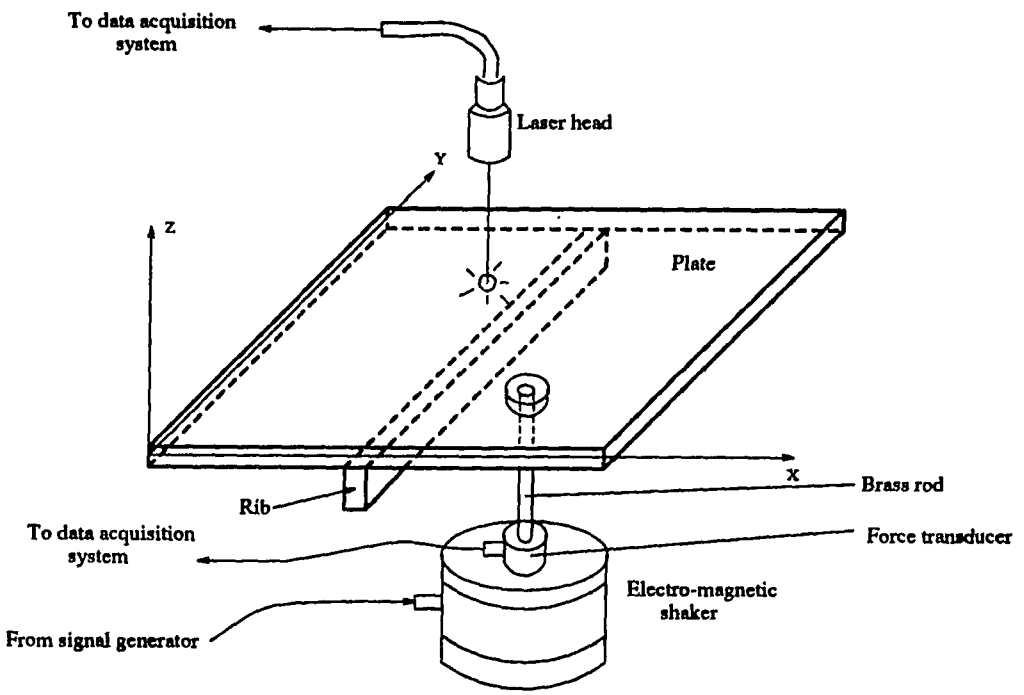

Figure 4.5: Plate set up

ments. It can also be used to make velocity measurements by inputting the velocity and force signals. When using this program, the signal to drive the shaker, and therefore the plate, needs to be generated by a separate signal generator, and can be either single frequency or broadband noise.

The program *rimpulsef* was also used in this investigation. It is similar to *intrun* except that *rimpulsef* generates a chirp signal that is directed to the shaker to excite the plate.

A chirp signal is a sine wave whose frequency sweeps over a specified frequency range during a certain amount of time, while at a given time, it only has one frequency component. A time signal and the frequency spectrum of a chirp is shown in Figure 4.6 and Figure 4.7, respectively. The chirp sweeps from 800 Hz to 1200 Hz in 0.25 seconds. The advantage of a chirp signal over a broadband noise is that it has more energy concentrated at a single frequency. There is not enough time at any one frequency for a vibration mode to dominate. Thus off resonance data is improved when compared to a white noise excitation. Broadband measurements were much improved by using a chirp rather than band limited white noise.

4.1.4 Measurement procedure

To use the Polytec laser vibrometer for measuring the surface velocity, the plate surface should first be painted with a retro-reflective material. The metal surfaces used in this research do not reflect a sufficient amount of the laser beam. There is also commercially available retro-reflective tape which reflect the laser beam better than the paint; however, the tape is much more expensive than the paint and requires much more effort to cover an entire plate.

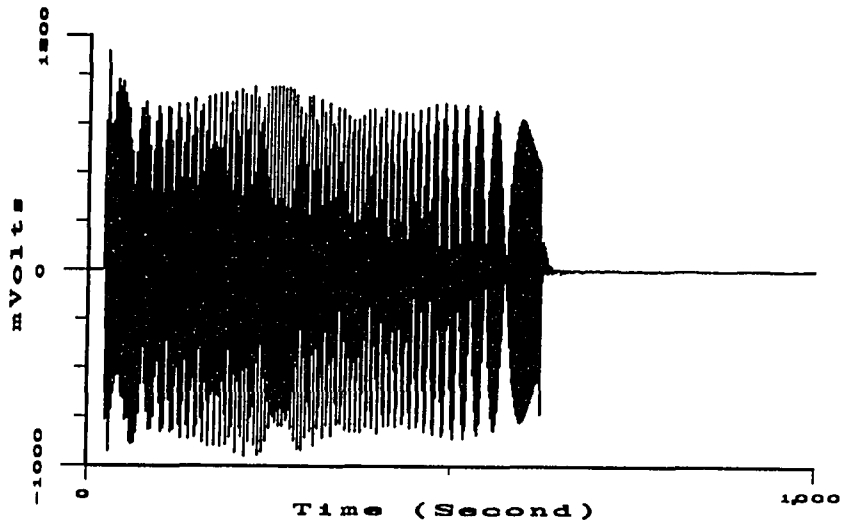

Figure 4.6: Time domain 800 to 1200 Hz chirp signal

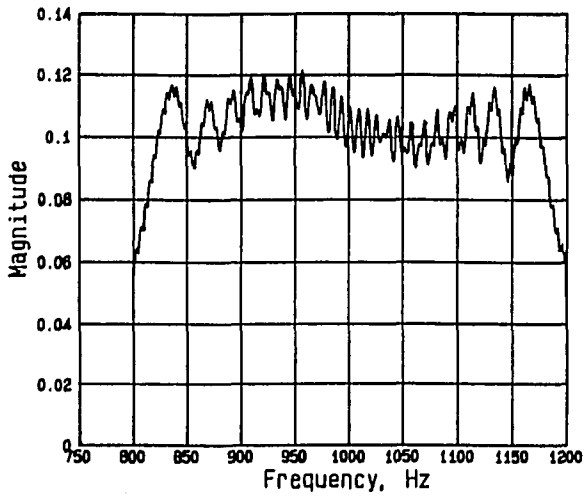

Figure 4.7: Frequency spectrum of the 800 to 1200 Hz chirp signal in Figure 4.6

The procedures to perform a measurement are:

1. Adjust the focus, the distance, and angle of the laser head to the plate to ensure that there is good reflection of the laser beam from the plate surface.

2. Turn on the signal generator to excite the plate through the electromagnetic shaker. If the chirp signal is to be used, then the signal comes out of the MassComp computer when the measurement program is run.

3. Adjust the output power of the signal generator to have enough power to excite the plate.

4. Check and adjust the signal amplifier to make sure that the measured signals have proper amplitudes to enter the data acquisition system.

5. Run the appropriate program to perform the measurement.

4.2 Procedure to Smooth Data

The measured plate velocity is usually not smooth enough due to the bad reflectivity of the plate surface at certain points. Figure 4.8 shows the velocity of a plate with absorptive boundaries at 201 Hz (details of the plate will be described in the next section). There are some dips in the velocity profile that could not be eliminated by repainting the plate surface. So, a B-spline algorithm was developed to eliminate the discontinuity. Since the velocity is complex, the procedure of smoothing the data is performed to the real and imaginary parts of the velocity.

The basic idea of the smoothing procedure is to use the velocity value at *good* points to estimate those at the *bad* points and replace the *bad* points with estimated *good* values. In order to do so, one must first locate the *bad* points. In the procedure of this research, I visually decide which points are *bad* and determine their grid

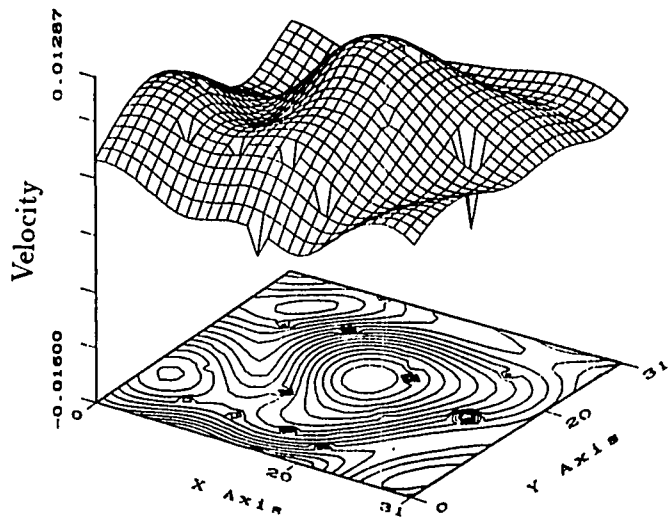

Figure 4.8: Velocity of plate with absorptive boundaries excited by a point force at the center of the plate, frequency f=201 Hz, before smoothing

coordinates. For example, in Figure 4.8, the dip that is closest to the lower left corner of the velocity patch has grid coordinates (7, 6) which means it is located in the velocity matrix in the seventh column and sixth row.

After locating the *bad* points, the entire data set is to be split into two sets, data set I and data set II as shown in Figure 4.9 for a one-dimensional case. The value of the *bad* points in the data set I can be evaluated by the data set II and vice versa. The data is split in such a way that every other point is in the same data set. In a two-dimensional case, the same idea is used in either the x or y directions. Figure 4.10 shows the way to split the data in a two-dimensional case. This algorithm, due to the fact that it splits the data into two sets, is called the *two-patch* method. This method works better for those dips at a single point. If there are a few consecutive *bad* points, the following *one-patch* method works better.

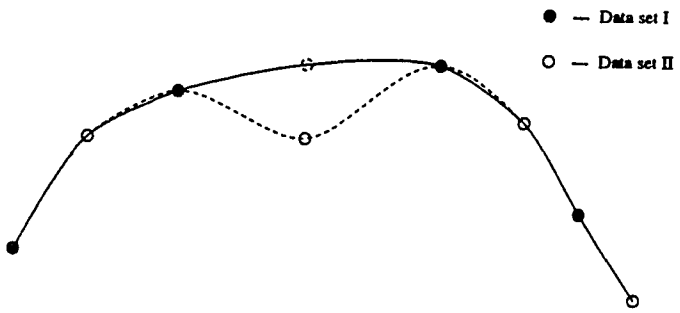

Figure 4.9: The sketch of the method to smooth data

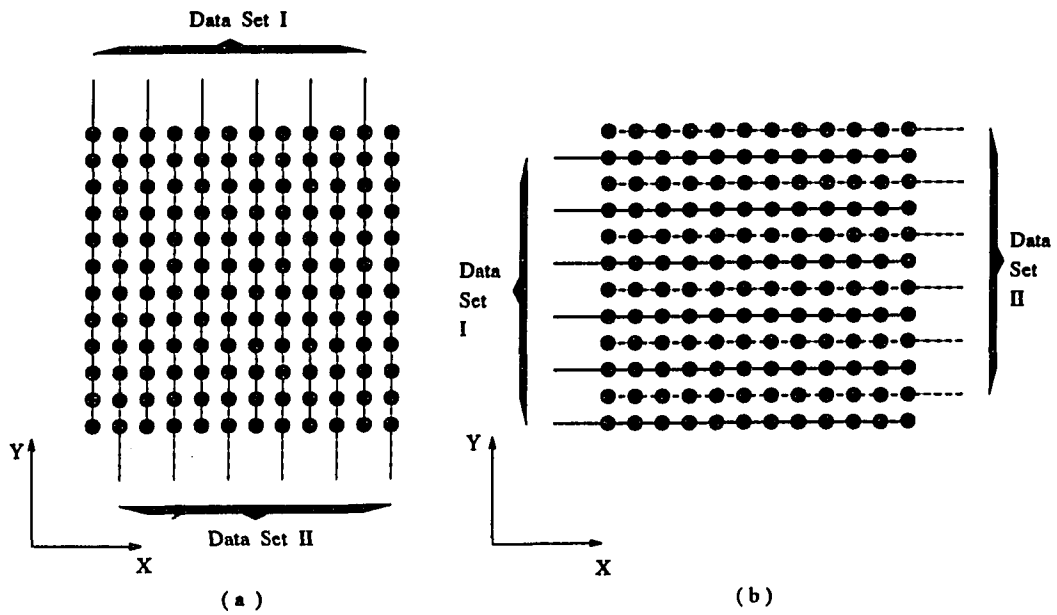

Figure 4.10: The sketch of the *two-patch* method to split data in the two-dimensional case

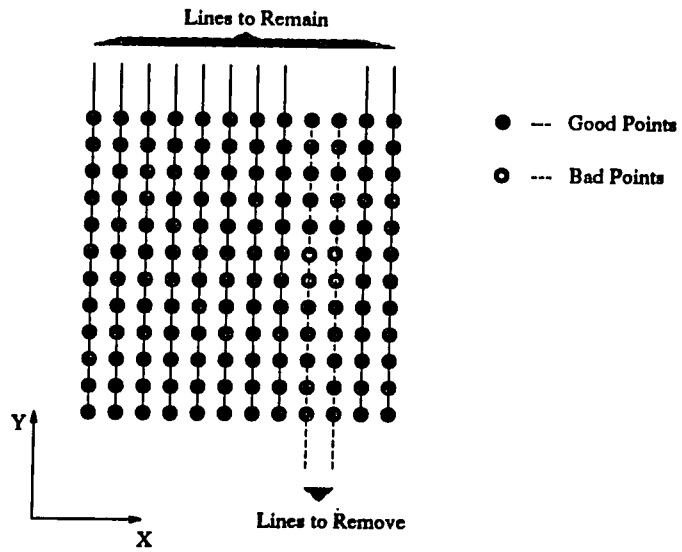

Figure 4.11: The sketch of the *one-patch* method to split data in the two-dimensional case

The *one-patch* method keeps the data as one set, but eliminates those lines of data that contain *bad* points. New values at those *bad* points are evaluated by the remaining data. Figure 4.11 shows a sketch of the *one-patch* method.

B-spline method is used to create data at the *bad* points. In this research, subroutines in the NAG mathematical library were called to perform the B-spline calculation. Figure 4.12 is a block diagram of the smoothing program.

The smoothing program requires the user to input the number of *bad* points, the grid coordinates of the *bad* points and choose either the *one-patch* or the *two-patch* method. Also, a control variable that defines the accuracy of the B-spline is need. The program will split the data according to the user's choice, evaluate the value at the *bad* points, and put the evaluated data back to where they should be.

The velocity for the plate with absorptive boundaries at 201 Hz before smoothing

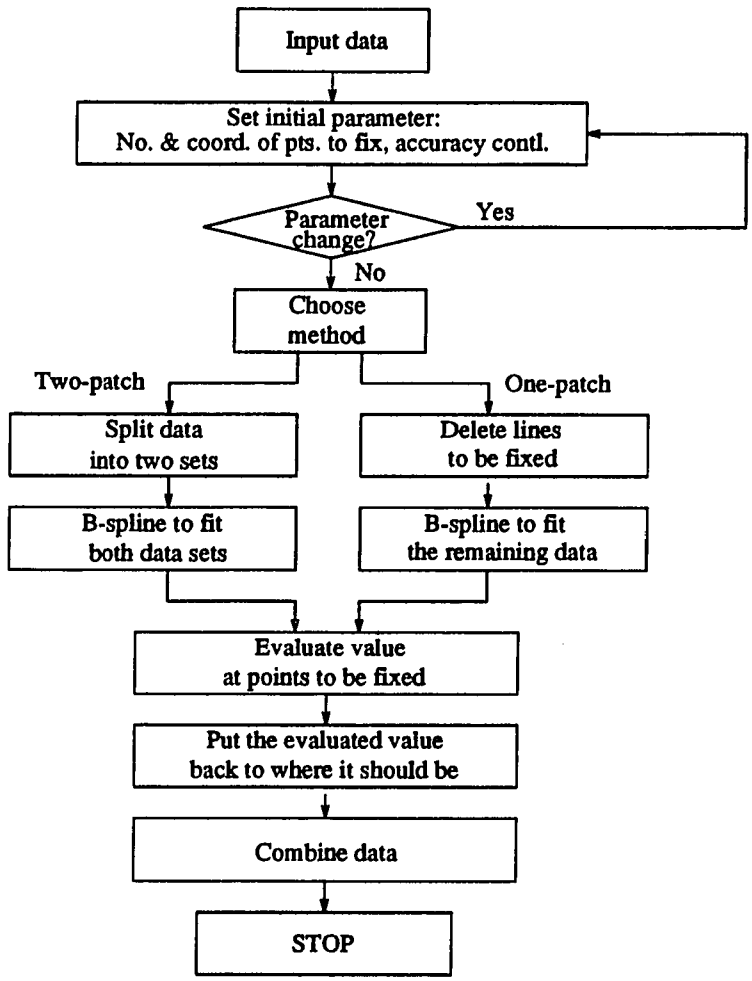

Figure 4.12: Block diagram of the smoothing program

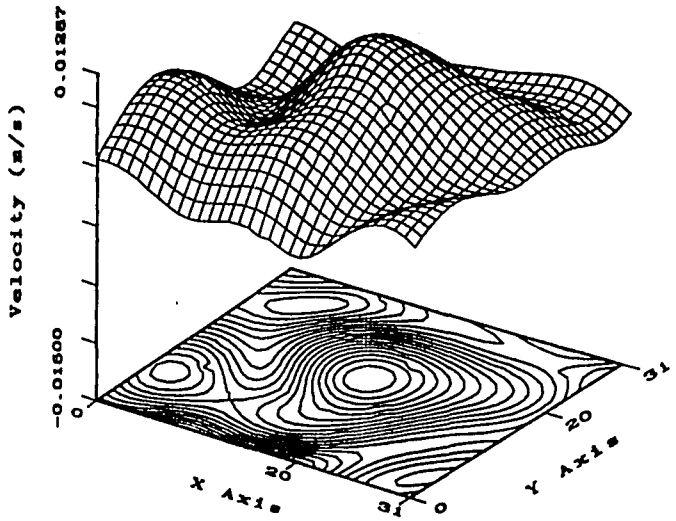

Figure 4.13: Velocity of a plate with absorptive boundaries excited by a point force at the center of the plate, frequency f=201 Hz, after smoothing

is shown in Figure 4.8. The smooth result is shown in Figure 4.13. Those individual dips were fixed by the *two-patch* method, while the dip with four points on the right side of the plate was fixed by the *one-patch* method. Comparing Figures 4.8 and 4.13, it is shown that the smoothing procedure is very effective.

The necessity of the smoothing procedure is shown in Figure 4.14 to Figure 4.17. Figures 4.14 and 4.16 show the results before the data was smoothed while Figures 4.15 and 4.17 show those after the data was smoothed. Figures 4.14 and 4.15 are the force distribution function and Figures 4.16 and 4.17 are the structural intensity. These quantities were calculated from the velocity of the plate with absorptive boundaries which is shown in Figure 4.8 (before smoothing) and Figure 4.13 (after smoothing). Without smoothing, both the force distribution function and structural intensity are noisy and the source location can not be determined, even when win-

dowing in the real space and filtering in the wavenumber domain were both applied in the calculation (the influence of windowing and filtering will be discussed in the next chapter). After smoothing, the results are less noisy and the source location is clear in both the structural intensity and force distribution function.

4.3 Description of the Structures Under Test

In this study, measurements were performed on four different plates with different boundaries and configurations as shown in Figure 4.18 (a), (b), (c) and (d). All four plates were made of aluminum and had a thickness of 0.003175 meters.

The plate in Figure 4.18 (a) is supported by velcro strips around the boundaries to simulate a free plate. The plate was 0.71 by 0.6 meters in dimension. The velocity measurement was made over the whole area of the plate. The excitation force was located at the point 0.56 meters from the left edge and 0.16 meters from the bottom edge. At 84 Hz, which theoretically corresponds to the (2, 1) mode, the measured velocity is shown in Figure 4.19. In this measurement, the excitation signal is a single frequency sine wave. The measurement clearly shows the modes.

For the plate in Figure 4.18 (b), sand bags were used to support the boundaries with the intent to absorb energy at the boundaries, simulating an infinite plate. A rib, which is the same material and thickness as the plate, is located at the center of the plate along the x axis. The rib is attached perpendicular to the plate as shown in Figure 4.5. The plate dimension was 1.2 by 1.2 meters and the measurement was over a patch 0.31 by 0.31 meters. The velocity at 292 Hz is shown in Figure 4.20. The excitation was also a single frequency sine wave. From the measurement, it is clear that the rib acts as a restraint that obstructs the vibration from being transferred

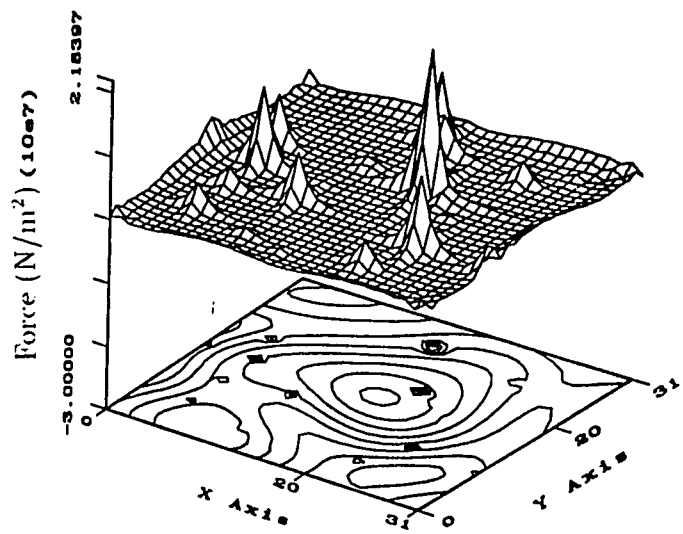

Figure 4.14: Force distribution function of a plate with absorptive boundaries, velocity not smoothed as in Figure 4.8, f=201 Hz

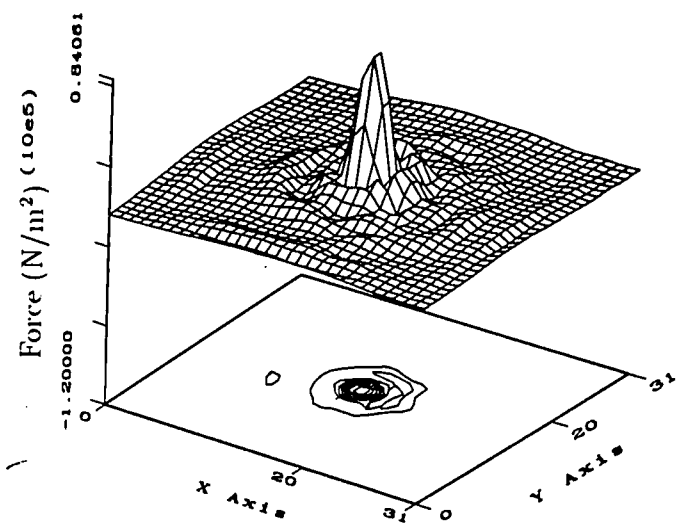

Figure 4.15: Force distribution function of plate with absorptive boundaries, velocity smoothed as in Figure 4.13, f=201 Hz

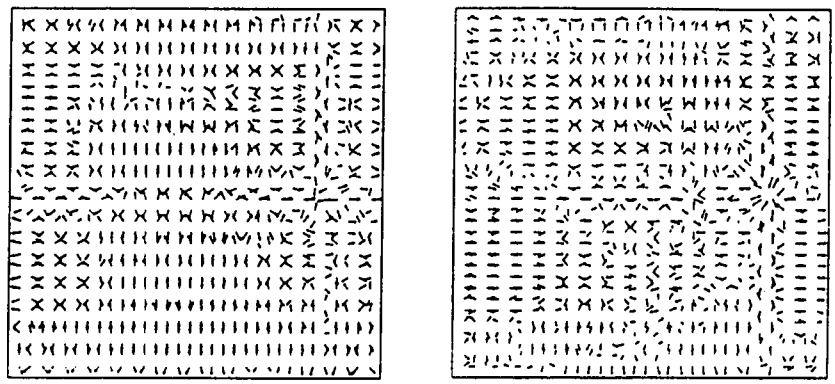

Figure 4.16: Structural intensity of a plate with absorptive boundaries, velocity not smoothed, f=201 Hz, (left. active intensity, right. reactive intensity)

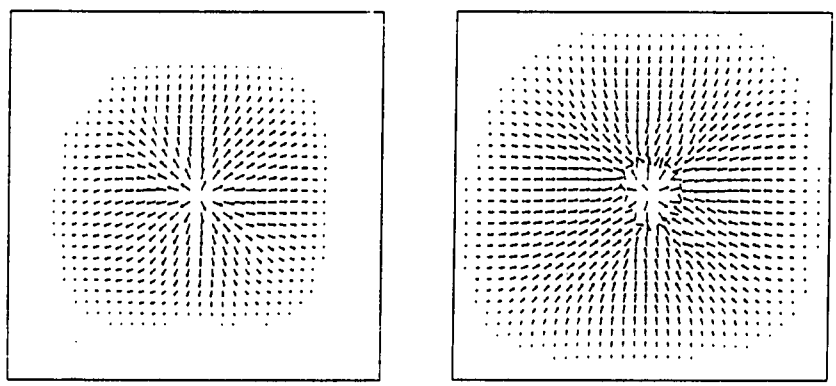

Figure 4.17: Structural intensity of a plate with absorptive boundaries, velocity smoothed, f=201 Hz, (left. active intensity, right. reactive intensity)

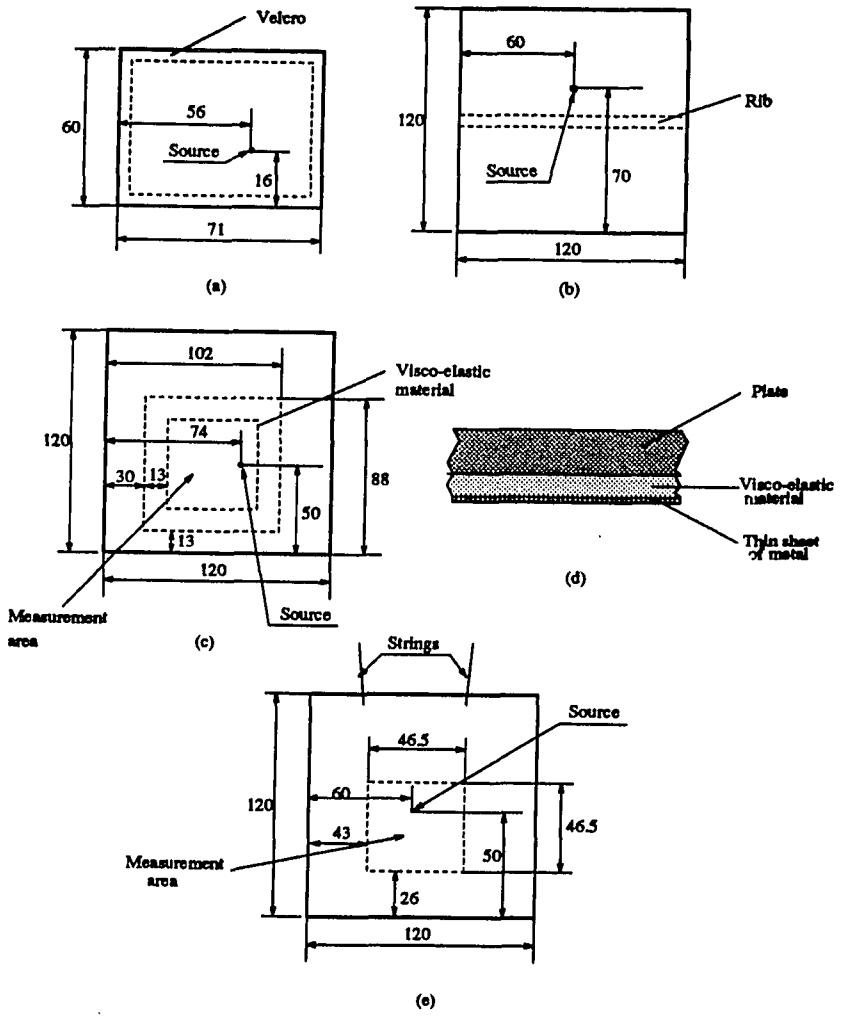

Figure 4.18: Three plates used in the measurement and simulations. (a). Simply supported plate. (b). Infinite plate with a rib. (c). Infinite plate with visco-elastic damping. (d). Visco-elastic material attached to plate. (e). Plate hung by strings

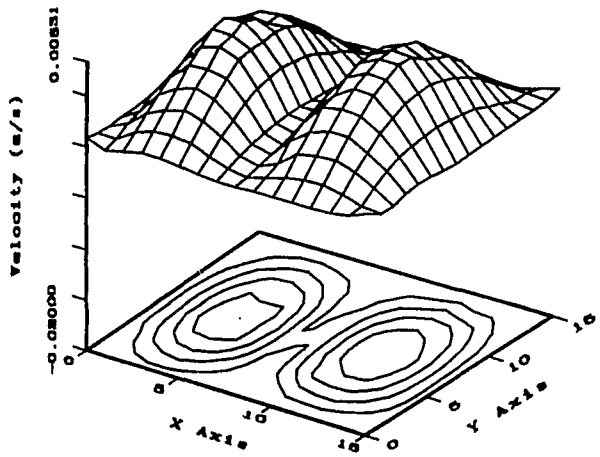

Figure 4.19: Measured velocity of the velcro supported plate at 84 Hz

past the rib. More details on the effect of the ribs will be discussed in Chapter 6, when the structural intensity and force function results are shown.

For a homogeneous plate shown in Figure 4.18 (c), a band of visco-elastic material was placed around the measurement area in order to better damp the vibrating energy so as to better simulate an infinite plate. The visco-elastic material was attached to the plate in the way shown in Figure 4.18 (d). The damping material is 3M's Scotchdamp^{TM} visco-elastic material. It is a double sided sticky material. The damping material was stuck to the plate. On the other side of the damping material, a layer of thin aluminum sheet (0.00127 meters in thickness in this case) was added. When the plate vibrates, the thin layer of metal tends to constrain the stretch of the surface of the plate through the visco-elastic material by producing a shear stress in the damping layer. The damping material damps out some of this shear energy.

The plate dimension was the same as the ribbed plate. The measured area is as

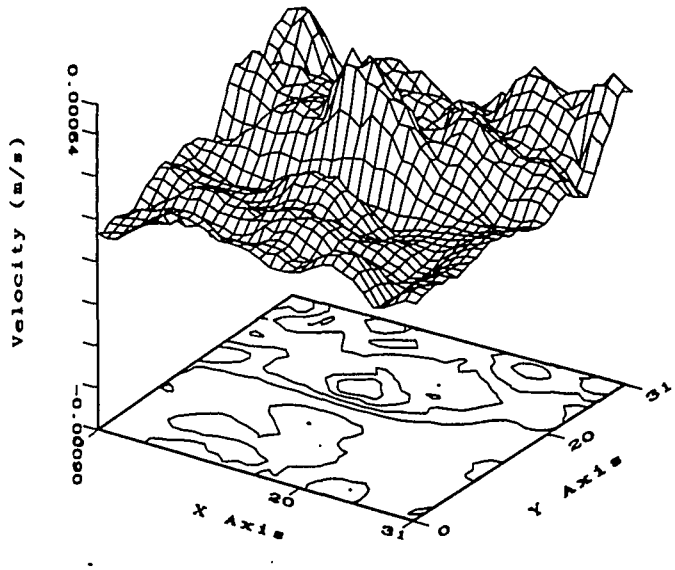

Figure 4.20: Measured velocity of the sand bag supported plate at 292 Hz

shown in Figure 4.18 (c). A chirp signal ranging from 800 Hz to 1200 Hz was used to excite the plate at the location shown in Figure 4.18 (c). The frequency response function of the plate is shown in Figure 4.21. The velocity measured at 1000 Hz is shown in Figure 4.22.

The plate in Figure 4.18 (e) is hung by two strings. It is intended to simulate very reverberant conditions. The purpose of this plate is to locate the damping on the plate using the structural intensity. The damping material and the way it is attached to the plate are as shown in Figure 4.18 (d).

More velocity measurement results will be shown in Chapter 6 together with the resulting structural intensity and the force distribution function that are calculated from the measured velocity.

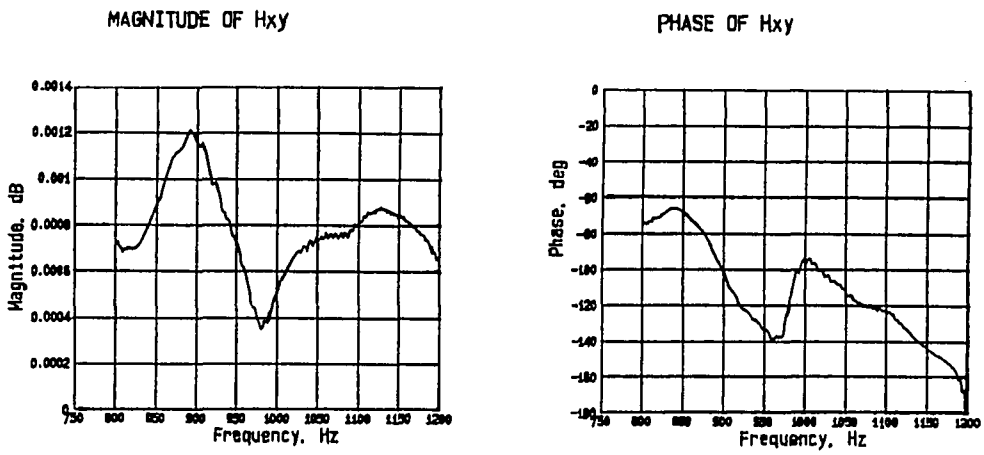

Figure 4.21: Frequency response function of the sand bag supported plate with visco-elastic damping around the measured area, force at the point 0.2 m away from the center

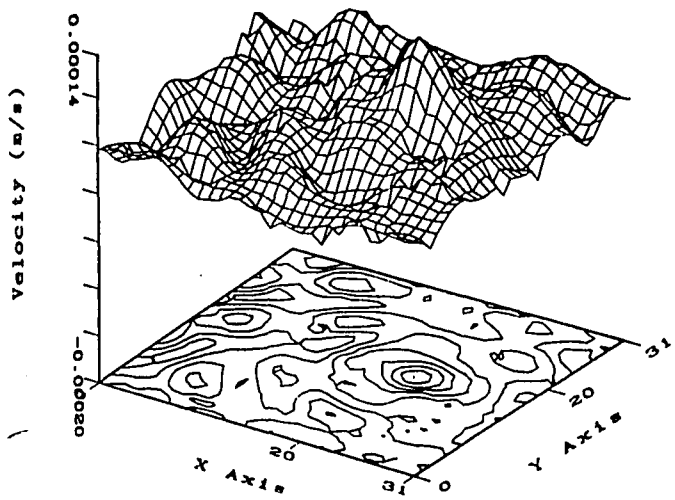

Figure 4.22: Measured velocity of sand bag supported plate with visco-elastic damping around the measured area, force at the point 0.2 m away from the plate center, frequency f=1000 Hz

CHAPTER 5. WINDOWING AND FILTERING

In the process of calculating the structural intensity and the force distribution function according the calculation described in Chapter 2 and 3, the Fast Fourier Transform (FFT) method is to be used in taking the spatial derivatives of the plate surface velocity. In this process, certain signal processing techniques are required to achieve reasonable results. Although spatial data is being processed, techniques originally developed for processing time domain signals are used. In this study, these techniques include windowing in the spatial domain and filtering in the wavenumber domain. Windowing is used to make the measured surface velocity smoothly decay to zero at the measurement edges. Filtering is used to remove noise in the wavenumber domain that gets amplified by the processing techniques.

This chapter is a discussion of the necessity of windowing and filtering and the influences of windowing and filtering on the calculation of the structural intensity and the force distribution function. It is shown that windowing and filtering are useful tools, but one must be aware of their limitations. These techniques are not based on plate theories. They are used in this research to overcome numerical difficulties in the calculations.

5.1 Windowing and Filtering

Mathematically, windowing and filtering involve multiplying the original data (or function, for example F_{before}) by a weighting function W to get a new function, for example F_{after}:

$$F_{after} = F_{before} * W, \tag{5.1}$$

In the calculation of the structural intensity and the force distribution function, the FFT is performed on the velocity, which is a two-dimensional function of spatial variables x and y. So the window and filter functions are also two-dimensional.

The following are some of the window and filter functions [30] that were used in this investigation:

1. Hanning window:

$$w(x,y) = \begin{cases} \frac{1}{4}(1 - cos(\frac{2\pi x}{L_x}))(1 - cos(\frac{2\pi y}{L_y})) & 0 \le x \le L_x, \quad 0 \le y \le L_y \\ 0 & \text{otherwise} \end{cases}, \tag{5.2}$$

This is the most used window type in this study. It is a cosine function in both the x and y directions. At $x = 0, L_x$ and $y = 0, L_y$, $w(x,y) = 0$. And at $x = \frac{1}{2}L_x, y = \frac{1}{2}L_y$, the window function $w(x,y) = 1$. A plot of the Hanning window function is shown in Figure 5.1.

2. Hamming window:

$$w(x,y) = \begin{cases} (0.54 - 0.46cos(\frac{2\pi x}{L_x})) \\ (0.54 - 0.46cos(\frac{2\pi y}{L_y})) & 0 \le x \le L_x, \quad 0 \le y \le L_y \\ 0 & \text{otherwise} \end{cases}, \tag{5.3}$$

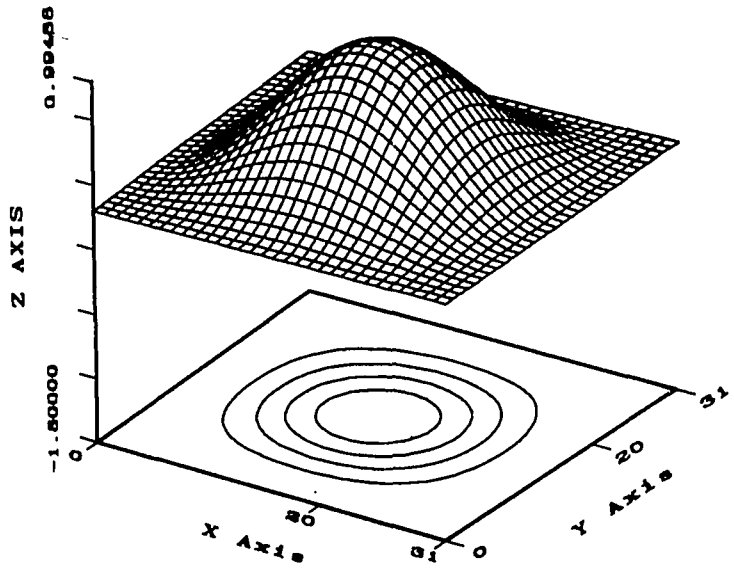

Figure 5.1: Hanning window function

Comparing the formula of the Hamming window with that of the Hanning window, we find that they are basically the same except that they have different coefficient in front of the cosine functions of the spatial variables x and y. From the plot of the Hamming window in Figure 5.2, we see that the Hamming window is wider than the Hanning window, and at $x = 0, L_x, y = 0, L_y$, the Hamming window does not go to zero.

3. Kaiser-Bessel window:

$$w(x,y) = \begin{cases} (1 - 1.24cos(\frac{2\pi x}{L_x}) + 0.244cos(\frac{4\pi x}{L_x}) \cdot \\ -0.00305cos(\frac{6\pi x}{L_x}))(1 - 1.24cos(\frac{2\pi y}{L_y}) \\ +0.244cos(\frac{4\pi y}{L_y}) - 0.00305cos(\frac{6\pi y}{L_y})) & 0 \le x \le L_x, \quad 0 \le y \le L_y \\ 0 & \text{otherwise} \end{cases} , \tag{5.4}$$

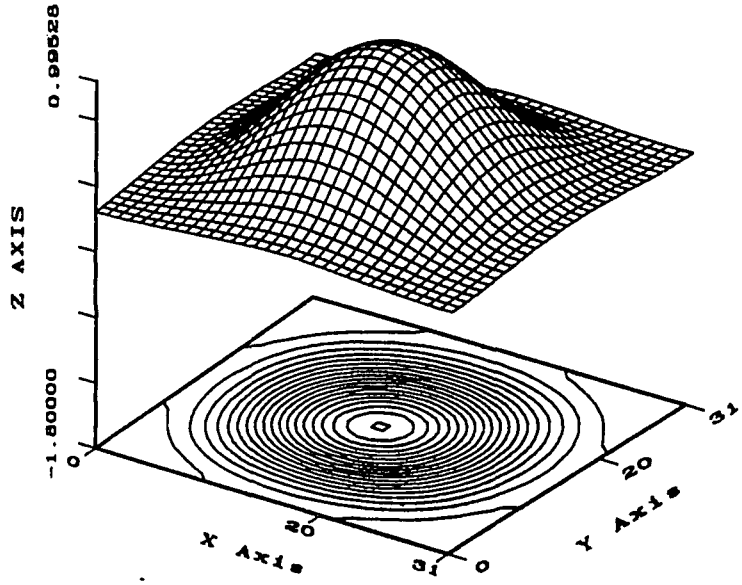

Figure 5.2: Hamming window function

The Kaiser-Bessel function also has maximum value (which is 1) at the center of the defined area and zeros on the boundaries of the same area, i.e., $w(x,y) = 0$ at $x = 0, L_x, y = 0, L_y$. Figure 5.3 shows the Kaiser-Bessel window function. It can be seen that Kaiser-Bessel function has a sharper peak than do the Hanning or Hamming functions.

4. Filter

The following function is used in the wavenumber domain (k-space) for the purpose of filtering as well as in the real domain for the purpose of windowing.

$$w(k_x,k_y) = \begin{cases} 1 - 0.5e^{(\frac{\frac{k_r}{k_{r0}}-1}{\alpha})} & k_r \leq k_{r0} \\ 0.5e^{(\frac{1-\frac{k_r}{k_{r0}}}{\alpha})} & \text{otherwise} \end{cases}, \tag{5.5}$$

where:

$k_r = \sqrt{k_x^2 + k_y^2}$,

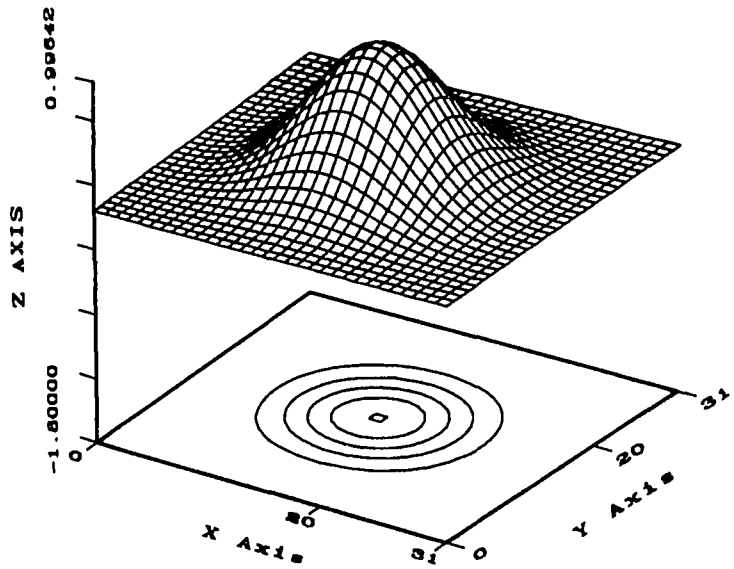

Figure 5.3: Kaiser-Bessel window function

k_{r0} defines the filter width,

α defines the filter slope.

In using the filter, one can choose the parameters k_{r0} and α to change the filter configuration. The larger k_{r0} is, the wider the filter is. On the other hand, a small value for α corresponds to a sharp step while a large value for α corresponds to a broad step. Figure 5.4 and Figure 5.5 show two filters with different parameters.

In the above filter equation, if we define

$$k_{r0}^2 = k_{x0}^2 + k_{y0}^2, \tag{5.6}$$

in such a way that k_{x0}, k_{y0} satisfy the oval equation, i.e.,

$$\frac{k_{x0}^2}{a^2} + \frac{k_{y0}^2}{b^2} = 1, \tag{5.7}$$

where:

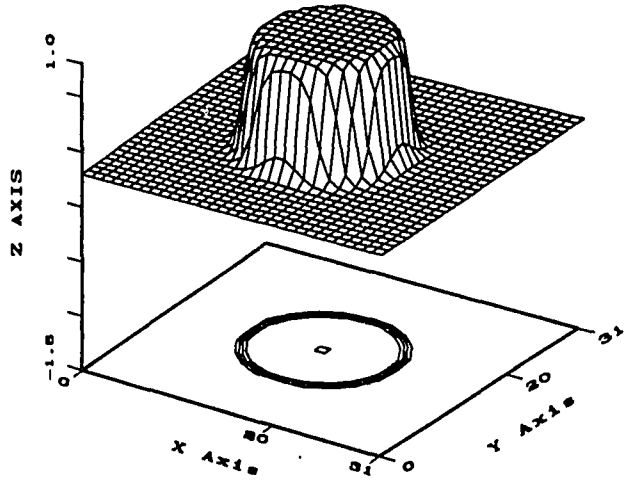

Figure 5.4: Filter function: $k_{r0} = 100.0, \alpha = 0.05$

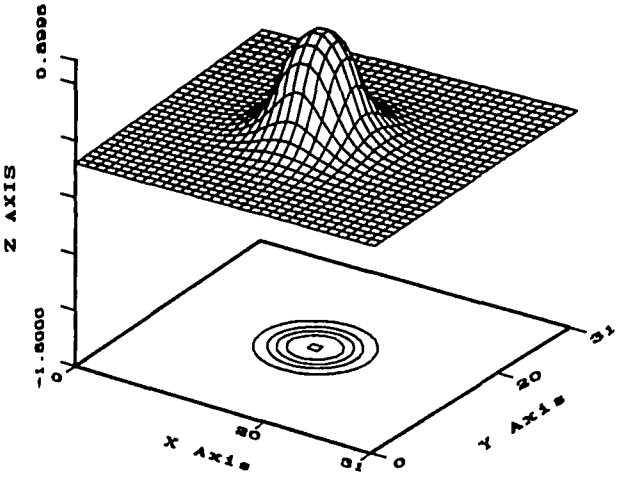

Figure 5.5: Filter function: $k_{r0} = 50.0, \alpha = 0.5$

a is the defined as the longer axis of the oval.

b is the defined as the shorter axis of the oval, and

$$k_{x0}^2 = \frac{a^2 b^2}{a^2 tan^2\theta + b^2}, \tag{5.8}$$

$$k_{y0}^2 = \frac{a^2 b^2 tan^2\theta}{a^2 tan^2\theta + b^2}, \tag{5.9}$$

where

$tan\theta = \frac{k_y}{k_x}$,

then the filter can be defined as a oval filter in the desired domain (real domain or wavenumber domain) by choosing different values for a and b. Figure 5.6 shows an oval filter with parameters $a = 20, b = 10$ and $\alpha = 0.05$. The oval filter can be used in the case where the original function (or discrete data) has different filtering needs in different directions.

5.2 Necessity of Using Windowing and Filtering

In this section, the necessity of using windowing and filtering in the calculation of the structural intensity and the force distribution function is discussed. An example is shown to demonstrate the usefulness of windowing and filtering.

5.2.1 Windowing

Windowing is to multiply the original function in the spatial domain by a window function. The purpose is to ensure for the FFT's that the function decays smoothly at the edges of the measurement. In this investigation, the plate aperture is always

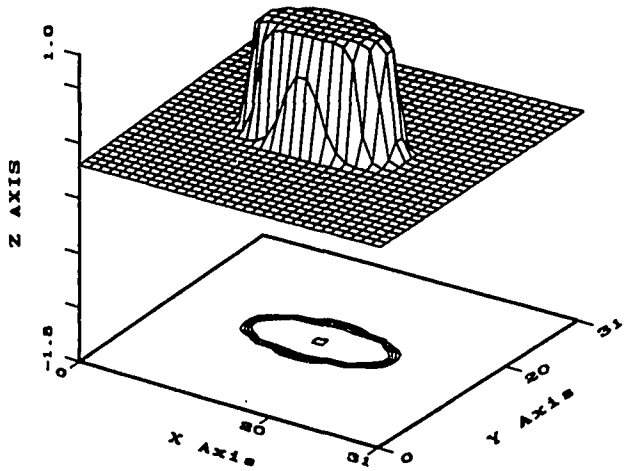

Figure 5.6: Oval filter, $a = 100, b = 50, \alpha = 0.05$

finite. But the velocity on the plate boundaries is not necessarily zero (actually, the velocity on boundaries usually is non-zero). So, windowing forces the spatial velocities to zero at the boundaries. Thus, in using an FFT, the discontinuity introduced by assumed periodicity is removed. In Figure 5.7, the original data is a cosine function which does not equal zero at chosen boundaries ($x = 0, 4\pi$). To force the boundary values to zero, the original function is multiplied by a Hanning window function. The result is the solid line that has zeros at the boundaries.

Again, the example that was used to demonstrate the smoothing procedure in Chapter 4 was used to show the usefulness of windowing. The smoothed velocity, which is in Figure 5.13, was used to calculate the force distribution function and structural intensity. Before applying windowing and filtering, the force distribution is very noisy on the boundaries, as well as at some interior points (see Figure 5.8). The source location is not shown at all. Structural intensity is also very noisy, as

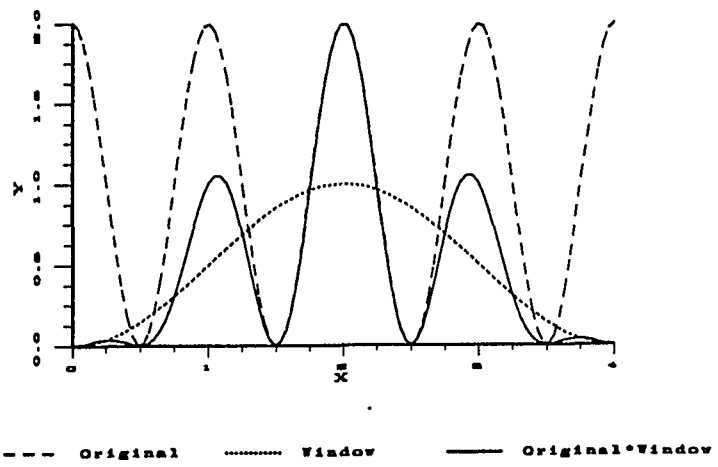

Figure 5.7: Windowing to remove discontinuity

shown in Figure 5.9.

After using a Hanning window shown in Figure 4.13 on the velocity, the noisy peaks in the force distribution function and random arrows in structural intensity at the plate boundaries are eliminated, Figures 5.10 and 5.11. But, noise still exists in the interior region of the plate for both the force distribution function and the structural intensity. To remove the noise from the interior region of the plate, filtering is to be used.

5.2.2 Filtering

The reason for interior noise in the force distribution function and the structural intensity is that even with windowing in the real space, there are still high wavenumber components in the plate velocity. These components, caused by measurement noise, can not be seen in Figure 5.12 since they are small. As described in Chapter

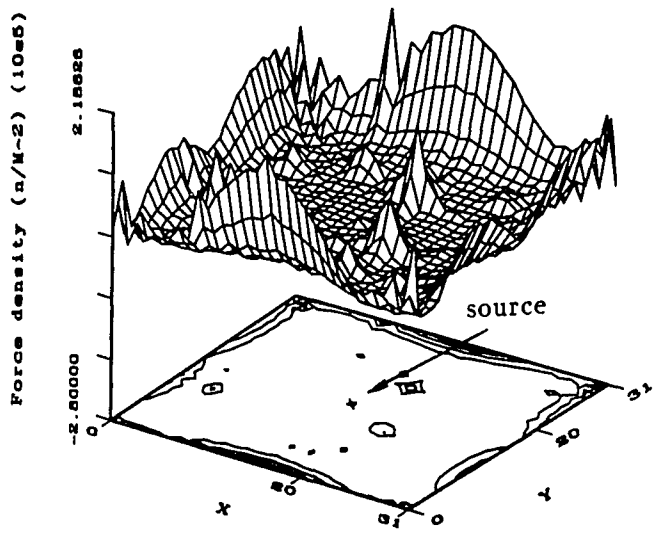

Figure 5.8: Force distribution function from the measured velocity of an absorptive boundary plate with a point excitation, frequency f=201 Hz, no windowing or filtering was applied

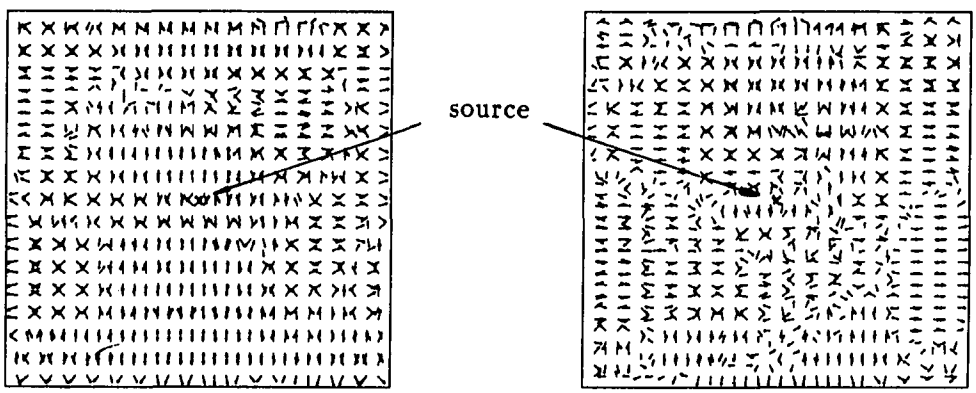

Figure 5.9: Structural intensity from the measured velocity of an absorptive boundary plate with a point excitation, frequency f=201 Hz, no windowing and filtering was applied, (left. active, right. reactive)

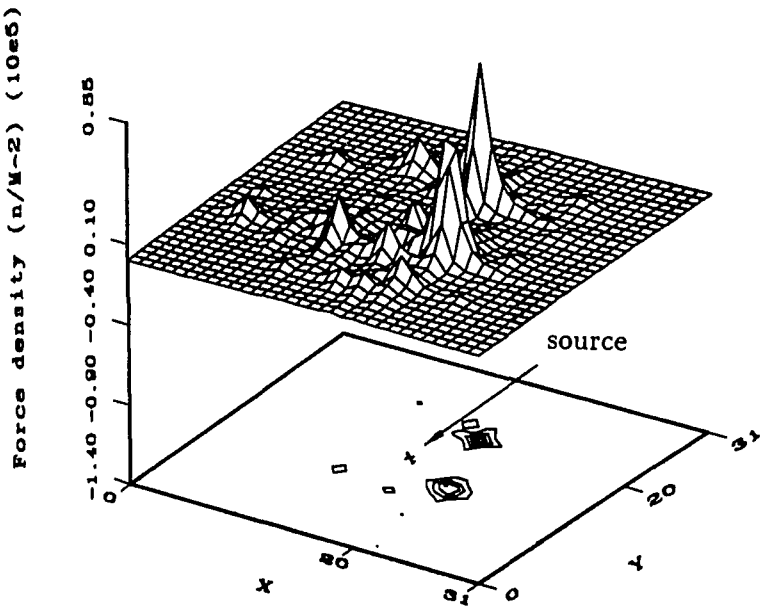

Figure 5.10: Force distribution function from the measured velocity of an absorptive boundary plate with a point excitation, frequency f=201 Hz, with a Hanning windowing, no filtering

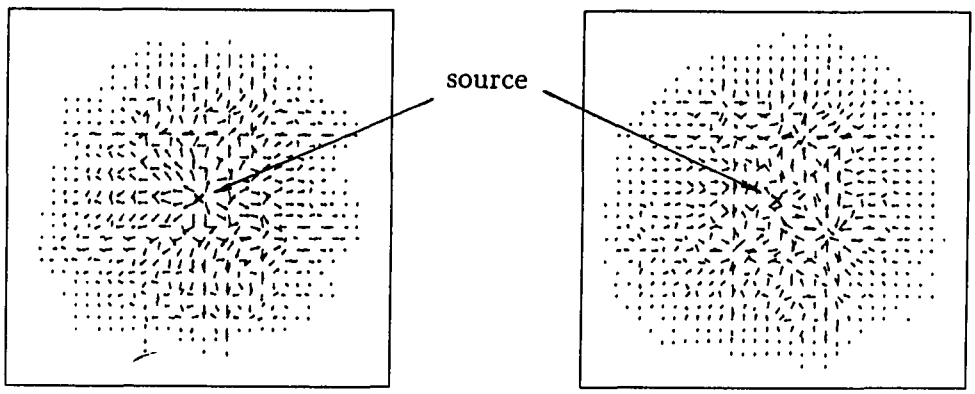

Figure 5.11: Structural intensity from the measured velocity of an absorptive boundary plate with a point excitation, frequency f=201 Hz, with a Hanning windowing, no filtering, (left. active, right. reactive)

3, the force distribution function and structural intensity in the wavenumber domain are proportional to the product of wavenumber domain velocity $\mathcal{F}(\bar{W})$ and the cubic of wavenumbers k_x^3, k_y^3, i.e.,

$$\bar{q} \propto (\mathcal{F}(\bar{W})k_x^3, \mathcal{F}(\bar{W})k_y^3), \tag{5.10}$$

$$\bar{I} \propto (\mathcal{F}(\bar{W})k_x^3, \mathcal{F}(\bar{W})k_y^3), \tag{5.11}$$

where

$\bar{q}$ is the wavenumber domain force distribution function,

$\bar{I}$ is the wavenumber domain structural intensity.

This situation is similar to taking a higher order derivative using Fourier Transforms. The small, nondominate peaks at high wavenumber can become very high peaks after being multiplied by the cubic of the wavenumber. As a result, noise is enlarged in the force distribution function and structural intensity. Figure 5.13 shows the k-space force distribution before a filter was used. We see that the high wavenumber components show up as noisy peaks.

Filtering is to multiply the original wavenumber domain velocity (or displacement) by a filter function to repress the small, high wavenumber components of the plate velocity. Figure 5.14 shows the filtered wavenumber domain velocity. Figure 5.15 shows the wavenumber domain force function with filtering. The dramatic change of the function by filtering is clear by comparing Figure 5.13 and Figure 5.15.

The force distribution function, Figure 5.16, is calculated by the inverse Fourier Transform of the data shown in Figure 5.15. The force location is clearly shown in the force distribution function and the interior noise is eliminated.

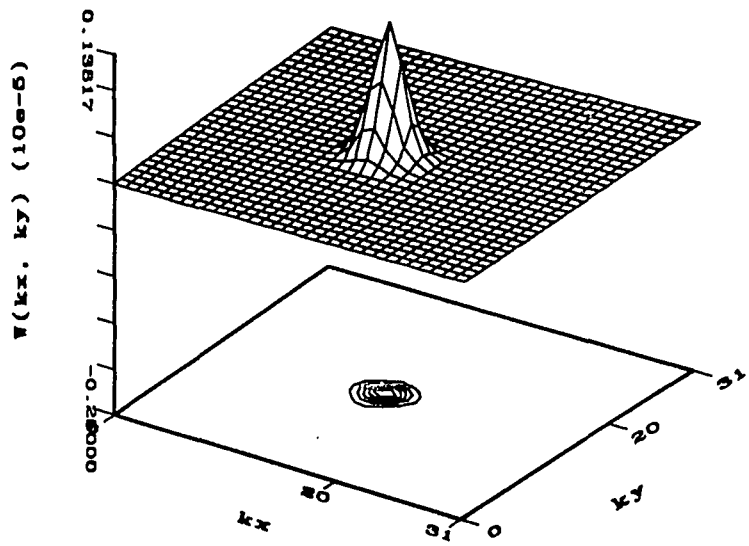

Figure 5.12: Wavenumber domain velocity with a Hanning window for the velocity shown in Figure 5.13, no filtering

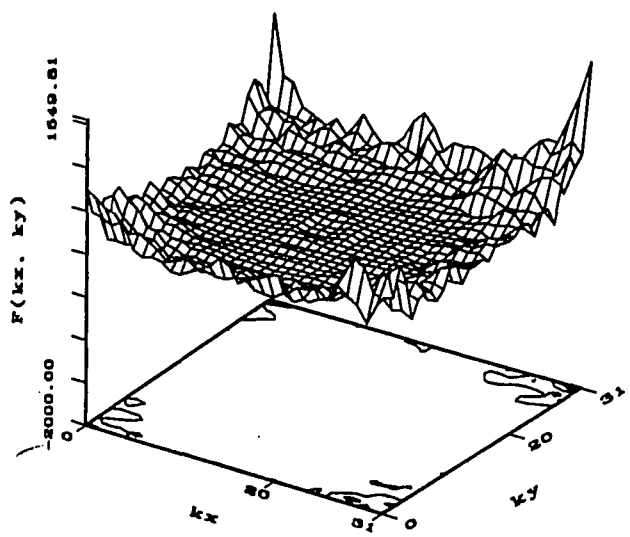

Figure 5.13: Wavenumber domain force distribution function with a Hanning window for the velocity shown in Figure 5.13, no filtering

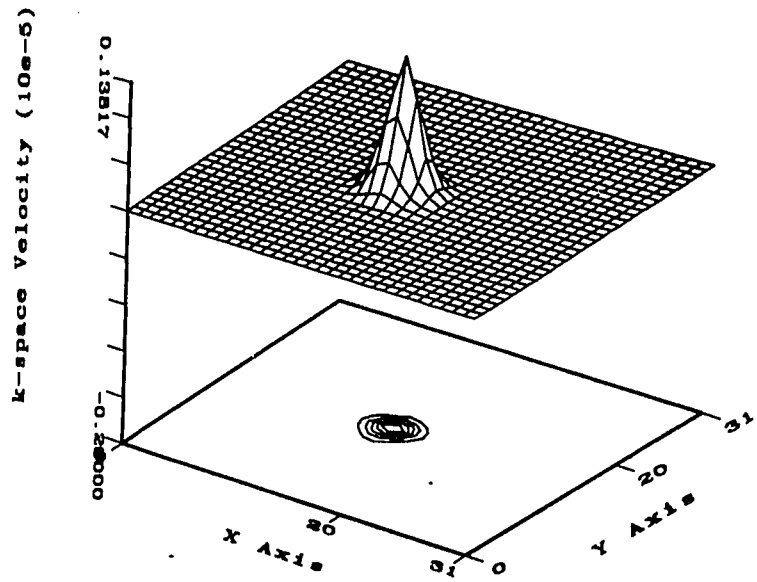

Figure 5.14: Wavenumber domain velocity with a Hanning window for the velocity shown in Figure 5.13, with filter (80, 80, 0.05)

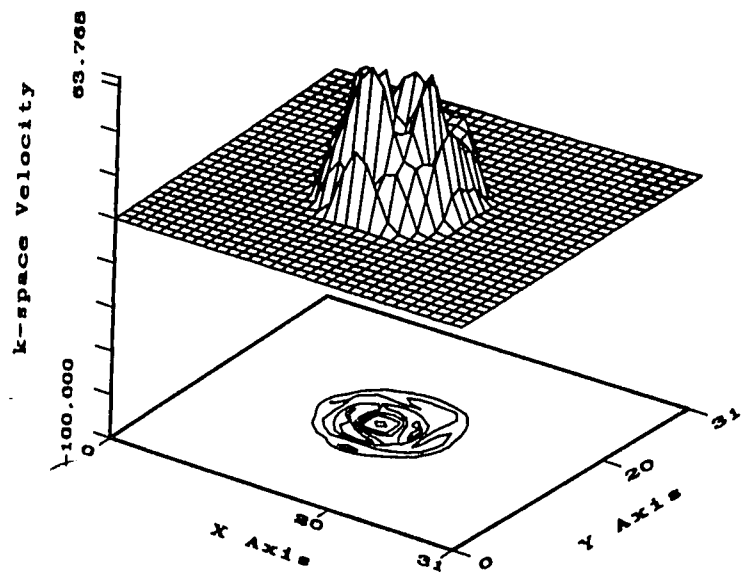

Figure 5.15: Wavenumber domain velocity with a Hanning window for the velocity shown in Figure 5.13, with filtering (80, 80, 0.05)

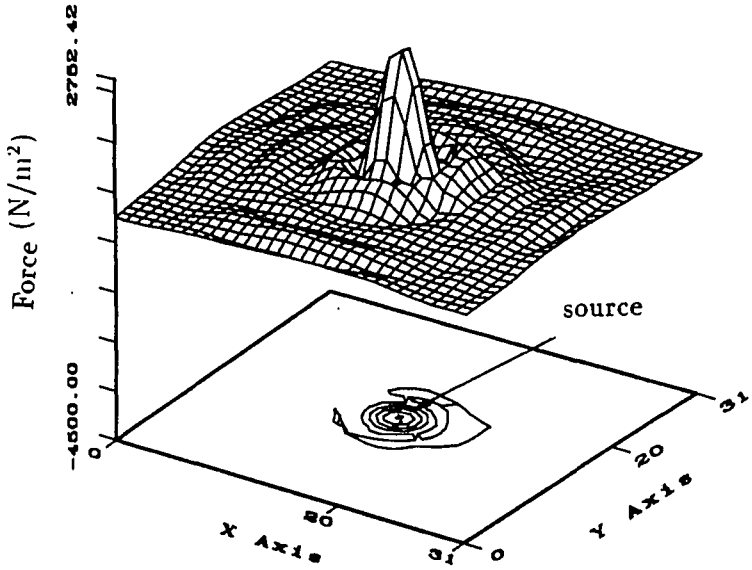

Figure 5.16: Force distribution function for the velocity shown in Figure 5.13, with a Hanning window and filtering (80, 80, 0.05)

Figure 5.17 is the corresponding structural intensity for the same case with Hanning window and filter. Again, the source location is clearly shown.

From the above example, we can see that windowing and filtering are necessary in the calculation of force distribution function and structural intensity by using a Fast Fourier Transform (FFT). Windowing removes the discontinuity at the boundaries of the measured data, while filtering removes the noise of the measured data in the wavenumber domain.

Windowing and filtering are effective techniques in the calculation of structural intensity and the force distribution function and in showing the source location. However, they introduce errors and sometimes remove useful information. The next section discusses the effect of windowing on the force magnitude.

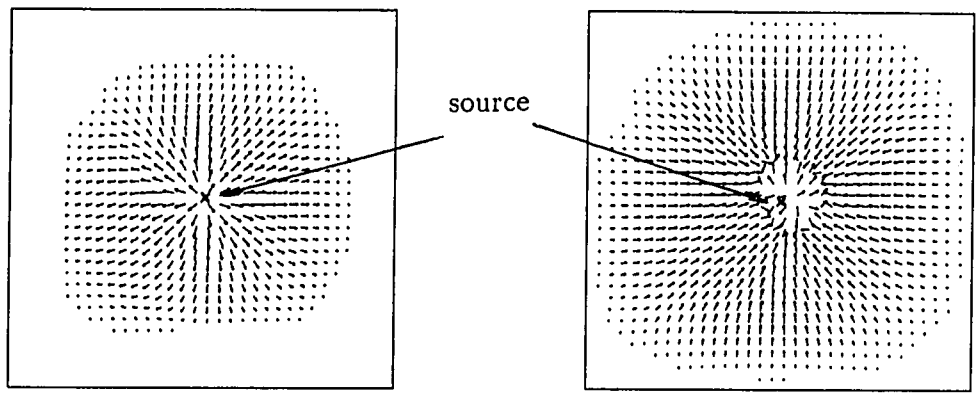

Figure 5.17: Structural intensity for the velocity shown in Figure 5.13, with a Hanning window and filtering (80, 80, 0.05), (left. active, right. reactive)

5.3 Effect of Windowing

5.3.1 Effect of windowing on the force distribution function

The example that I used in the previous sections is the case that a plate has an excitation force located at the center of the plate or the part of the infinite plate under study. In practical cases, the excitation force may be located anywhere in the plate. The question is can we still locate the source(s) and can we estimate the magnitude of the excitation force?

Here, the analytical velocity for an infinite plate with a point source is used to calculate the force distribution function with a Hanning window. The velocity was calculated by Juang [21] over a 2 meters by 2 meters aperture of the infinite plate. The plate thickness is 0.01 meters. A point force with a magnitude of 1 Newton at 292 Hz is applied to the plate. First, the influence of a Hanning window on the

velocity with a point source at the center of the plate is shown. Then, as the point source is moved away from the plate center, the influence of windowing on the force location and magnitude is studied.

Figure 5.18 and Figure 5.19 show the velocity of the plate with a point source at the plate center before and after the Hanning window is applied, respectively. Comparing the two plots, it is seen that the major change occurs at the boundaries, i.e., the window makes the velocity have zero boundary values. Figure 5.20 and Figure 5.21 show the difference between velocities before and after windowing and the percentage error introduced by windowing. We can see, as we expect, the major differences are on the boundaries. The percentage error introduced on the boundaries is as high as 100% while in the center is only as low as 0.5%. From this result, we expect that the force magnitude will not be influenced much by windowing if the force is located close to the center of plate. However, the force magnitude will be significantly affected by windowing if the force is located away from the plate center. This hypothesis is proven to be true later in this section.

Now, let us look at the same plate with the excitation force moved away from the center of the plate. The excitation force is now located half way between the plate center and its lower left corner. Velocities before and after windowing are shown in Figure 5.22 and Figure 5.23. The differences between the velocities due to windowing and the percentage error are shown in Figure 5.24 and Figure 5.25, respectively.

From Figure 5.24 and Figure 5.25, it is seen that the Hanning window not only forces the velocity at the boundaries to be zero, but also reduces the velocity peak which is not at the center of the plate. The differences due to windowing in Figure 5.24 shows that the maximum difference occurs at the point where the velocity peak

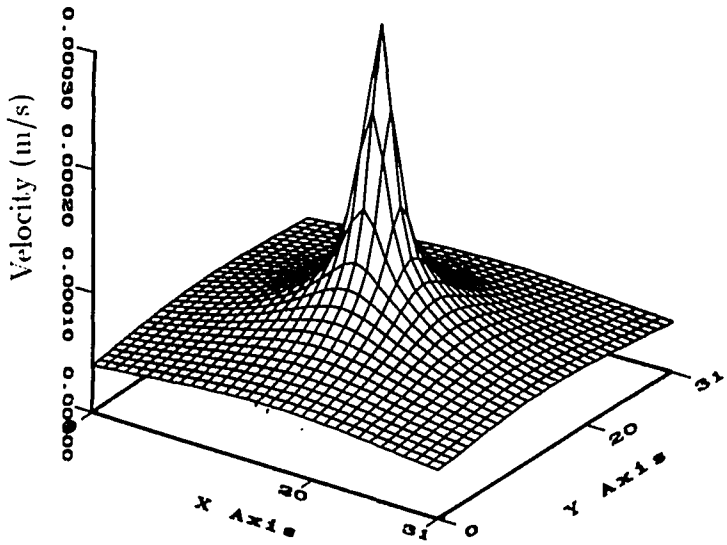

Figure 5.18: Velocity of an infinite plate with a point source at the center. frequency f=250 Hz, before windowing

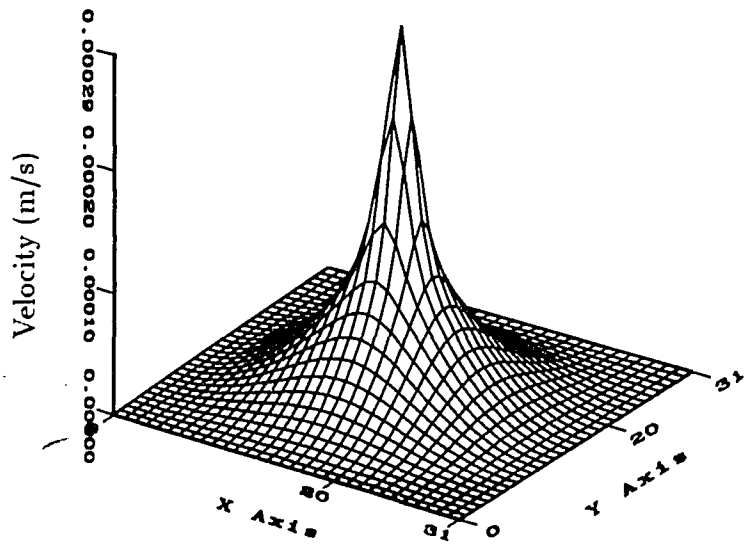

Figure 5.19: Velocity of an infinite plate with a point source at the center, frequency f=250 Hz, after applying a Hanning window

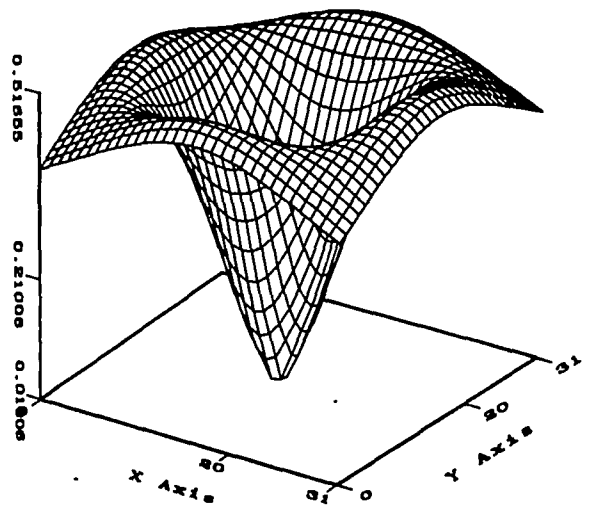

Figure 5.20: Difference of the velocity shown in Figure 5.18 and Figure 5.19

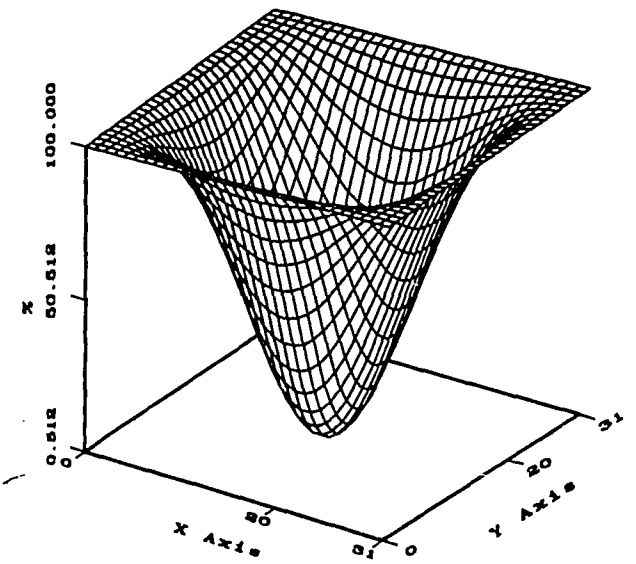

Figure 5.21: Percentage error introduced by the Hanning window for the velocity in Figure 5.18

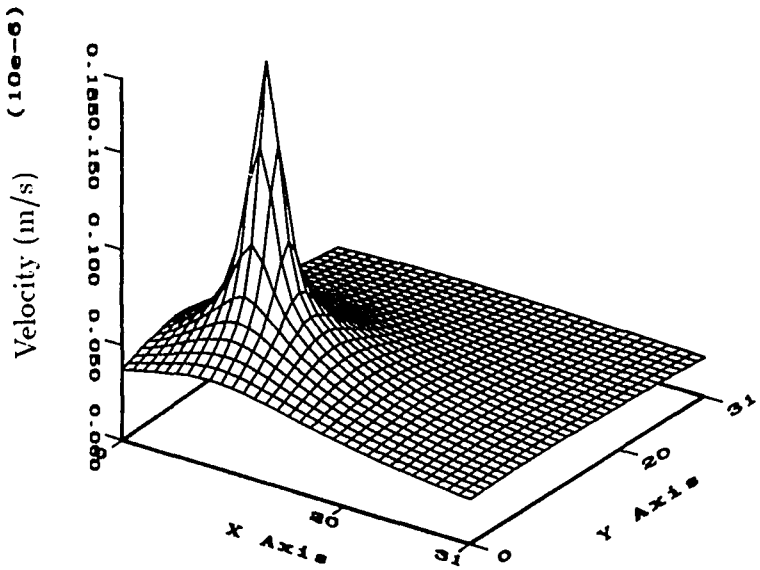

Figure 5.22: Velocity of infinite plate with a point source away from the center, frequency f=250 Hz, before windowing

is while the minimum difference is at the center of the plate.

From the above examples, we see that windowing does cut down the velocity peaks. Now, let us look at the influence of windowing on the force distribution function.

Figure 5.26 is the force distribution function before windowing for the case of the force acting on the center of the plate. There is noise on the boundaries. After windowing, Figure 5.27 shows the source location nicely. The noise at the boundaries has been eliminated. The difference between the force functions before and after windowing is shown in Figure 5.28, in which we see that the major difference is at the boundaries. Windowing actually does not greatly affect the peak of the force. The percentage error of the force distribution function due to the Hanning window is shown in Figure 5.29.

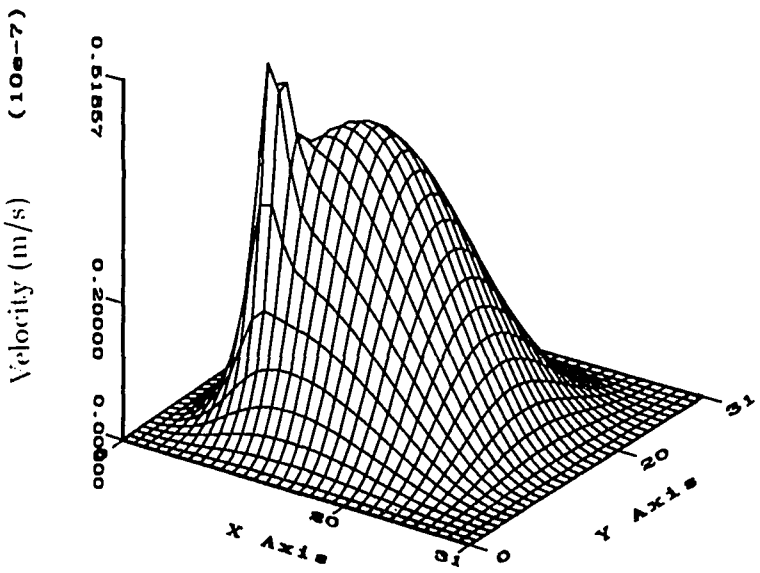

Figure 5.23: Velocity of infinite plate with a point source away from the center, frequency f=250 Hz, after applying a Hanning windowing

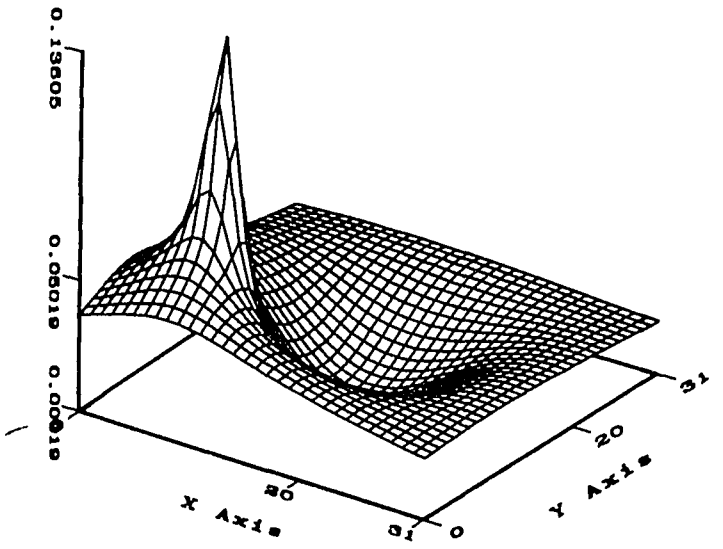

Figure 5.24: Difference of the velocities shown in Figure 5.22 and Figure 5.23

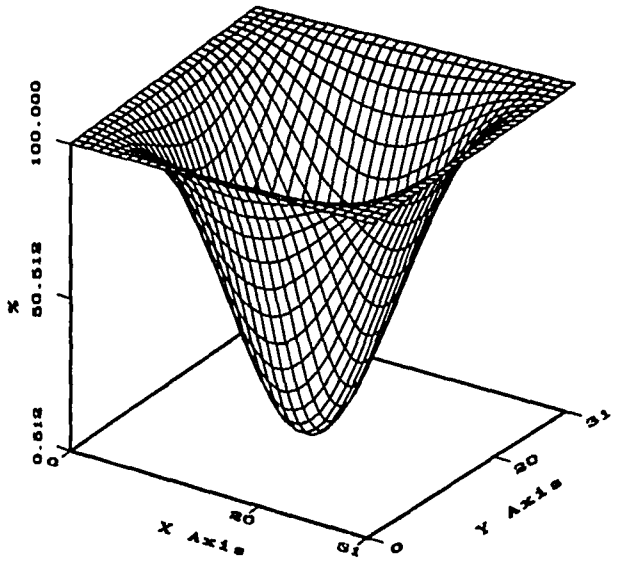

Figure 5.25: Percentage error introduced by the Hanning window for the velocity in Figure 5.22

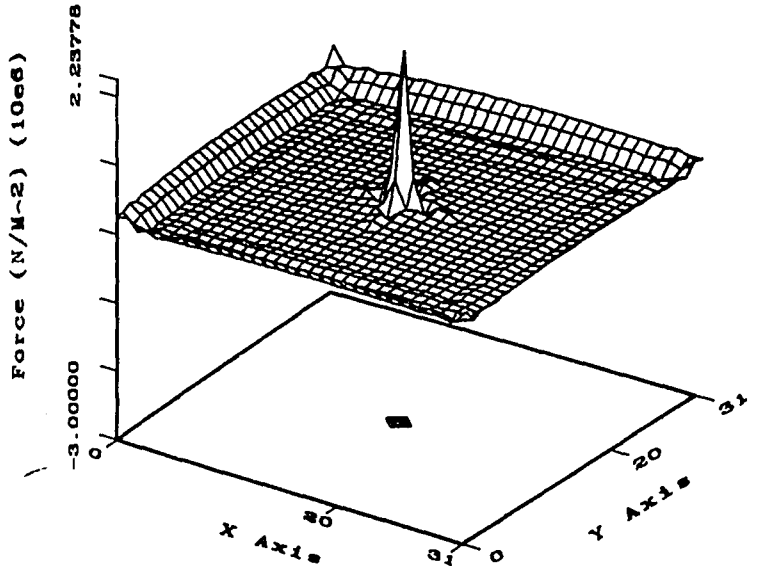

Figure 5.26: Force distribution function of an infinite plate with a force at the center of the plate, frequency f=250 Hz, before windowing

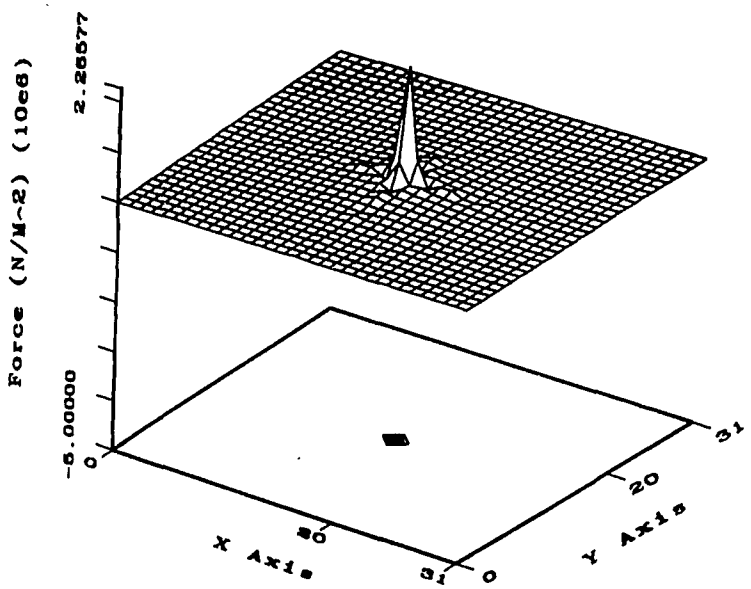

Figure 5.27: Force distribution function of an infinite plate with a force at the center of the plate, frequency f=250 Hz, after applying a Hanning window

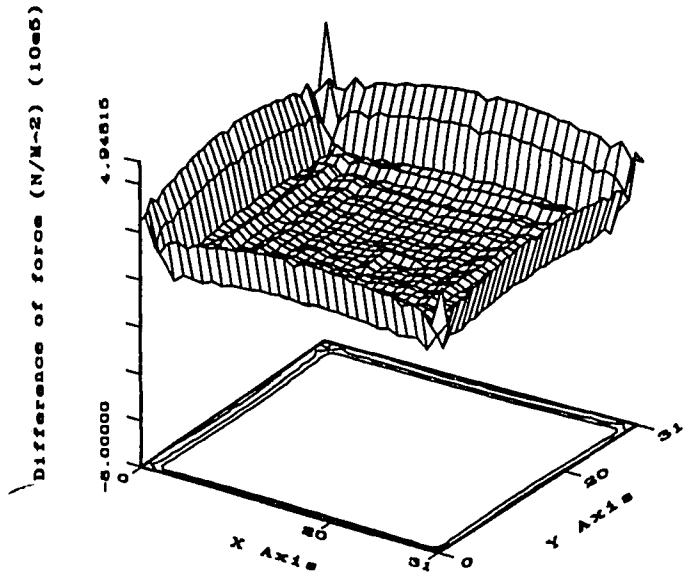

Figure 5.28: Difference between the force distribution functions of an infinite plate with a force at the center of the plate, before and after windowing

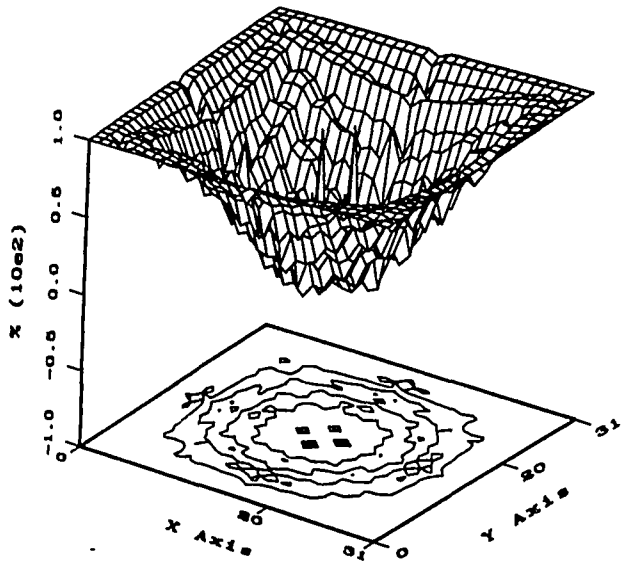

Figure 5.29: Percentage error of the force distribution function in Figure 5.26 due to a Hanning window

For the case in which the force is moved half way to the lower left corner, the force function is shown in Figure 5.30 and Figure 5.31 for velocities before and after windowing, respectively. From the plot in Figure 5.32, showing the difference between the two force functions, it is clear that windowing causes a lot of difference at the force location. Figure 5.33 shows the percentage error of the force distribution function caused by windowing.

Comparing the results from the above two case, we see that windowing does have an effect on the force magnitude as the excitation force is moved away from plate center.

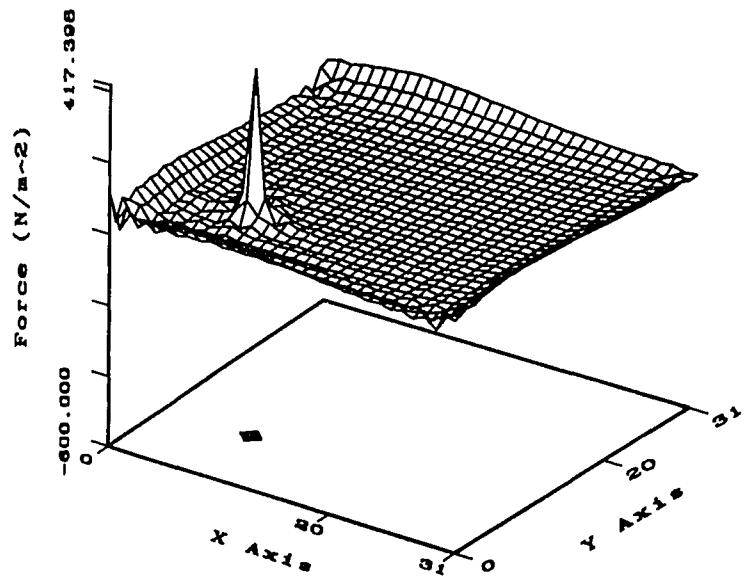

Figure 5.30: Force distribution function for an infinite plate with a point source between the plate center and the plate's lower left corner, frequency f=250 Hz, before windowing

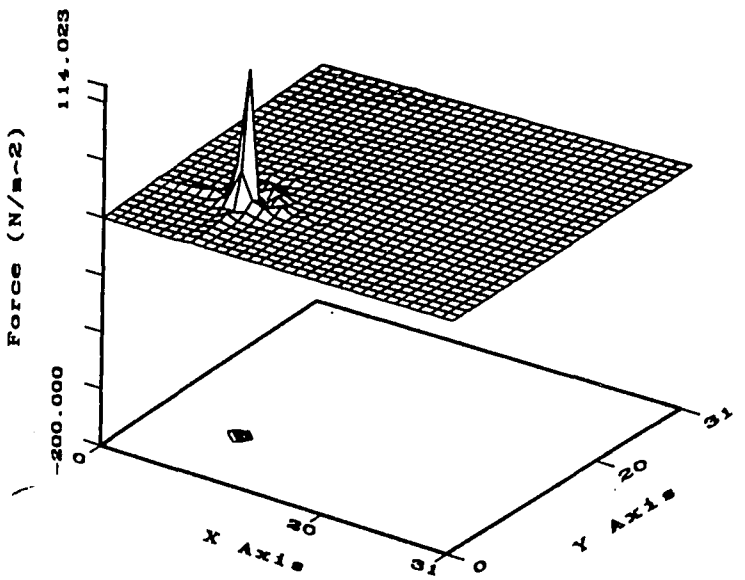

Figure 5.31: Force distribution function for an infinite plate with a point source between the plate center and the plate's lower left corner, frequency f=250 Hz, after applying a Hanning window

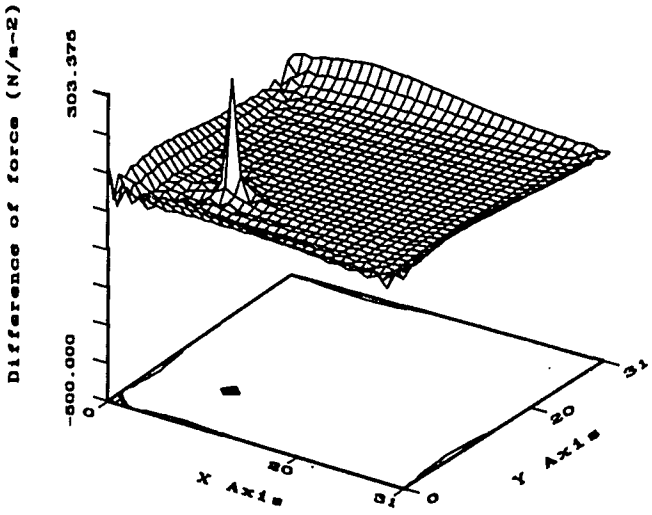

Figure 5.32: Difference between the force distribution functions in Figure 5.30 and Figure 5.31

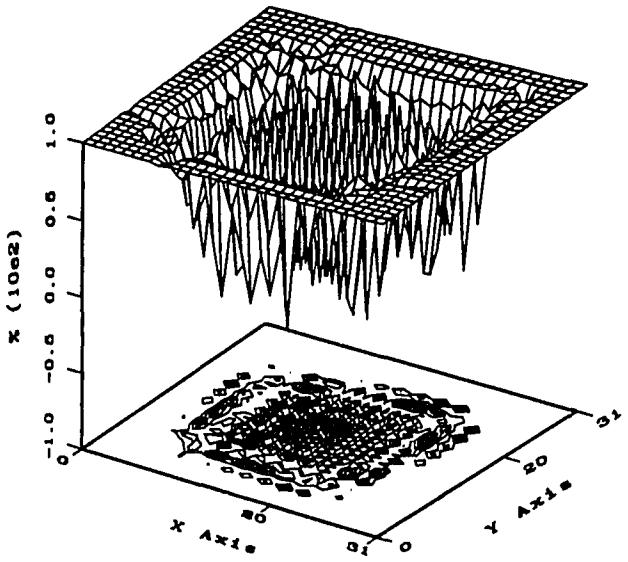

Figure 5.33: Percentage error of the force distribution function for the side force case due to windowing

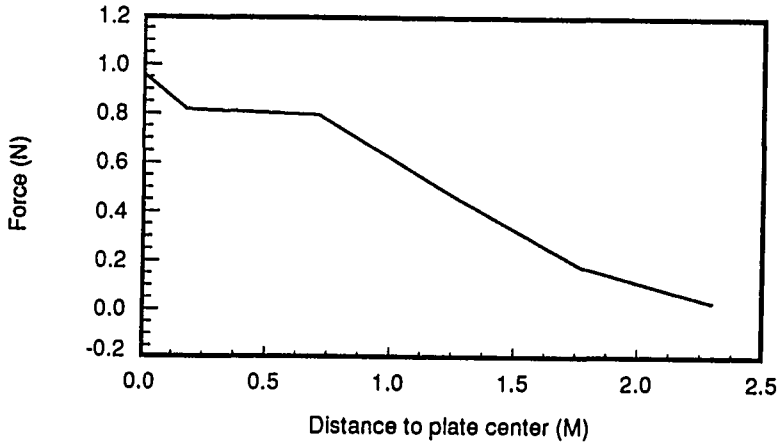

Figure 5.34: Force magnitude vs distance of the force away from the plate center

5.3.2 Correction of the force magnitude

To correct the effect of windowing on the force magnitude, we took the same infinite plate as described in the above section. The force was moved gradually from the center of the plate to the lower left corner of the plate. At each location, the force magnitude was calculated as described in Chapter 3. Figure 5.34 shows that the force magnitude decreases as the force is moved away from the center of the plate. Figure 5.35 shows the window function along the same line that the force magnitude was calculated. Comparing Figures 3.34 and 3.35, we see that the force magnitude decreases in the same way the window function does as the force is moved away from the plate center. This means that the decrease of the force magnitude is caused by the window function.

To correct the force magnitude, we need to divide the calculated force magnitude by the value of the window function at the point of the force location. Figure 5.36

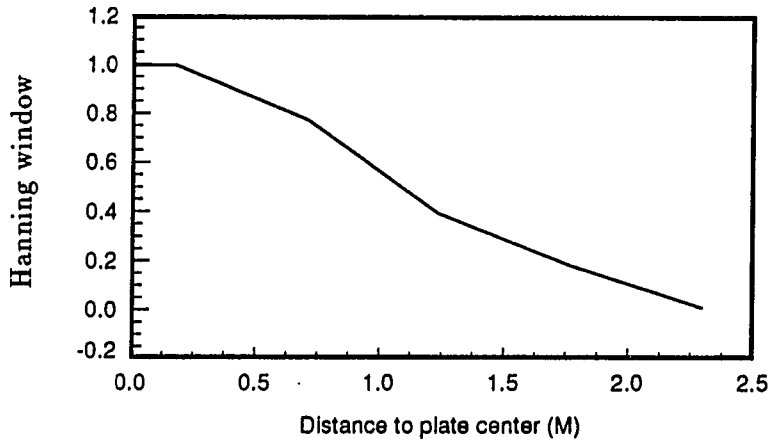

Figure 5.35: Window function along the same line as the force magnitude

shows the corrected force magnitude that is calculated by dividing the force magnitude in Figure 5.34 by the window function. It can be seen that in a fairly large range from the plate center, the force magnitude is corrected to within 15 % of its actual value which is 1 Newton. However, For the forces that are located very close to the measurement boundaries (about 25 % of the total distance between the plate center and the measurement boundary), the force magnitude can not be recovered.

5.4 Effect of Filtering

The purpose of filtering in the wavenumber domain is to remove the noise in the wavenumber spectrum. To achieve this goal, the proper filter size is crucial. If the filter size is too large, the noise may not be removed and the structural intensity and the force distribution function may be noisy. If the filter size is too small, useful information may be removed along with noise, and we may not be able to locate

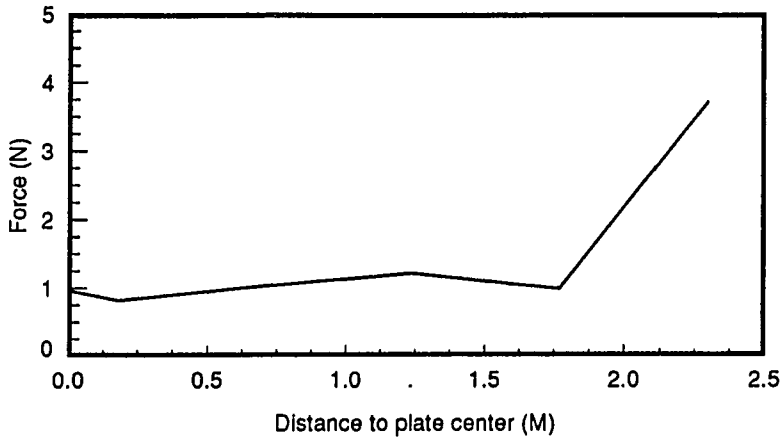

Figure 5.36: The force magnitude after being normalized by the window function

sources. Figure 5.37 shows a force distribution function with a filter that is too large for the velocity in Figure 4.13. Figure 5.38 shows a force distribution function with a filter that is too small. In this research, the filter size is usually determined by a visual inspection of the velocity wavenumber spectrum. Usually, there is a big peak in the center of the plot as shown in Figures 3.1 and 5.12. As a rule of thumb, the filter size is chosen that it just encloses the large central peak. All other noise is filtered out. Sometimes, it is necessary to fine tune the filter size around the chosen value to get better results. Figure 5.39 and Figure 5.40 show how the integrated force magnitude and input power change as the filter size changes for the calculated velocity for the infinite plate with a point source at 250 Hz. It is seen that a larger filter size results in larger force magnitude and vise versa. Figure 5.41 and Figure 5.42 show the integrated force magnitude and the input power as functions of filter size for the measured velocity (Figure 4.13) of the sand bag supported plate with a

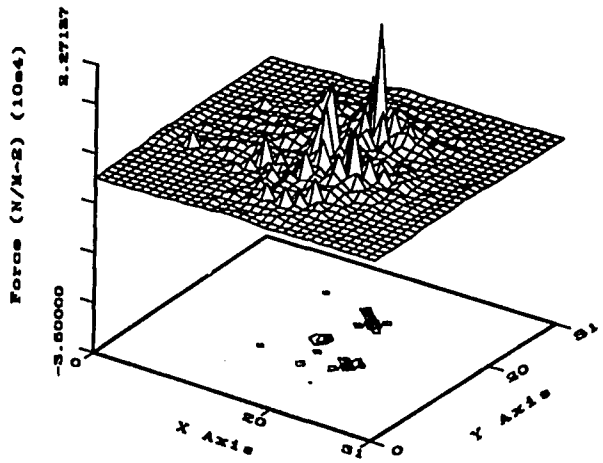

Figure 5.37: Force distribution function with filter size that is too large.

point source at the plate center. It can be seen that for analytical and experimental data, the force magnitude and the input power change differently as the filter size changes. It is not possible to find a single curve that can be used to correct the force magnitude and the input power to compensate for filtering. So, the problem with using filtering is that a different filter size gives different values for the calculated force magnitude and the input power, although filtering helps in locating sources.

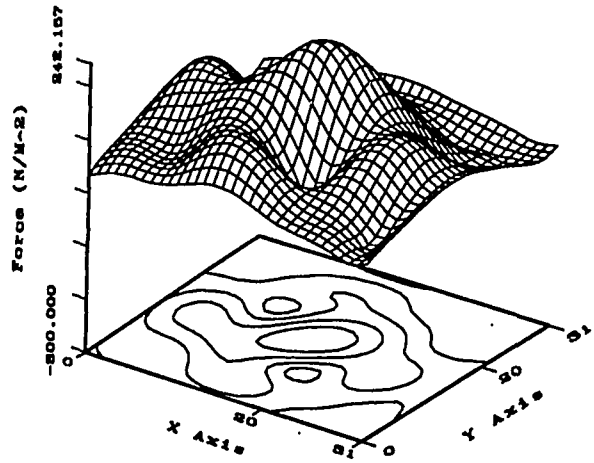

Figure 5.38: Force distribution function with filter size that is too small

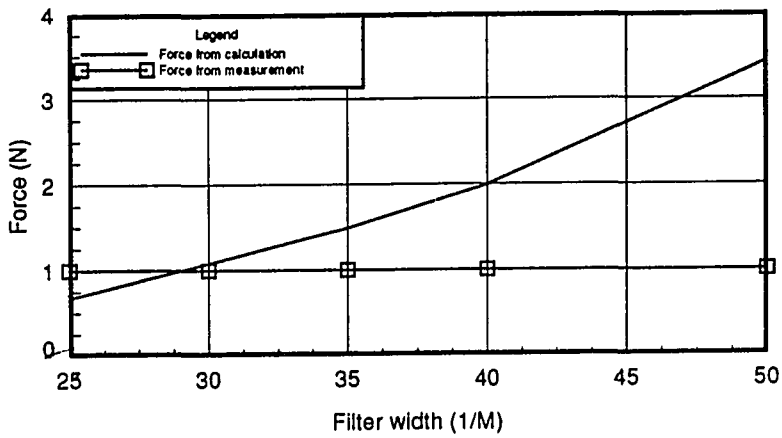

Figure 5.39: Influence of the filter size on the force magnitude, analytical data

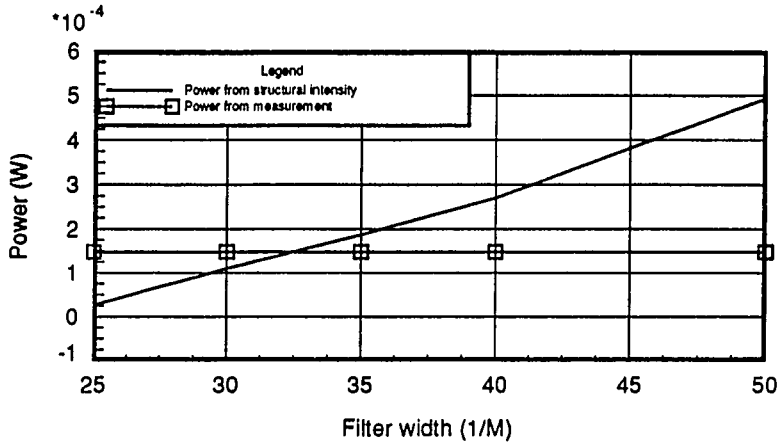

Figure 5.40: Influence of the filter size on the input power, analytical data

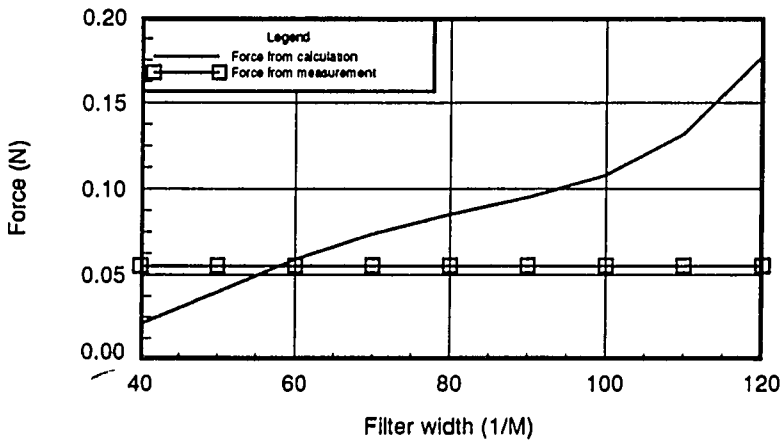

Figure 5.41: Influence of the filter size on the force magnitude, measured data

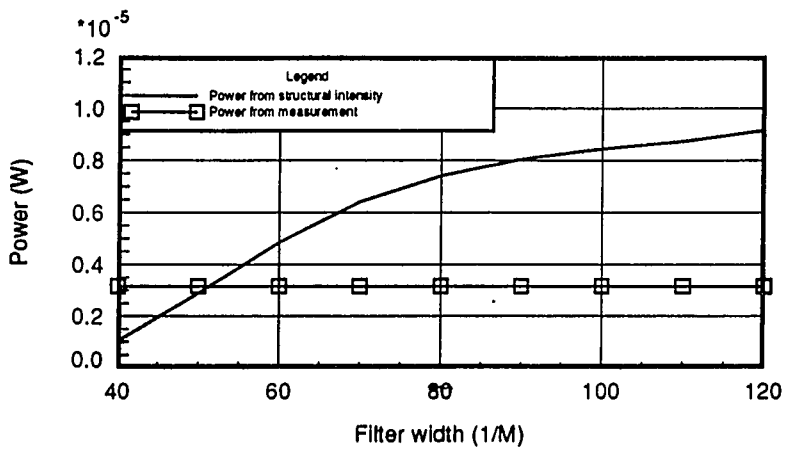

Figure 5.42: Influence of the filter size on the input power, measured data

CHAPTER 6. RESULTS

Based on the structural intensity and force distribution function formulations in Chapter 2 and the calculation procedure described in Chapter 3 and Chapter 5, the structural intensity and force distribution function can be calculated for plate type structures. This chapter will show some of the results for both analytical plate displacements and the measured plate displacements.

In this chapter, the source locations will be determined by using both the structural intensity and the force distribution function from measured data from different plates. The magnitude of the excitation force and the power of the excitation force input to the plate will be calculated from the force distribution function and the structural intensity and compared to the measured data.

Also shown in this chapter are results for the cases where there are two forces exciting the plate. The structural intensity and the force distribution function are used to locate the two sources.

Because the structural intensity shows the energy transported in the vibrating structure, it is expected to show the location of damping in a vibrating structure. This chapter illustrates some results to show the damping location and the effectiveness of the damping using structural intensity.

6.1 Source Location

In this section, the structural intensity and the force distribution function is calculated for the plates described in Figure 4.18 (c) to show how the source location can be determined from the structural intensity and the force distribution function. The plate velocity is measured by the laser Doppler vibrometer as described in Chapter 5.

For the 1.2 m $\times$ 1.2 m plate shown in Figure 4.18 (c), the plate with sand supported boundaries and visco-elastic damping around the measurement area, the excitation force is 20 centimeters to the right of the center of the plate. The measured velocity, the structural intensity and the force distribution function are shown in Figure 6.1, Figure 6.2 and Figure 6.3, respectively. As described in Chapter 5, the excitation is a chirp signal with frequency ranging from 800 Hz to 1200 Hz. Here, only the result for 1000 Hz is shown. In calculating the structural intensity and the force distribution function, the Hanning window and filter were used as discussed in Chapter 4. The parameter for the digital filter in the wavenumber domain is (80, 80, 0.05).

It can be seen from Figure 6.2 and Figure 6.3 that the source location is very nicely shown by both the structural intensity and the force distribution function. In the structural intensity plot, it shows clearly that the structural intensity points away from the the point where the source is located. In the force distribution function, a peak shows up at the point where the force is acting, showing the source location.

Now, it is shown that the source location can be seen from both the structural intensity and the force distribution function. The question is whether or not it is possible to determine the magnitude of the input power from the structural intensity

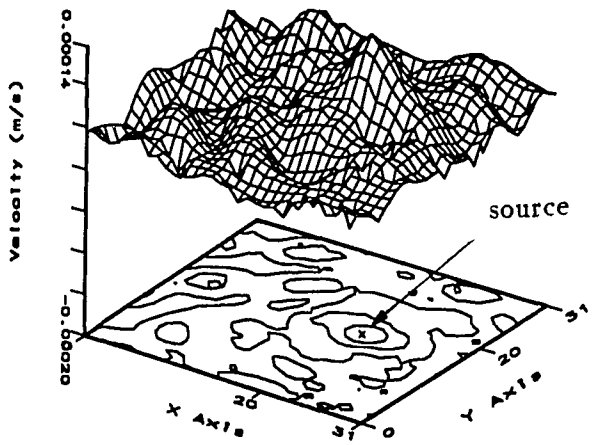

Figure 6.1: Velocity of the plate with visco-elastic damping around the measured area, f=1000 Hz

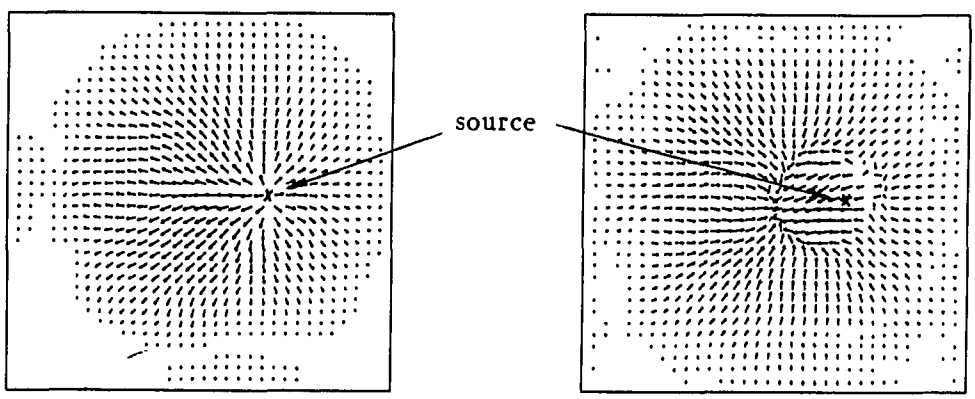

Figure 6.2: Structural intensity of the plate with visco-elastic damping around the measured area, f=1000 Hz. (left. active, right. reactive)

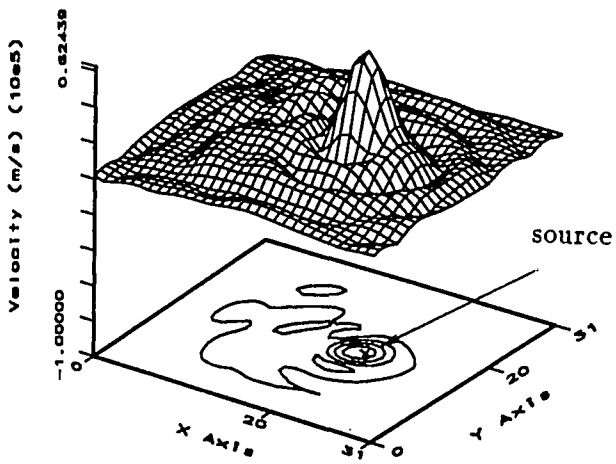

Figure 6.3: Force distribution function of the plate with visco-elastic damping around the measured area, f=1000 Hz

and the force distribution function.

In Chapter 4, it has been shown that for an infinite plate with a point source, the force magnitude and the input power to the plate can be determined to very good accuracy if the force magnitude is corrected by the window function. Here, for the plate with visco-elastic damping around the measured area, the input power is calculated from both the structural intensity and the power function over a frequency range of 800 Hz to 1100 Hz. Figure 6.4 shows the calculated input power and the measured input power as a function of frequency. Also, from the force distribution function, the force magnitude is calculated over the same frequency range. Figure 6.5 shows the comparison of the calculated force magnitude and the force magnitude measured by the force transducer located between the shaker and the plate. The method to calculate the force magnitude and the input power is discussed in Chapter

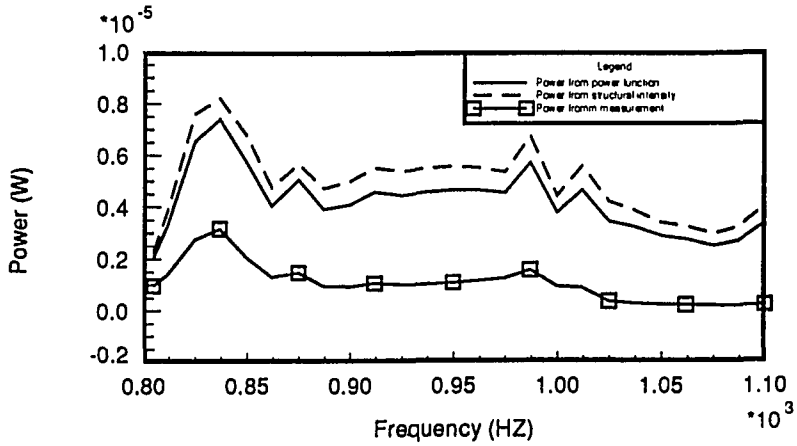

Figure 6.4: Comparison of the input power for the plate with visco-elastic damping around the measured area

3.

It is obvious that both the calculated input power and the force magnitude vary in much the same way the measured quantities do. This means that the calculation is not sensitive to the frequency change. For each single frequency, the difference between the calculated value and the measured value is due to the fact that in the calculation, signal processing techniques such as windowing and filtering are used. Heavy filtering (smaller filter size) may be needed to show the location of the source, but may cause significant differences in the force magnitude and the input power. This difficulty in matching input force and power magnitude from measurement data remains yet to be solved.

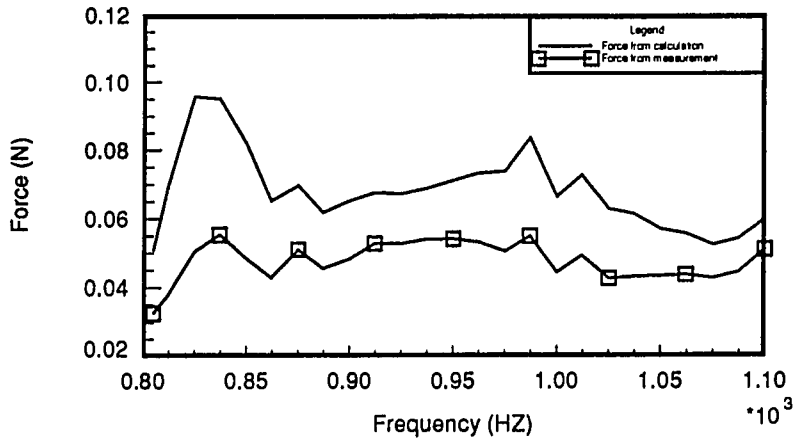

Figure 6.5: Comparison of the force magnitude for the plate with visco-elastic damping around the measured area

6.2 Ribbed Plate

Ribs on plate-like structures change the plate stiffness and the vibration of the plate. Using the structural intensity, we can decide how the energy flow is affected by the ribs. The force distribution function is also used to study the influence of the ribs on the plate.

From Juang's study of an infinite plate with a rib and a point force excitation, the displacement is shown in Figure 6.6 [32]. The portion of the plate under study is 0.31 meters by 0.31 meters. The plate thickness is 0.01 meters, and the frequency is 292 Hz. The rib is attached in the same way as shown in Figure 4.18 (e). It can be seen from the displacement (Figure 6.6) that the rib constrains transmission of the vibration past the rib. The structural intensity and force distribution function corresponding to the displacement in Figure 6.6 are shown in Figure 6.7 and Figure

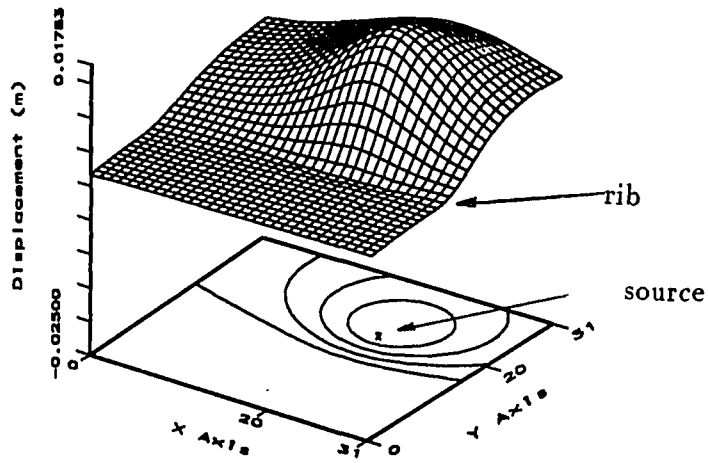

Figure 6.6: Displacement of the ribbed plate with a point force, f=292 Hz, analytical data, from [32]

6.8, respectively.

A measurement was also performed for a ribbed plate that is shown in Figure 4.18(b). The plate thickness is 0.003 meters. And the plate boundaries were supported by sand bags to simulate absorptive boundaries. The measured velocity has been shown in Figure 4.20. The corresponding structural intensity and the force distribution function are shown in Figure 6.9 and Figure 6.10 , respectively.

The source location can be determined easily from the structural intensity for the analytical data Figure 6.7. For measured data, the structural intensity does not show the source as clearly as in the analytical data case.

The rib can be seen from the structural intensity for the analytical data in Figure 6.7. The energy flows into the area of the plate where the rib is located. This means that the rib is actually absorbing energy so as to constrain the plate vibration. For

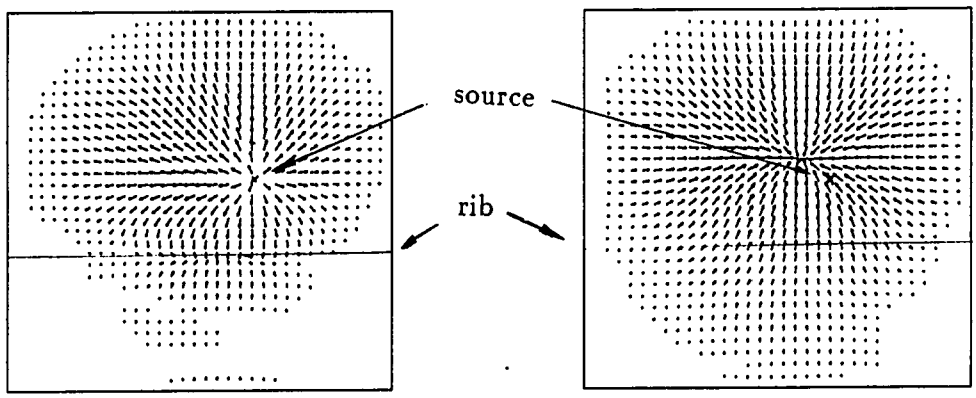

Figure 6.7: Structural intensity of the ribbed plate with a point force, f=292 Hz, from analytical data, (left. active, right. reactive)

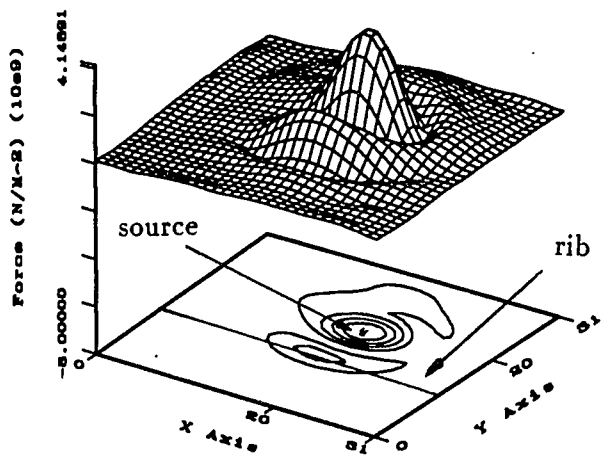

Figure 6.8: Force distribution function of the ribbed plate with a point force, f=292 Hz, from analytical data

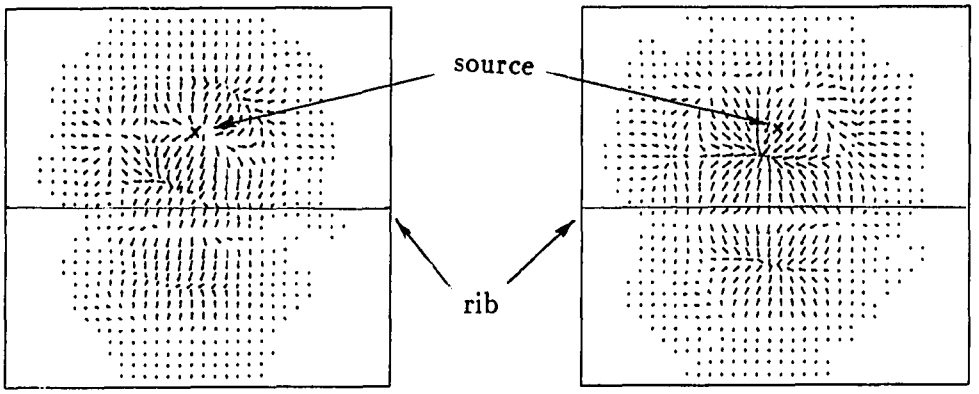

Figure 6.9: Structural intensity of the ribbed plate with a point force, f=292 Hz, from experimental data, (left. active, right. reactive)

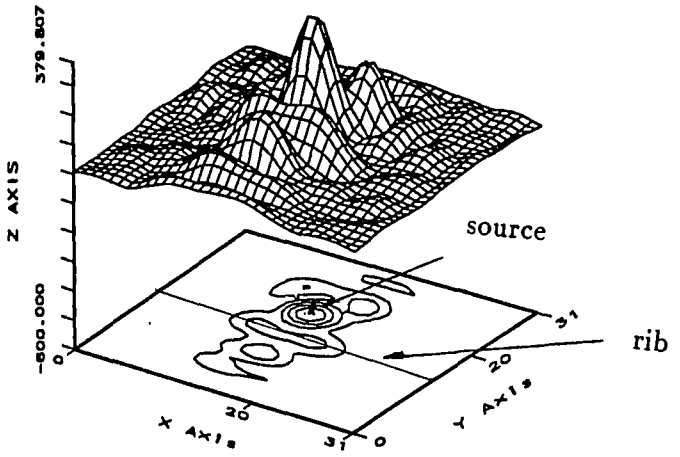

Figure 6.10: Force distribution function of the ribbed plate with a point force, f=292 Hz, from experimental data

an infinite plate, the energy is transmitted along the rib to infinity. This phenomenon can not be seen from the measured data because the rib and the plate are finite.

The force distribution function shows the source location better than the structural intensity does. In Figures 6.8 and 6.10, the source location is very clear for both analytical and experimental data. Also, the rib is shown as a force peak due to the fact that there is interaction between the plate and the rib while the plate is vibrating. In other words, there is a constraint force on the plate by the rib, and the constraint force is shown in the plot of the force distribution function.

There are two reasons that the constraint force between the plate and the rib appear to be more like a concentrated force than a line force. First, around the point the force is located, there are more vibrations of the plate than away from the excitation. Therefore, there is a larger force constraining the plate close to the point excitation than away from it. Secondly, as has been pointed out before, signal processing techniques are used in the calculation of the force distribution function. Windowing and filtering may have removed some of the useful information close to the edges of the plate. Thus, the constraint force on the plate will not be clearly seen close to the plate boundaries.

6.3 Multiple Forces

For a plate with a single excitation force, it has been shown in the first section of this chapter that the source location can be clearly shown by both the structural intensity and the force distribution function. In this section, we show some results for a plate with two excitation forces. The analytical displacement data for an infinite plate and experimental data for a sand bag supported plate will be discussed.

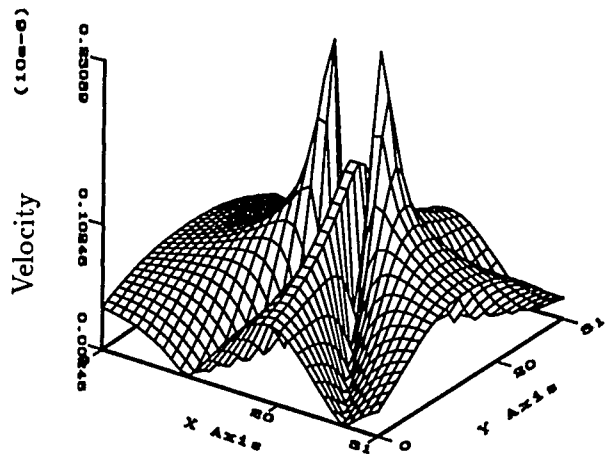

Figure 6.11: Velocity of the homogeneous plate with two point forces, f=250 Hz, from analytical data

The displacement shown in Figure 6.11 is for the same infinite plate as described in the previous sections with two in phase forces applied to the plate.The corresponding structural intensity and the force distribution function are shown in Figure 6.12 and Figure 6.13, respectively. Both the structural intensity and the force distribution function show the source locations clearly.

The structural intensity and the force distribution function are not as effective at distinguishing the two sources for measured velocity data. The following figures (Figures 6.14, 6.15, 6.16) show the measured velocity, the structural intensity, and the force distribution function for the plate in Figure 4.18 (b) with two forces exciting it. Again, the two forces are in phase. One of the force is located at the center of the plate. The other is 0.12 meters on the right of the plate center.

One reason that the structural intensity and the force distribution function do

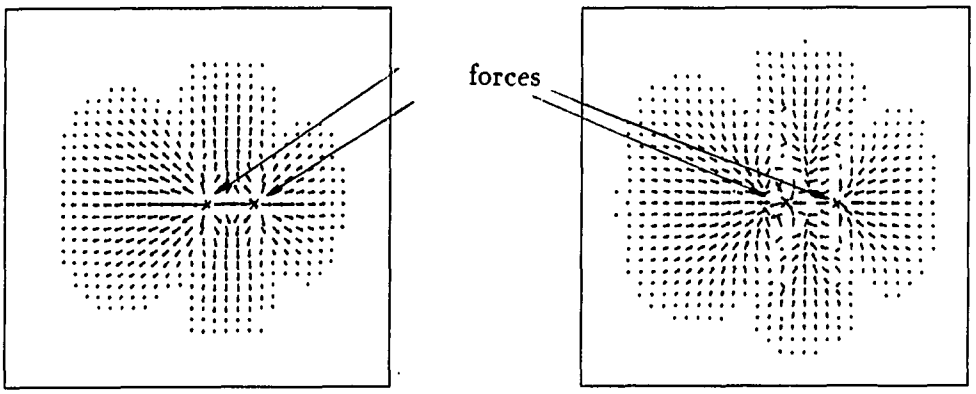

Figure 6.12: Structural intensity for the homogeneous plate with two point forces, f=250 Hz, from analytical data, (left. active, right. reactive)

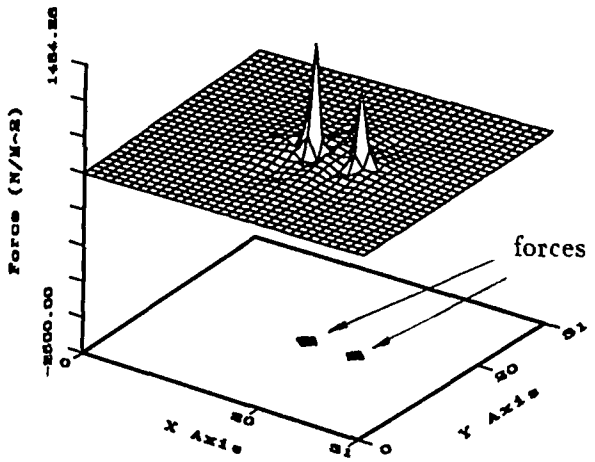

Figure 6.13: Force distribution function for the homogeneous plate with two point forces, f=250 Hz, from analytical data

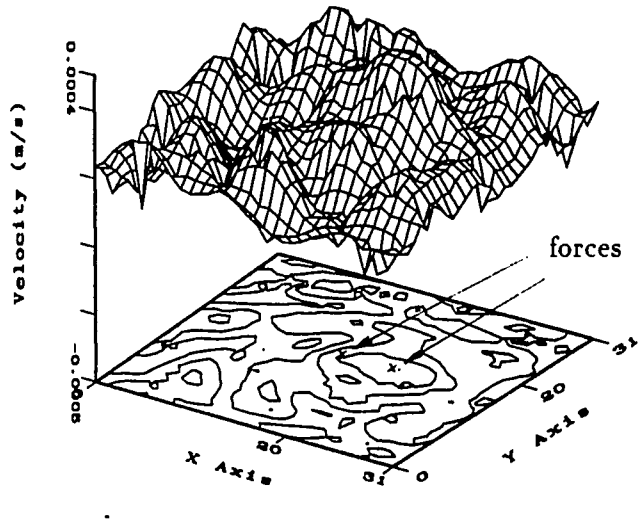

Figure 6.14: Velocity of the sand supported plate with in phase forces, f=1000 Hz, from measured data

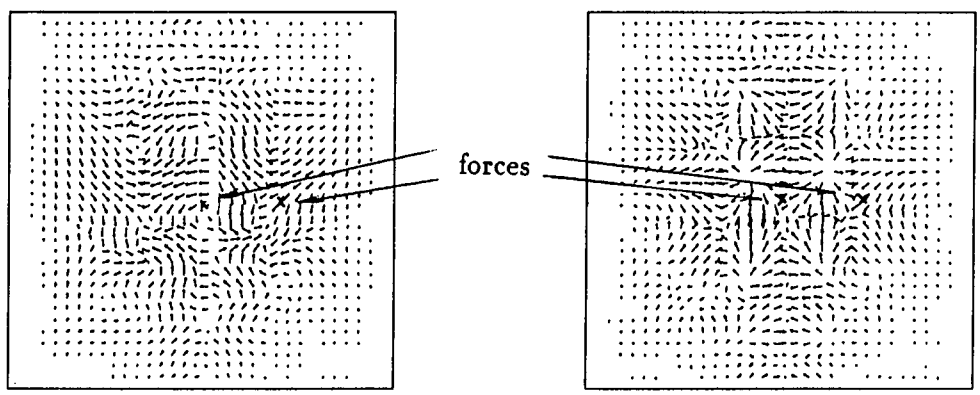

Figure 6.15: Structural intensity of the sand supported plate with in phase forces, f=1000 Hz, from measured data, (left. active, right. reactive)

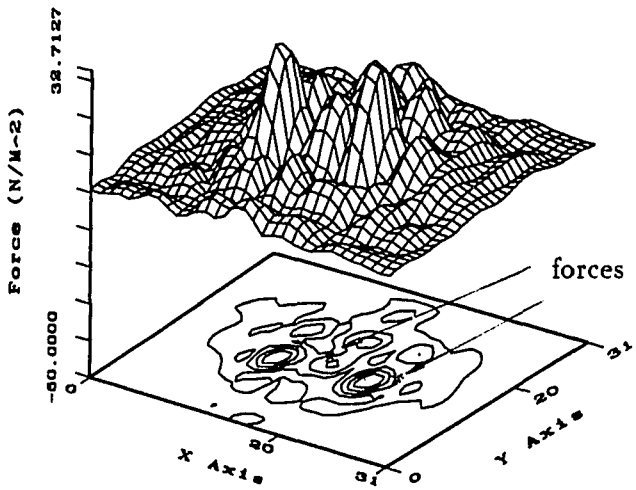

Figure 6.16: Force distribution function of sand supported plate with in phase forces, f=1000 Hz, from measured data

not show the source location clearly for measured data is that there is interference between the two forces. This makes the numerical calculation more difficult. In the single force case, there are more ripples appearing around the force peak in the measured data compared to the synthetic data (see Figure 6.17 and Figure 6.18). Also note that the spatial width of the force peak is much greater for the measured data. Both the ripple and width increases because a smaller filter is needed with measured data. For the two force case, the ripples and the spatial width from each force add up and the actual forces are not easily distinguishable from all the ripples.

One thing that may help in getting better results in distinguishing the two forces for measured data is to increase the spatial resolution of measurement points. Figure 6.19 shows a force distribution function for the synthetic data. This set of 16 by 16 data is over an area of 2.0 by 2.0 meters. Figure 6.20 shows a force distribution

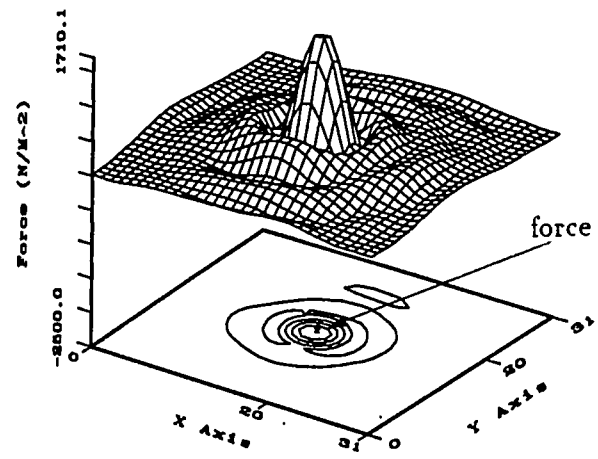

Figure 6.17: Force distribution function from measured data

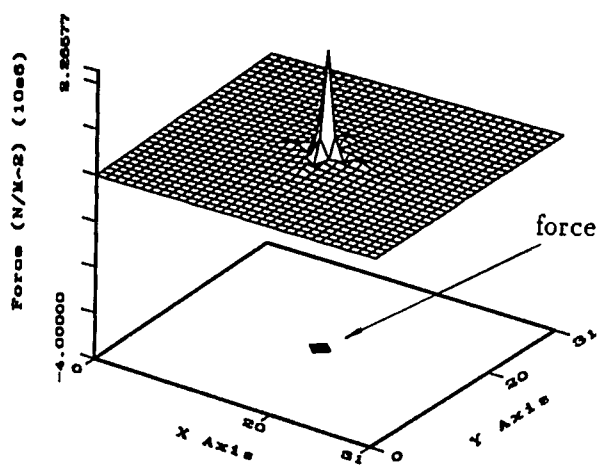

Figure 6.18: Force distribution function from synthetic data

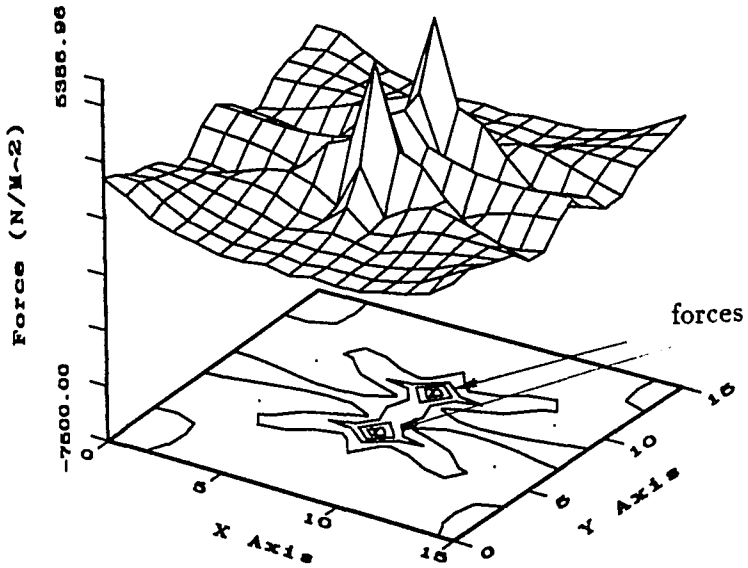

Figure 6.19: Force distribution function of a larger aperture (lower resolution)

function for another set of 16 by 16 points. But it is over an area of 1.0 by 1.0 meters. The data for Figure 6.20 shows a better separation between the two forces than the data for Figure 6.19. From the two plots, it is seen that the force peak is clearer in the case of higher resolution. For measured data, it is expected that better results could have been obtained if measurements of higher resolution had been performed. Due to the limitation of the equipment, this work is not done.

6.4 Locating Damping in the Plate

In a vibrating structure, the vibrational energy can be absorbed by the material damping. Since the structural intensity represents the energy flow in the structure, the structural intensity is investigated to see if it can locate damping material added to a vibrating structure.

A plate of dimension 1.2 by 1.2 meters with a thickness of 0.003 meters is used.

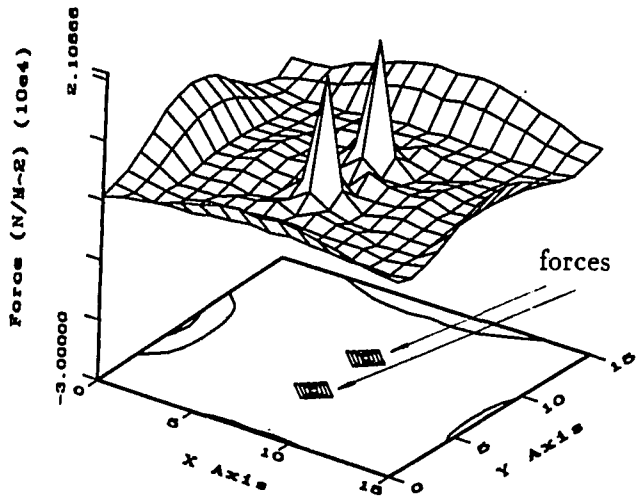

Figure 6.20: Force distribution function of a smaller aperture (higher resolution)

The plate was hung by two strings (as shown in Figure 4.18 (e)). Two measurements were performed on the same plate. The first one is the plate without damping material on it, representing a very reverberant plate. The velocity is measured over an area of 0.46 by 0.46 meters as shown in Figure 4.18 (e). The measured velocity is shown in Figure 6.21. Since this is a very reverberant plate, the vibrational energy reflects back and forth in the plate. The structural intensity is shown in Figure 6.22. Figure 6.23 shows the structural intensity caused by bending, twisting and shearing vibrations in the plate. These three terms correspond to the three terms in Pavić's structural intensity formula. The force distribution function is shown in Figure 6.24, in which, the force location can be seen.

The second measurement is for the same plate with a five inch wide strip of constrained layer damping material placed across the plate as shown in Figure 4.18 (e). A measurement was performed over the same area as in the above measurement.

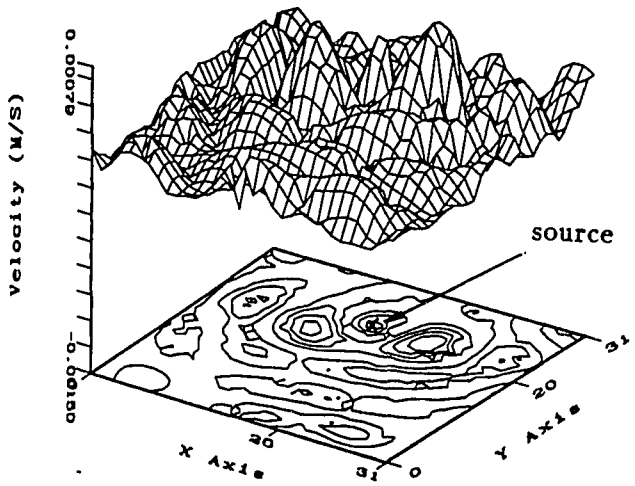

Figure 6.21: Velocity of the reverberant plate, f=1045 Hz

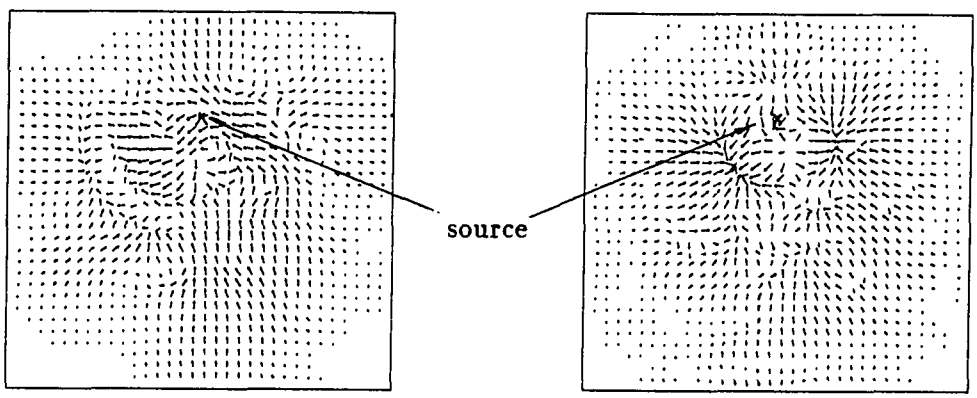

Figure 6.22: Structural intensity of the reverberant plate, f=1045 Hz, (left. active, right. reactive)

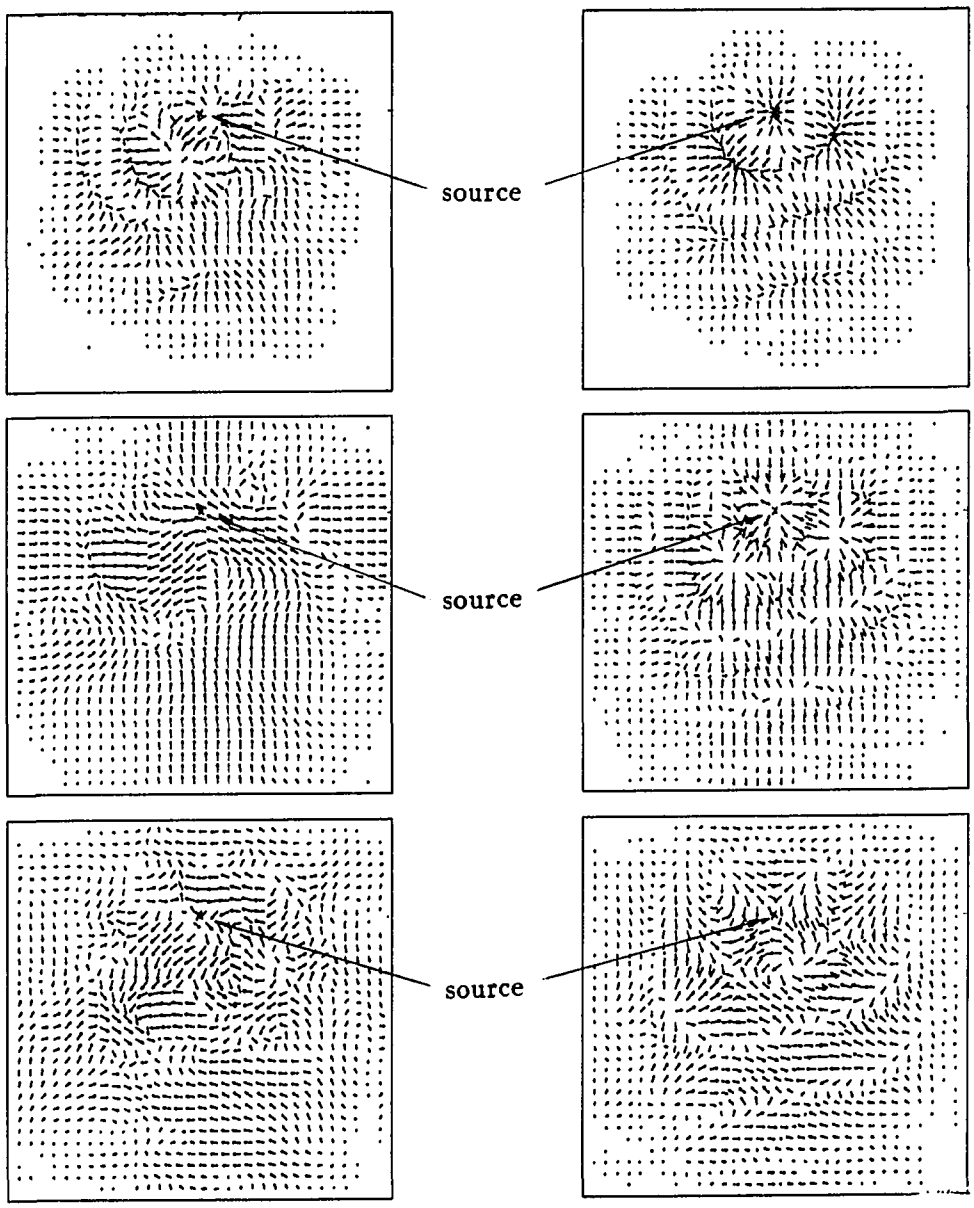

Figure 6.23: Structural intensity of the reverberant plate, (top) for bending vibration, (middle) for twisting vibration, (bottom) for shearing vibration, f=1045 Hz, (left. active, right. reactive)

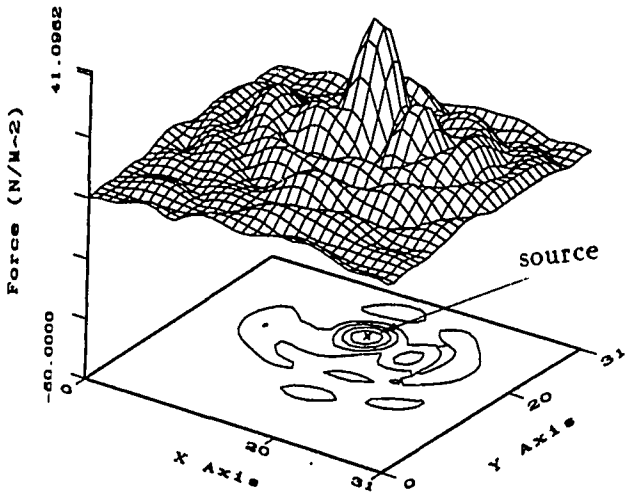

Figure 6.24: Force distribution function of the reverberant plate, f=1045 Hz

The velocity in this case is shown in Figure 6.25. Since the damping is placed on a very reverberant plate, it is expected that a lot of energy is to be absorbed by the damping. The structural intensity, shown in Figure 6.26, shows energy being absorbed by the damping material. A detailed look at the structural intensity caused by bending, twisting and shearing waves in the plate is shown in Figure 6.27. Since the damping layer is designed to damp out vibration that causes shear stresses in the damping layer as described in Chapter 5, it is not effective in damping out twisting vibration. So, the structural intensity from the twisting vibration does not show energy flowing into the damped area. For bending and shearing vibrations, which cause shear stresses in the damping layer, it is clearly shown that there is energy flowing into the damped area. Table 6.1 shows the amount of energy that flows through the boundaries of the area where the damping material is located. The minus sign means the energy flows into the damped area. It can be seen that among

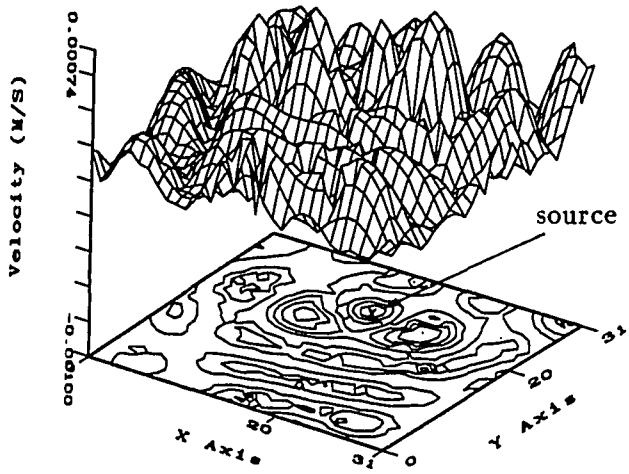

Figure 6.25: Velocity of the plate with damping, f=1034 Hz

the total amount of the absorbed energy, 61.2 % is the bending wave energy, and 34.8 % is the shearing wave energy. Only 4 % of the damped energy is the twisting energy, although the magnitude of the twisting structural intensity is even larger than that of the shearing structural intensity.

In the force distribution function, shown in Figure 6.28, the excitation force is clearly seen. But the damping is not. This means that the damping is not absorbing energy by applying a normal force to the plate.

The effectiveness of the damping also depends on the location of the damping material on the plate. Figures 6.29, 6.30 show the velocity and the structural intensity of the same measurement at 998 Hz. From the velocity in Figure 6.29, it is seen that a single resonance mode of the plate dominates at this frequency. However, the damping material is located around a nodal line, a location where little energy can

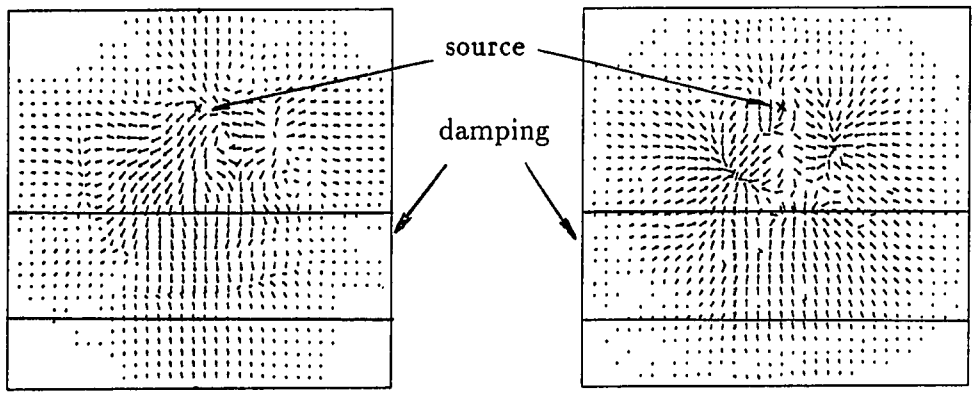

Figure 6.26: Structural intensity of the plate with damping, f=1034 Hz, (left. active, right. reactive)

Table 6.1: Energy absorbed by the damping material

	Absorbed Energy (W)	% of the total	Mag. of Max. Int.
Total	-0.1298×10^{-4}	100	2.0496^{-4}
Bending wave	-0.7948×10^{-5}	61.2	1.4295^{-4}
Twisting wave	-0.5138×10^{-6}	4.0	6.3596^{-5}
Shearing wave	-0.4514×10^{-5}	34.8	1.2119^{-5}

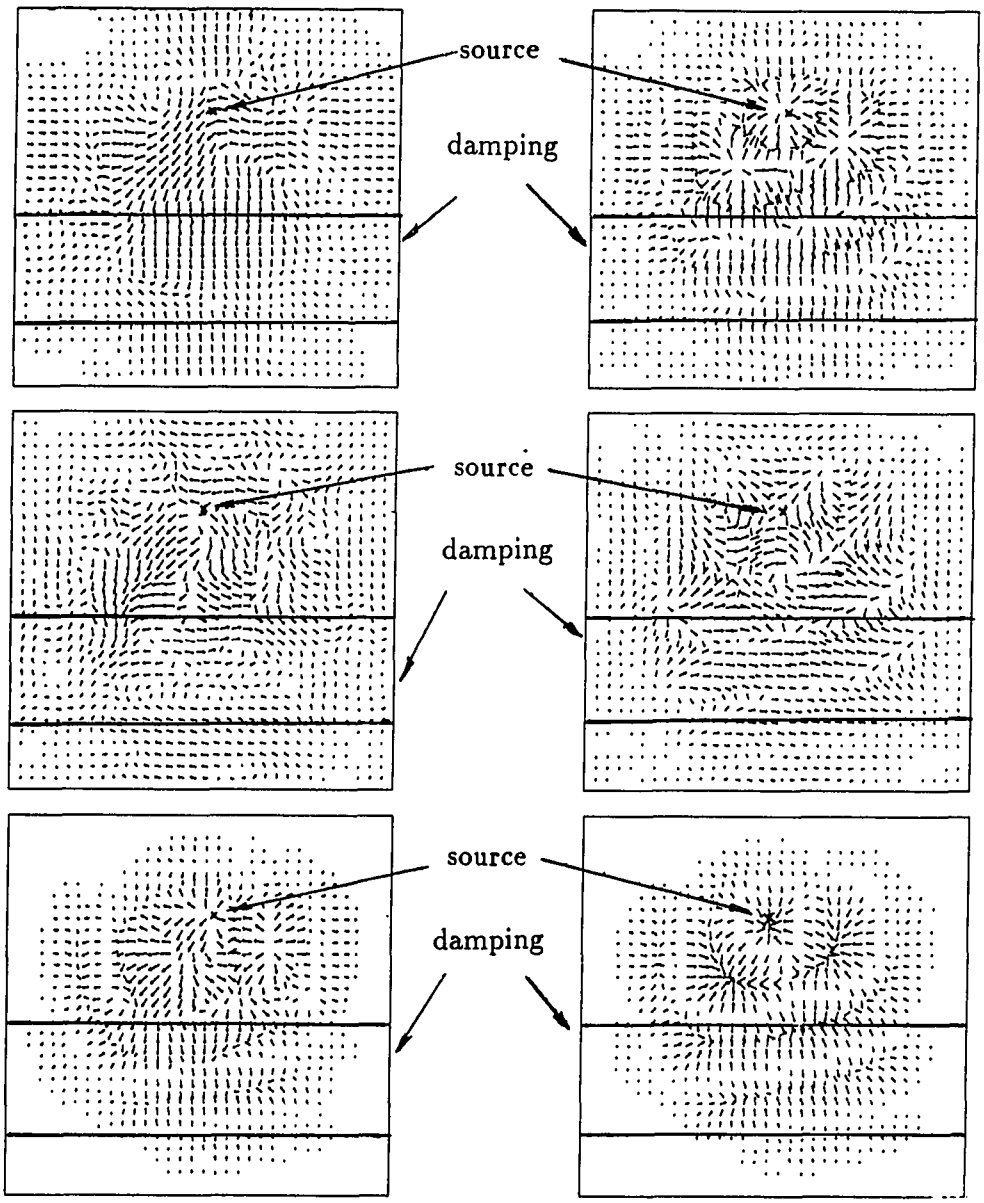

Figure 6.27: Structural intensity of the plate with damping, (top) for bending vibration, (middle) for twisting vibration, (bottom) for shearing vibration, f=1034 Hz, (left. active. right, reactive)

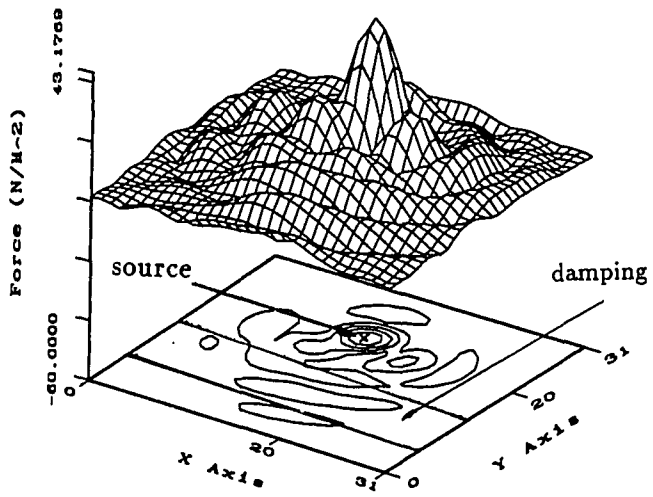

Figure 6.28: Force distribution function of the plate with damping, f=1034 Hz

be absorbed. Thus, in Figure 6.30, the structural intensity does not show clear energy flow into the damped area.

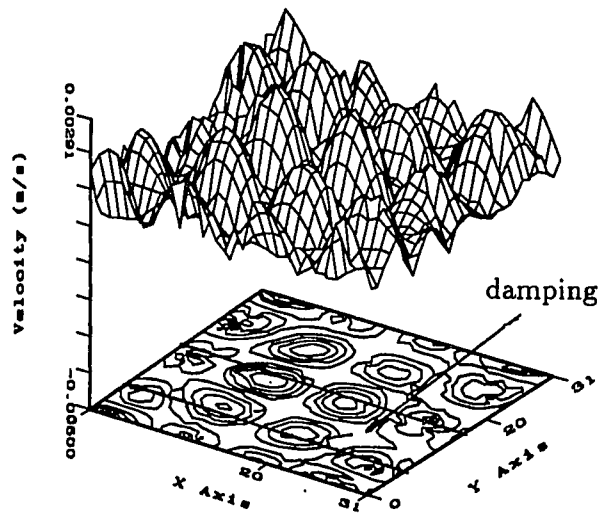

Figure 6.29: Velocity of the plate with damping, f=998 Hz

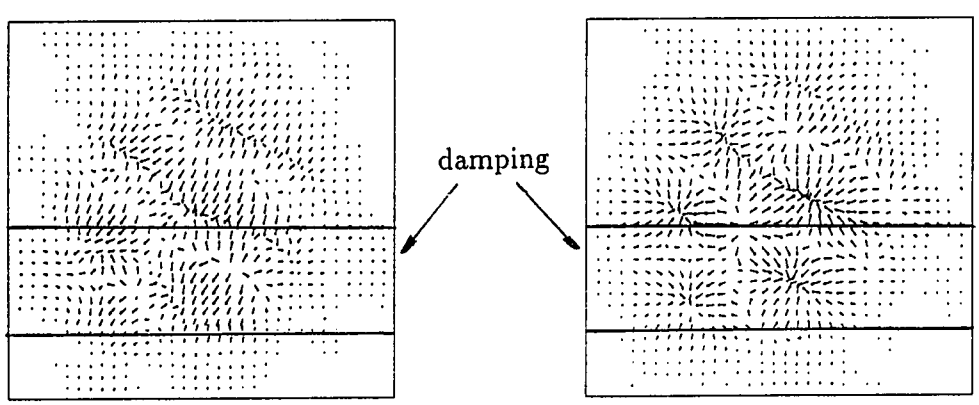

Figure 6.30: Structural intensity of the plate with damping, f=998 Hz, (left. active, right. reactive)

CHAPTER 7. SUMMARY

7.1 Summary and Conclusions

The objective of the thesis is to locate sources on plate type structures by using the structural intensity and the force distribution function. To achieve this goal, it is necessary to first study the formulations of the structural intensity. There have been many studies in this problem. Different formulas were derived based on different assumptions for plates. Pavić's structural intensity formula is based on classical (or pure bending) plate theory. While Romano's formula takes into account the effect of shear and rotary inertia. Because of the differences in assumptions, the two formulations are different. Pavić's formula requires only the out of plane displacement (or velocity) and up to third order spatial derivatives of the displacement. Romano's, on the other hand, needs all the three displacement components but only the first derivatives of the displacement components. At low frequencies (the corresponding wave length is longer than the plate thickness), the influence of the rotary inertia and shear is not significant in the calculation of the structural intensity.

The major purpose for the study on the structural intensity is to locate sources. Studies by Romano and Williams [15] pointed out that the vector form of the plate inplane displacement can be used for source identification. In addition, Romano, Abraham and Williams [33], Williams [16], and Pascal et al. [12] pointed out that

the divergence of the structural intensity is equal to the power injected into the plate. So the divergence of the structural intensity can be used to locate the sources. In this thesis, a force distribution function is introduced for locating sources. The force distribution function can be obtained through a set of plate motion equations. In this research, Mindlin's equations of plate motion [2] are used to calculate the force distribution function. This dissertation shows that the force distribution function is a very effective way of showing sources for plate like structures. Also, the plate inplane displacement components are obtained through solving Mindlin's equations of motion. These inplane components are useful in calculating the structural intensity by using Romano's intensity formula.

The normal displacement (or velocity) of the plate is required in calculating both the structural intensity and force distribution function. A laser Doppler vibrometer and a computer controlled data acquisition system are used in measuring the plate normal velocity. The measurement system is described in the thesis. Since in practical measurements, noise exists in the measured velocity, a B-spline algorithm is developed to smooth the measured data. Results show that the algorithm is effective in removing some of the noise in the measured velocity.

The formulations of the structural intensity and force distribution function are straight forward along with the overall method of implementing them using measured data. However, actually getting good results takes a lot of manipulating the data. Because derivatives are needed in the calculations and they are implemented in wavenumber domain, measurement noise is greatly amplified. Thus, filtering and windowing was shown to be an important tool to get reasonable results. However, this also removes information. For example, the windowing and filtering made it

possible to locate a single force on a plate, but also made it impossible to locate two forces on the plate. Also, a force close to the plate boundaries can not be located due to windowing. In this thesis, the effect of windowing and filtering on the location of sources and on the calculation of the force magnitude and input power is studied. Results show that using the window function, the input force magnitude can be corrected to within 18 % error when the force is not close to the plate boundaries. On the other hand, choosing a proper filter size is crucial in locating sources. As a rule of thumb, the filter size should be just large enough to enclose the center peak in the wavenumber spectrum of the plate velocity, slight adjustments may be needed in practical calculations.

A few different plates were used for measuring the velocity and calculating the structural intensity and the force distribution function. Source locations are very nicely shown in both the structural intensity and the force distribution function. For measured data, it is difficult to match the calculated force magnitude and input power with those from directly measured by a force transducer. However, it is shown that over the measured frequency band, the force magnitude and the input power from calculations change as a function of frequency in the same way as those from a direct force transducer measurement. However, the magnitude has a discrepancy.

The structural intensity and the force distribution function are also used in the study of a rib and damping materials attached to a plate. Results show that a rib constrains the plate vibration by applying a constraint force on the plate. It absorbs vibrational energy when the vibrational wave passes across it. Damping material used in this research does not apply a normal force to the plate. It absorbs energy by producing a shear stress in the visco-elastic layer and absorbs the shear energy.

It is more effective in damping out bending and shearing vibrations than twisting vibrations. All this can be seen from the force distribution function and decomposing the structural intensity into the different wave types.

7.2 Suggestions on Further Work

This research has been primarily concerned on the implementation of the calculation of the structural intensity and the force distribution function along with some analysis of the influence of ribs and damping on vibrations from an energy point of view. In the calculations, a digital Fast Fourier Transform (FFT) is used. It is clear that the FFT creates difficulties in the numerical calculations. Windowing and filtering can help improve the results. But they introduce some other difficulties. It is recommended that further study be conducted to seek ways to overcome the numerical problems.

The structural intensity formula used in this thesis are for homogeneous plates. However, the plate with a rib is also studied by using these formulas. It is suggested that the influence of ribs on the structural intensity be studied to verify the validity of the structural intensity formula. A possible approach is to calculate the structural intensity by the formulas for homogeneous plates and by directly using the structural intensity definition in Equation (2.1) with the velocities and stresses. The velocities and the stresses in the plate cross section can be calculated, for example, by finite difference methods.

The force distribution function has been shown to be an effective way of locating sources for plate type structures. It would be interesting to see if it is effective in locating sources for other types of structures. In fact, for any type of structure,

it is possible to find a force distribution function provided that there exists a set of governing equations of motion for the structure and some of the vibration components can be determined by either analytical or measurement methods. A cylindrical shell is a good choice for the structure because there are existing governing equations of motion.

REFERENCES

[1] L. Rayleigh, "Theory of Sound," Dover Publications, New York, 1945, 2nd edition

[2] H. Lamb, "On Waves in an Elastic Plate," *Proceedings of the Royal Society of London*, A93, 114-128, 1917

[3] S. Srinivas, C. V. Joga Rao, A. K. Rao, "An Exact Analysis for Vibration of Simply-Supported Homogeneous and Laminated Thick Rectangular Plates," Department of Aeronautical Engineering, Indian Institute of Science, Bangalore, India, 1969

[4] S. Timoshenko, "Vibration Problems in Engineering," D. VanNostrand Co. Inc., New York, 1937, 2nd edition

[5] E. Reissner, "The Effect of Transverse Shear Deformation on the Bending of Elastic Plates," *Journal of Applied Mechanics,* 12, pp69-77, 1945

[6] Y. S. Uflyand, "The Propagation of Waves in the Transverse Vibration of Bars and Plates," Prikl. Mat. Meh., 12, pp287-300, 1948

[7] R.D. Mindlin, "Influence of Rotary Inertia and Shear on Flexural Motion of Isotropic, Elastic Plates," *Journal of Applied Mechanics,* 1951, pp31-38

[8] D. U. Noiseux, "Measurement of Power Flow in Uniform Beams and Plates," *Journal of the Acoustic Society of America,* Vol 47, No.1 (part 2) 1970, pp238-243

[9] X. Morse and X. Feshback, "Methods of Theoretical Physics," Part I, McGraw-Hill, New York, 1953

[10] G. Pavić, "Measurement of Structural Borne Wave Intensity, Part I: Formulation of the methods," *Journal of Sound and Vib.,* Vol. 49(2), 1976, pp221-230

[11] E. G. Williams, H. D. Dardy, R. G. Fink, "A technique for Measurement of Structure-borne Intensity in Plates," *Journal of Acoustic Society of America,* 78(6), december 1985

[12] J. C. Pascal, T. Loyau, J. A. Mann, "Structural Intensity from Spatial Fourier Transformation and BIHIM Acoustic Holography Method," *Proceedings of the International Congress on Intensity Techniques,* CETIM, Senlis, France, 1990

[13] A. L. Pate, Y. Zhang, R-C. Wei, D. D. Dennink, "Determination of Structure-born Intensity in Plates from Acoustic Imaging," *Proceedings of the International Congress on Intensity Techniques,* CETIM, Senlis, France, 1990

[14] S. Hayek, M. J. Pechersky, et al, "Measurement and Analysis of Near and Far Field Structural Intensity by Scanning Laser vibrometery," *Proceedings of the International Congress on Intensity Techniques,* CETIM, Senlis, France, 1990

[15] A. J. Romano, E. C. Williams, "On the Theoretical and Experimental Applications of a Poynting Vector Formulation for Thin Shells and Plates," *Proceedings of the International Congress on Intensity Techniques,* CETIM, Senlis, France, 1990

[16] E. Williams, "Structural Intensity in Thin Cylindrical Shells," *Journal of Acoustic Society of America,* 89(4), Part 1, April 1991

[17] Y. Zhang, A. L. Pate, J. A. Mann III, "A Study on Source Localization in Plates," *Presentation at the 123rd Meeting of the Acoustical Society of America,* Salt Lake City, Utah, May 1992

[18] Chi-Teh Wang, "Applied Elasticity," McGraw-Hill Book Company, Inc, New York, 1953

[19] E. H. Kennard, "The New Approach to Shell Theory: Circular Cylinders," *Journal of Applied Mechanics,* pp33-40, March 1953

[20] P. M. Naghdi, J. G. Berry, "On the Equations of Motion of Cylindrical Shells," *Journal of Applied Mechanics,* pp160-166, 21, 1954

[21] L. Cremer, M. Heckle, E. E. Ungar, "Structural-Borne Sound," Chapter 11, Second Edition, Springer-Verlag, New York, 1972

[22] M. C. Junger, D. Feit, "Sound, Structures, and Their Interaction," Second Edition, The MIT Press, Cambridge, Massachusetts, 1986

[23] F. Fahy, "Sound and Structural Vibration — Radiation, Transmission and Response," Academic Press, New York, 1985

[24] A. D. Pierce, "Acoustics, An Introduction to Its Physical Principles and Applications," Acoustical Society of America, New York, 1989 Edition

[25] L. E. Kinsler, A. R. Frey, A. B. Coppens, J. V. Sanders, "Fundamentals of Acoustics," Third Edition, John Wiley and Sons, 1980

[26] J. A. Mann III, J. Tichy, "Acoustic Intensity Analysis: Distinguishing Energy Propagation and Wave-front Propagation," *Journal of Acoustical Society of America,* 90(1), July 1991

[27] J. S. Bendat, A. G. Piersol, "Engineering Application of Correlation and Spectral Analysis," John Wiley & Sons, New York, 1980

[28] R. N. Bracewell, "The Fourier Transform and Its Application," McGraw-Hill, New York, 1986

[29] R. J. Unglenieks, "Determining three Components of Motion for Vibrating Surfaces Using the Laser Doppler Method," Master's thesis, Iowa State University, 1991

[30] Brüel & Kjær, "Technical Review," No. 2, 1989

[31] J. D. Achenbach, "Wave Propagation in Elastic Solids," North-Holland Publishing Company, New York, 1984

[32] Tien-bin Juang, "Vibrational and Acoustic Response of Ribbed Plates," Ph.D. Thesis, Iowa State University, 1993

[33] A. J. Romano, P. B. Abraham, W. G. Williams, "Analysis of the Structural Intensity in a Driven Finite, Cylindrical Shell,"